Materiel and IT Command
Ministry of Defence

A Cylinder Pressure Measurement System for Main Diesel Engines

Assessing the Added Value for the Royal NL Navy

2025.MME.9069

J.M.T. Bongartz

Delft University of Technology

TU Delft

Materiel and IT Command
Ministry of Defence

A Cylinder Pressure Measurement System for Main Diesel Engines

Assessing the Added Value for the Royal NL Navy

by

J.M.T. Bongartz

to obtain the degree of Master of Science
at the Delft University of Technology,
to be defended publicly on Wednesday July 16, 2025 at 10:00 AM.

Student number:	9093200	
Thesis number:	2025.MME.9069	
Project duration:	November 1, 2024 – July 16, 2025	
Thesis committee:	Dr. ir. P. de Vos	TU Delft—chairman
	Dr. ir. R. Geertsma	TU Delft / Netherlands Defense Academy
	Ir. Y. Linden	TU Delft / Netherlands Defence Academy

Front cover: Ocean-going Patrol Vessel HNLMS Groningen (www.defensie.nl)
Back cover: idem (www.marineschepen.nl)

An electronic version of this thesis is available at `http://repository.tudelft.nl/`.

TU Delft

Preface

My interest in, and fascination with, cylinder pressure measurement began in 2002/2003 when I was assigned as Junior Engineering Officer aboard the multi-purpose frigate HNLMS Van Galen. At the time, I accepted without question the advice of the Chief Propulsion Engineer, namely that the exhaust gas temperatures of all cylinders of our diesel engines should be as uniform as possible. To achieve this, we manually adjusted the output of the individual high-pressure fuel pumps. The only cylinder-specific metric readily available was exhaust gas temperature—and thanks to these adjustments, the temperatures aligned almost perfectly.

However, I later reviewed reports based on cylinder pressure measurement of our cruising diesel engines, which revealed a striking disparity in individual cylinder performance. Some cylinders were barely producing more than idle output, while others delivered significantly above average power, even up to the point of overloading. This experience taught me the importance of not relying solely on exhaust gas temperature as a performance indicator.

I was more than a bit surprised, when I learnt, in 2012, while serving as Head of Engineering aboard the ocean-going patrol vessel HNLMS Groningen, that fuel injection on our main engines was controlled based on exhaust gas temperature. My immediate question was: how does that affect cylinder pressure? The answer came closer in 2019, when, working with the Department of Maritime Systems of the Defence Materiel Organisation, I was involved in the acquisition and installation of a cylinder pressure measurement system on HNLMS Groningen. Bringing the system to full operational status, I had to overcome several challenges, partly due to the onset of the COVID-19 pandemic soon after the contract was signed, but even more so because the system was not initially fully compatible with the engines. Despite these obstacles, the system was successfully brought into operation, thanks in large part to the support of the Royal Netherlands Navy's Maintenance Organisation (DMI). I am especially grateful to Wouter Mooij of DMI, without whose technical expertise, ingenuity, and hands-on involvement, the system would never have come to life.

With a fully operational cylinder pressure measurement system installed on an active vessel, I was inspired to make this system the focus of my MSc thesis. Until then, I had doubted whether I would ever find the time to complete my degree alongside a full-time job, family commitments, ownership of an old farmhouse with a decent piece of land (and the work that comes with it), and other responsibilities. However, this project had already demanded a significant portion of my working time and was beginning to generate a wealth of data, information, and insights of academic relevance. With effective time management and, perhaps, some much-needed guidance, I began to believe that finishing my thesis was within reach.

That guidance came largely from Youri Linden, who was just beginning his PhD project and proved invaluable in reviewing my early drafts and helping me stay on track. A big thank-you is in order for Youri. I also owe gratitude to Rinze Geertsma and Peter de Vos, who, while too busy to concern themselves with every detail, encouraged me to maintain focus on the bigger picture. My thanks also go to Konstantinos Kiouranakis, who generously shared his deep insights during several in-depth discussions covering multiple aspects of my research. In addition, I am grateful to Henk Knoll—my thermodynamics teacher and later colleague at the NL Defence Academy—whose knowledge and experience with critical aspects of cylinder pressure measurement greatly enriched my understanding.

I also want to thank my parents for their constant support and unwavering confidence in me. Their steady presence over the years has meant more than I can express. But foremost, I want to thank Vera and our wonderful children, Roos and Joris, who inspire me every day to strive for what truly matters. Without Vera's unwavering support and encouragement, this thesis would never have been completed. Over the past months, I've fallen short in contributing my fair share at home—if I ever truly did—and I know I have some making up to do.

J.M.T. Bongartz
Delft, July 2025

Summary

Cylinder pressure measurement of diesel engines can be a step toward enabling condition-based maintenance, moving beyond traditional maintenance strategies based solely on engine running hours. This thesis investigates the application of a continuous cylinder pressure measurement system for condition monitoring of marine diesel engines. It addresses the question how such a system can be used effectively for the analysis of engine performance, combustion, and fault detection and diagnosis of a naval vessel's main engines. To answer this question, a comprehensive methodology is proposed and tested on an ocean-going patrol vessel of the Royal Netherlands Navy. The main diesel engines of this vessel have been retrofitted with a permanent, multi-cylinder pressure measurement system, enabling simultaneous, high-frequency, crank-angle-resolved pressure acquisition. The setup includes piezoelectric sensors, a crank-angle encoder, and a custom synchronisation mechanism.

In order to obtain useful information from the raw cylinder pressure data, these data have to be preprocessed first. Preprocessing steps applied in this thesis include:

1. Synchronising pressure data with crank angle using a method that determines the TDC shift based on a temperature-entropy diagram of a non-firing engine.
2. Applying the correct pressure offset, preferably using the air intake manifold pressure. Alternatively, if this pressure is too unsteady, a linear least-squares regression method is used.
3. Averaging the cylinder pressures over 25 cycles to reduce random noise.
4. Applying cubic-spline smoothing to reduce non-random noise. A tunable smoothing parameter dictates the trade-off between curve smoothness and fidelity to the original data.

The preprocessed data are subsequently used to derive several performance and combustion-related indicators, using a single-zone heat-release model. Performance indicators include indicated mean effective pressure (IMEP), compression pressure, and peak pressure. Combustion characteristics are assessed through net heat release, thermodynamic efficiency, and crank angles corresponding to key energy release thresholds.

Cylinder-to-cylinder comparison of these parameters enables the identification of anomalies that may indicate underlying faults. Rejection criteria should be defined based on manufacturer guidelines, though these may need to be adapted. Notably, since OEM specifications only cover peak pressure and exhaust gas temperature, these criteria can be supplemented with operational experience. A structured diagnostic approach involves distinguishing whether the root cause lies in compression (e.g., valve leakage, excessive blowby) or combustion (e.g., injector malfunction).

In this study, particular attention was given to a suspected malfunctioning fuel-injection pump, identified through deviating exhaust gas temperature. However, analysis of pressure-derived parameters did not support this diagnosis; instead, another cylinder was found to exhibit signs of underperformance. This study further argues that IMEP is a more reliable parameter than peak pressure, while the angle of peak pressure is of limited diagnostic value. Exhaust gas temperature is also found to be less effective for localising faults.

In conclusion, the results of this study suggest that cylinder pressure measurement holds substantial promise for condition monitoring applications. However, validation of rejection criteria requires actual fault cases, which highlights the need for a database of known faults, including their symptoms. The study also recommends routine system checks, automation of data processing, and clear assignment of system ownership. It also recommends to implement a method for determining the correct TDC shift for the engine under load.

Contents

1
Introduction

The topic of this thesis is the marine diesel engine, the workhorse of the vast majority of naval and merchant vessels, used for propulsion (as the main engine) and power generation (as the auxiliary engine). Thanks to its favorable fuel economy and proven reliability, the diesel engine has served as the primary power source for ships for over a century. As maintenance strategies evolve, there is an increasing interest in applying data-driven methods to improve reliability and efficiency of diesel engines. This research examines the use of data obtained from cylinder pressure measurement as a step toward enabling condition-based maintenance for the main diesel engines on a specific class of vessels within the Royal Netherlands Navy.

This introductory chapter begins by outlining the motivation for the thesis, including a description of the underlying problem (Section 1.1). It then presents the research questions (Section 1.2), followed by the plan of approach (Section 1.3). Lastly, the structure of the thesis is described (Section 1.4).

1.1. Motivation

The Holland-class ocean-going patrol vessels (OPV's) of the Royal Netherlands Navy (RNLN) are manned with a small crew, much smaller than crews of similar-size frigates in use of the RNLN. This is enabled by a high degree of automation. However, the limited size of both the crew and the ship's engineering department limits the capacity to perform all required maintenance tasks. In addition, unforeseen defects that require repair, compete with the already scarce capacity available for scheduled maintenance. In particular, the vessels' main diesel engines require significant maintenance capacity from the engineering crew. In case of engine failure there is often too little time and resources available for adequate root-cause analysis and repair. As a result, maintaining the availability and reliability of the main diesel engines is a continuous challenge.

Traditionally, marine diesel-engine maintenance is time-based, i.e., based on engine running hours and/or calendar time, rather than engine condition. There is, however, an ongoing trend from time-based maintenance towards potentially more efficient maintenance programs such as predictive or condition-based maintenance: maintenance based on the condition of an asset. This allows the maintenance actions to take place before a failure occurs, i.e., not too late, and from an efficiency perspective, preferably not too early [70]. Condition-based maintenance requires measurement, data acquisition and processing of data on the condition of the asset, in support of maintenance decision making. In many situations, this approach has proven to provide better results in preventing unexpected failures and reducing total maintenance costs than other maintenance programs [33].

In recent years, fault detection and diagnosis (FDD) methods have been designed for marine diesel engines. These methods have proven vital in maintaining the efficiency and reliability of marine diesel engines [43]. An important parameter suitable for assessing engine health is the cylinder pressure [71]. Measurement of cylinder pressure, in addition to engine health assessment, may be used for many purposes. Examples hereof are online combustion failure detection [40, 54], prediction of emission formation [27, 41], noise control [55], estimation of cylinder trapped mass [75], the study of ignition timing [26], or cylinder-pressure based engine control [25] to name just a few.

In line with the trend sketched above, and in order to improve their availability and reliability, the main diesel engines of one of the RNLN OPV's, HNLMS Groningen, have been equipped with a cylinder pressure measurement system. Furthermore, the Netherlands Ministry of Defence (NL MOD) considers to have a cylinder pressure measurement system installed on diesel engines in future RNLN ships. HNLMS Groningen's system is intended to measure the pressures of all cylinders of the two four-stroke, medium-speed, V12 diesel engines.[1] An important feature of the system will be to measure and process the pressures of all cylinders simultaneously and continuously. This is a big contrast with the manual cylinder pressure measurements traditionally performed within the RNLN on medium-speed diesel engines; here cylinder pressures are taken sequentially, which may take up to 30 minutes per engine per measurement, generating no more than one data set once a year. Real-time cylinder pressure measurement and analysis allow the state of the engine to be assessed at any instant. Hence, it may help to identify failures in an early stage and to analyse the cause of occurring failures. Moreover, the ability to record cylinder pressure data more frequently allows for meaningful trend analysis and opens the door to machine learning applications by building an extensive dataset. In this way, continuous cylinder pressure monitoring represents a significant step toward condition-based maintenance in diesel engines.

1.2. Research objective

The RNLN aims to make optimal use of the installed cylinder pressure measurement system on its OPV HNLMS Groningen. Looking ahead, the NL MOD also intends to evaluate whether the operational benefits of such systems justify their costs for potential integration into future naval platforms. The objective of this research is to evaluate how a cylinder pressure measurement system can be effectively applied on naval vessels to support the analysis of engine performance, combustion processes, and fault detection. This includes understanding the system's technical implementation, identifying performance and combustion-related indicators from pressure data, and assessing the system's diagnostic capabilities. Through this, the study aims to determine the added value of cylinder pressure data over traditional engine monitoring parameters and to establish a foundation for data-driven engine condition assessment in maritime operations. Thus, the main research question that is addressed in this thesis is:

> *How can a cylinder pressure measurement system of a naval vessel's main engines be used effectively for the analysis of engine performance, combustion, and fault detection and diagnosis?*

The effective implementation of a cylinder pressure measurement system on a naval vessel requires careful consideration of several key aspects, each leading to specific research questions. The following thematic overview presents these aspects, along with the corresponding subquestions:

a) System understanding and implementation

1. What are the key components and operating principles of a cylinder pressure measurement system?
2. What are the technical and operational requirements for implementing such a system on the main engines of a naval vessel?
3. How does the marine environment affect the accuracy and reliability of cylinder pressure measurements?
4. What preprocessing steps are required to convert raw cylinder pressure data into usable formats for analysis?

b) Engine performance and combustion analysis

5. What useful performance indicators can be derived from cylinder pressure data?
6. In what ways can cylinder pressure data provide additional value or insights beyond traditional performance parameters (e.g., fuel consumption, engine load, and power output)?
7. How can cylinder pressure data be used to characterise the combustion process in marine diesel engines?

c) Fault detection and diagnosis

[1]The reader is assumed to be familiar with the working principles of a turbocharged diesel engine.

8. Can a malfunctioning fuel-injection system be detected through cylinder pressure analysis?
9. How does pressure-based fault detection compare in accuracy and timeliness to other diagnostic methods?

Together, these thematically grouped subquestions form a comprehensive framework for addressing the main research question. The themes highlight the critical areas of cylinder pressure measurement. Understanding the system's technical foundations establishes a baseline for reliable data acquisition. Investigating its role in engine performance and combustion analysis reveals how operational insights can be derived from pressure data. Exploring fault detection capabilities underscores the system's diagnostic value. Collectively, these subquestions support a comprehensive assessment of the system's value and practical implementation.

1.3. Plan of approach

To systematically address the main research question, this thesis adopts a structured three-step approach. Each step contributes to answering specific subquestions and builds toward the development, validation, and demonstration of a comprehensive methodology for the analysis of cylinder-pressure data from marine diesel engines.

1. **Literature review:** The first step involves performing an extensive literature review. This review includes a thorough examination of existing studies, technical documentation, and academic publications relevant to cylinder-pressure data analysis, combustion diagnostics, and fault detection in diesel engines. The objective is to identify established methods, assess their applicability, and uncover existing gaps in knowledge.
2. **Methodology development:** In the second step, a methodology is developed dedicated to the analysis of cylinder-pressure data. The method is structured into four main components: preprocessing, performance analysis, combustion analysis, and fault detection and diagnosis. This step builds upon insights gained from the literature review and is designed to ensure methodological effectiveness and operational relevance.
3. **Method application and demonstration:** The final step involves applying and demonstrating the developed methodology using operational cylinder-pressure data obtained from the Royal Netherlands Navy vessel HNLMS Groningen. This practical implementation validates the effectiveness of the proposed approach and serves to answer the remaining subquestions by evaluating the methodology under real-world operating conditions.

1.4. Thesis outline

This thesis is organised as follows:

- **Chapter 2** reviews the relevant literature on cylinder pressure measurement, organised into four key themes: (1) system understanding and implementation, (2) data preprocessing, (3) engine performance and combustion analysis, and (4) fault detection and diagnosis (FDD). The chapter concludes by identifying a research gap.
- **Chapter 3** outlines the research methodology, which is based on analysing cylinder pressure data collected under comparable operating conditions across three different periods. The chapter also provides a detailed description of the implemented measurement system.
- **Chapter 4** describes the preprocessing steps applied to the raw pressure data to ensure accuracy and consistency. These include: (1) synchronisation of pressure and crank angle, (2) determination of pressure offset, and (3) pressure averaging and smoothing.
- **Chapter 5** presents the methodology used to assess cylinder performance and combustion characteristics, as well as to support fault detection and diagnosis. Diagnostic criteria are based on manufacturer guidelines and relevant literature.
- **Chapter 6** presents the results obtained by applying the proposed methodology to engine data collected during operational deployments at sea, recorded on three separate occasions over a period of eighteen months.
- Finally, **Chapter 7** provides the main conclusions and offers recommendations, including suggestions for further research.

2

Literature review

This chapter presents the main findings of the literature review conducted in support of this thesis. Section 2.1 introduces the fundamental principles of cylinder pressure measurement. Section 2.2 discusses data preprocessing techniques used to improve measurement accuracy and reliability. In Section 2.3, the potential for performance and combustion analysis based on cylinder pressure data is explored. Section 2.4 reviews various fault detection and diagnosis (FDD) methodologies applicable to diesel engine monitoring. Finally, Section 2.5 summarises the key insights from the literature and identifies the research gap addressed by this thesis.

2.1. System understanding and implementation

Modern cylinder pressure measurement systems comprise a set of components that together form a complete measurement chain. The role and function of each component in this chain are discussed in this section.

2.1.1. A typical measurement system - components

The cylinder pressure in a diesel engine (or any reciprocating internal combustion engine) varies with the position of the crankshaft. This variation results primarily from changes in cylinder volume, combustion processes, and heat transfer, and to a lesser extent from flow-related phenomena such as crevice flow and blow-by [28]. Hence, measurement of cylinder pressures may generate useful information related to engine operation, specifically to the compression and combustion stages, overall engine performance and performance of individual cylinders.

A system designed to measure the cylinder pressures of an internal combustion engine typically consists of the following components:

- Pressure transducers

  Several types of pressure transducers exist, e.g. piezoelectric, piezoresistive and optical sensors. Piezoelectric pressure transducers are by far the most commonly used type. This type of sensing element produces an electric charge proportional to the mechanical force (and pressure) applied to it. The element thus reacts only to a pressure *change*, which makes it unsuitable for static pressure measurements [62]. For cylinder pressure measurement, this is not an issue, since this type of measurement typically involves a highly dynamic environment and requires a highly dynamic measurement chain [47]. Piezoelectric pressure transducers are generally used because of their high frequency response and relative (but not complete) insensitivity to environmental conditions. Combustion engine research suggests that the most accurate measurement results are obtained when the sensors are flush mounted in the cylinder head [58], see Figure 2.1. However, this may increase the severity of thermal shock since the sensing element is then directly exposed to the extreme combustion temperatures. Thermal shock is a shift in sensor output caused by high rates of heat flux to the sensing element. Careful design of the transducer can limit its sensitivity to temperature changes: the transducer can be protected by a small front plate that has one or several passages leading to a small cavity volume in the vicinity of the transducer face. For detailed combustion analysis and extremely accurate measurement tasks, water-cooled

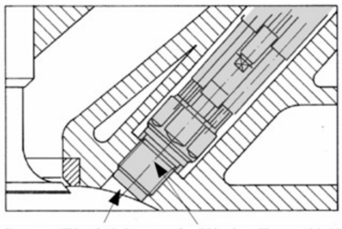

Figure 2.1: Flush mounted transducer [24]

transducers are commonly applied. In general, these are more stable and less sensitive to errors induced by thermal conditions than non-cooled transducers [62]. The water-cooled type is widely preferred for use in single-cylinder research engines, but is less suitable for small-bore engines because of spatial restrictions. Cylinder heads of medium speed, marine diesel engines usually have provisions for mounting an indicator valve. This can be used for (permanent) mounting of a pressure transducer as well. For mobile measurements, the pressure transducer is commonly mounted on the indicator valve and moved from one cylinder to another, in order to perform the pressure measurement on all cylinders [5].

- Charge amplifiers

  The charge amplifier converts the tiny electric charge signal produced by the pressure transducer into an output voltage for further processing. The charge amplifier should do so without affecting the signal or introducing any unwanted filtering effects [62]. The voltage may then be converted to an industry-standard 4-20 mA signal. This reduces the vulnerability to noise [19].

- Crank angle encoder

  The measured cylinder pressure must be referenced to the crank angle, which is the function of the crank angle encoder. Since the cylinder volume is a (usually known) function of the crank angle, it suffices to know this angle. Many engines are fitted with a toothed wheel and inductive sensors used by the engine management system to provide information on the crankshaft position. It is common practice to omit one tooth on the wheel in order to provide a reference point during every revolution [62]. For field applications, when the crank angle information from the engine management system is not available to the cylinder pressure measurement system, it will be necessary to install an inductive pick-up sensor to be used in combination with a toothed wheel, e.g. the engine's flywheel. It may be necessary to install an additional sensor to provide a reference point every revolution.
  Another way to determine the crank angle at any instant is to use an optical transmitter and receiver, combined with an engine-mounted marker disk. Its use, however, is mostly restricted to lab applications [1].

- Data acquisition and data processing

  The analog cylinder-pressure and crank-angle signals must be digitised and brought together to be processed further. A common method is to digitise samples at fixed time intervals and then transform time into crank angle by assuming a constant rotational speed during the engine cycle [1]. The sampling can also be triggered by a crank angle encoder so the cylinder pressure can be related to the crankshaft position [18]. In either case it is necessary to synchronise the crank angle with the cylinder pressure.

2.1.2. Performance requirements

In order for a cylinder pressure measurement system to provide useful data, following requirements need to be met:

- The measured pressure must be converted to absolute pressure by using the correct reference pressure [7]. Pressure referencing (or *pegging*) is necessary since commonly used pressure transducers only respond to a *change* of pressure [62].
- The phasing (or synchronising) of cylinder pressure versus crank angle should be sufficiently accurate, within 0.2° at least [28] or, for detailed combustion analysis, even within 0.1° [62, 68].
- A sufficient amount of data points must be available. The number of points that qualifies as sufficient, depends on the purpose of the measurement. For example, in order to calculate the gas temperature from the cylinder pressure, the number of data points would have to be at least 500 per crankshaft revolution [67]. In order to compare different pegging methods, Randolph [59] used pressure data with 1° increment (hence 'only' 360 data points per revolution). This does not contradict the previous point, as long as pressure and crank angle are well synchronised.
- The clearance volume must be accurately known [28]. This is equivalent to knowing the cylinder bore, stroke and geometrical compression ratio. These parameters are usually available from engine documentation.

2.2. Preprocessing cylinder pressure data

In order to obtain sufficiently accurate cylinder pressure data, it is necessary to limit following common sources of error [28]:

- incorrect phasing of cylinder pressure with crank angle;
- incorrect pressure referencing;
- fluctuations with regard to pressure signal;
- thermal shock of the pressure sensor.

The latter, thermal shock, may be virtually eliminated by careful design of the pressure sensor: special heat shields, coating of the transducer membrane, water cooling and temperature effect compensating design [56]. Thermal shock will not be discussed further here. The former three sources of error are now discussed in more detail.

2.2.1. Determination of TDC

Although it has no influence on the measured values of (absolute) cylinder pressure, incorrect phasing of the pressure with crank angle will lead to significant errors in the calculation of certain parameters, including *IMEP*, indicated efficiency and rate of heat release [13]. This is a consequence of the cylinder volume being derived from the crankshaft position. As a rule of thumb, every 0.1° phase error will increase the error in *IMEP* with 1% [6].

The position of top dead center (TDC) is usually taken as a reference to which the position of the crankshaft (crank angle) for a certain cylinder is expressed. When analysing cylinder pressure data, it is of vital importance, therefore, to determine TDC with sufficient accuracy. TDC may be determined by a static or a dynamic method. In the static method, a dial gauge is used to measure the distance from the fuel injector hole to the top of the piston. This distance is minimal at TDC, but the vertical displacement of the piston around TDC is too small to accurately determine TDC. It is better to start at a position around 90 degrees before the (expected) TDC position, note the distance and mark the position on the flywheel. Then slow-turn the engine until the same exact distance is measured on the dial gauge and mark the position on the flywheel. Now, TDC is the exact value in the middle of the two [62].

In contrast, dynamic methods make use of an engine during operation. Most methods use a motored, or non-firing, engine. In the (hypothetical) absence of heat transfer and other irreversibilities, the peak pressure would occur precisely at TDC, when cylinder volume is minimal. Because of inevitable heat transfer, however, the instant (or crank angle) of maximum pressure comes just before TDC. The difference between TDC and the angle of maximum pressure of a non-firing cylinder is called the *thermodynamic loss angle*, or simply *loss angle*. Hence, determining the (thermodynamic) loss angle is equivalent to establishing the position of TDC. The loss angle typically has a value of 0.5° to 1.0°. This

may seem like a minor value but the effects of a poor TDC determination are very significant: a 1° inaccuracy may lead to a 10% error in *IMEP* [3], and even a 25% error in total heat released during combustion [57]. The loss angle, therefore, needs to be taken into account. Nevertheless, assuming the maximum pressure to occur at TDC may be regarded as a fast and simple starting point.
Several methods exist to determine the thermodynamic loss angle. Explicit formulas have been derived for the loss angle as a function of the heat loss per crank angle [66]. However, if the heat loss is not known in sufficient detail, which will likely be the case with an engine in the field, this method will be unreliable.

Here is a short selection of the many dynamic methods that can be found in literature to determine TDC position:

- Tazerout [69] proposed a method based on inspection of a temperature-entropy diagram of a motored engine. When the position of TDC is incorrect, a loop is observed in the T-s diagram, around the maximum temperature. The loop scales with the magnitude of the error in TDC position. In order to construct the T-s diagram, the values of temperature and entropy need to be calculated at any instant.
- Stas [68] describes a method to determine TDC, based on a measured pressure-versus-crank angle (p-α) diagram of a motored engine cycle. The method follows the change of the polytropic exponents at the inflection points of compression and expansion curves. The method shows that the thermodynamic loss angle depends heavily on the heat transfer, and even on which heat transfer formula is being used.
- Nilsson [52] introduced a method based on symmetry of the pressure signal during compression and expansion of a non-firing cylinder. The method determines a pressure offset in order to account for heat transfer. Nilsson found the 'symmetry' method' to provide slightly better results than the 'inflection point' method. However, the effectiveness of the symmetry method relies heavily on the estimation of an exponent that varies from engine to engine, which may make the method less suitable as a general method.
- Oskam [53] applied a method that used the p-α diagram of a firing cylinder. The tangent to the graph of the derivative $dp/d\alpha$ is constructed in a descending part of the graph before TDC. Then, TDC is the position where the tangent intersects with the α axis. This method is extremely sensitive to fluctuations of the pressure signal; if the pressure trace is not very smooth, the method gives an inaccurate TDC value, leading to erroneous calculations of e.g. heat release or combustion temperature.

Table 2.1 presents an overview of the described methods to determine TDC, including assessment criteria that help to select a suitable method. The criterion *practicality* is the author's (subjective) interpretation of the simplicity versus difficulty to succesfully implement the method. Some methods require a substantive amount of estimation and calibration of parameters, making it sensitive to errors, hence less practical, whereas other methods require interpretation of cylinder pressure data only.

Table 2.1: comparison of methods to determine TDC

Method	practicality	accuracy	firing/motored
static	- -	++	n.a.
maximum pressure	++	-	motored
$T{-}s$ diagram (Tazerout)	+	+	motored
inflection points (Stas)	+/-	+	motored
symmetry (Nilsson)	+/-	++	motored
tangent (Oskam)	+/-	- -	firing

Which of the described methods is the most suitable, may differ from engine to engine. Based on the above the method by Tazerout appears to be the most suitable method to be implemented on board.

2.2.2. Pressure referencing

An inherent characteristic of piezoelectric pressure transducers is that these respond only to a *change* in pressure. Referencing the measured pressure to a known value (also called *zero-level correction* or pressure *pegging*), therefore, is a necessary step. Many methods, that can be divided into two classes, exist to determine the pressure offset. The first class uses an external (additional) pressure sensor in order to reference a measured cylinder pressure to the external pressure at some instant during the cycle. The second uses numerical algorithms on the gathered pressure data in order to determine the pressure offset [3].

In a leading study, Randolph [59] compared nine different pressure-referencing methods. Three of these made use of an extra pressure sensor, either in the intake or the exhaust manifold:

- The cylinder pressure at inlet bottom dead center (IBDC) is set equal to the absolute pressure in the intake manifold each cycle.
- The average cylinder pressure during the exhaust stroke is set equal to the exhaust backpressure.
- The pressure at exhaust TDC is set equal to the measured backpressure.

Pegging at IBDC proved to give better results than the other methods tested in this study, including numerical procedures like forcing a fixed or variable polytropic exponent during compression. Referencing to a single point, however, may lead to a very noisy pressure trace due to inevitable fluctuations (noise) in the signal from the pressure transducer. In order to reduce this potential for error, Randolph suggests taking the average of three pressures as the reference value: 1° before IBDC, at IBDC and 1° after IBDC. In addition, it is advisable to peg every cycle, preventing long-term drift of the piezoelectric devices.

Zhang [78] proposed a pegging algorithm that does not require an additional pressure sensor. Assuming that the compression phase is a polytropic process (i.e. $pV^n =$ constant), this algorithm uses a least-squares method to calculate the sensor offset as well as the cycle-to-cycle variation of the polytropic exponent n in an iterative procedure. The effectiveness of the proposed method was compared with that of two other algorithms:

- A least squares method with n assumed constant.
- A non-linear least squares method with variable n.

The first method performed poorly as a consequence of the assumption of a constant n. The second method resulted in severe oscillations of both n and pressure offset. In contrast, the proposed method was found to produce stable and reliable results, at acceptable computational cost.

It is also possible to determine the pressure offset as well as the TDC position simultaneously. The method developed by Baskovic et al. allows both values to be determined in a single calculation [3]. The method identifies characteristic deviations of the heat-release rate specific for the TDC and the pressure offset during the compression and expansion phase after combustion. A second refinement step can be done in order to obtain very accurate results. A drawback of the method is the fact that it is based upon a thermodynamic model, which incorporates heat transfer calculation, making it difficult to implement.

Table 2.2: comparison of pressure referencing methods

Method	practicality	accuracy	sensor/numerical
pegging at IBDC	++	++	sensor (intake)
average exhaust pressure	-	+	sensor (exhaust)
pegging at exhaust TDC	-	+/-	sensor (exhaust)
assuming constant n	+	-	numerical
variable n	+/-	+/-	numerical
cyclic variation of n	+/-	++	numerical
pressure offset and TDC	-	++	numerical

Table 2.2 gives an overview of the described methods to determine the pressure offset. As before, the criterion *practicality* reflects the author's view of the difficulty to successfully implement the method. Based on the above, it is obvious that pegging at IBDC will be the author's method of choice: the extra pressure sensor usually is available in the intake manifold and the method is accurate.

2.2.3. Smoothing the pressure trace

Several phenomena make it necessary for the cylinder pressure signal to be smoothed before it can be used for control purposes or diagnostics. Fuel injection and the rapid rate of combustion cause appreciable pressure fluctuations in the cylinder, which are measured by the pressure transducer. In addition, the position of the pressure transducer may give rise to significant acoustic pressure oscillations. Ideally, the pressure sensor should be flush-mounted in the combustion chamber, but often this is not possible. In that case, the indicator channel together with the volume of the chamber at the end of the channel, where the pressure sensor is mounted, will act as a Helmholtz resonator. The fast pressure rise at the entrance of the passage due to the combustion causes the gas to vibrate at a certain natural frequency, due to the compressibility of the gas. The frequency of the oscillating pressure waves is given by [73]:

$$f = \frac{c}{2\pi}\sqrt{\frac{A}{LV}} \tag{2.1}$$

where c is the velocity of sound, A the cross-sectional area of the channel, L the length of the channel and V the volume of the chamber. The velocity of sound $c = \sqrt{\gamma RT}$, where γ is the ratio of specific heats of the in-cylinder gases and R the specific gas constant. These oscillations are superimposed on the combustion pressure, see Figure 2.2, making information like e.g. peak pressure difficult to extract.

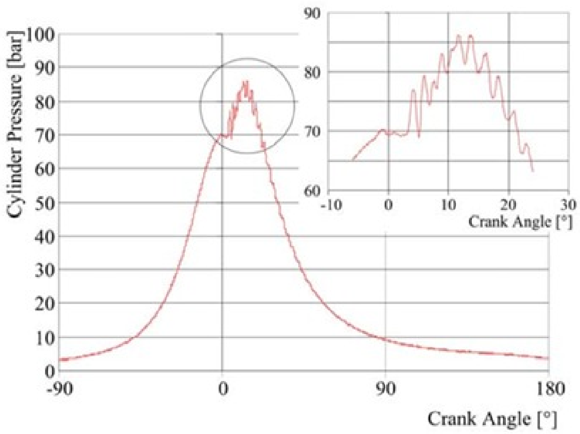

Figure 2.2: Fluctuations in pressure signal due to oscillations in indicator channel [24]

A typical indicator channel may consist of several tubes and passages of differing lengths and diameters, in which case the natural frequency of the pressure wave cannot be calculated using Eq. 2.1. As an alternative, the formula developed by Bergh and Tijdeman [4] can be used to describe the dynamic response of a pressure measuring system. This (elaborate) recursive formula is a complex transfer function of the pressure ratio between two adjacent volumes of the indicator channel. In a comparative study of three different methods (1. Helmholtz resonator, 2. organ pipe model, 3. Bergh and Tijdeman) to determine the resonance in indicator channels of different geometry, the method of Bergh and Tijdeman was found to give excellent agreement between theory and experiment [24].

Pressure fluctuations may lead to inaccurate pressure measurement and, as a consequence, to significant errors when computing e.g. the rate of heat release from cylinder-pressure data. This is the result of the differentiation involved in applying Eq. 2.6 and 2.8: differentiation amplifies the high-frequency noise and oscillations present within the pressure trace. It is therefore necessary to smooth the pressure trace before performing heat-release calculations [80].

A common first step in smoothing is averaging the pressures from many engine cycles. The resulting graph of the averaged cylinder pressure as a function of cylinder volume or crank angle is a much smoother one than the graphs of the individual cycles. Averaging is a simple and effective method to reduce the random noise of the pressure measurement. The method does, however, not eliminate systematic errors. Also, averaging many cycles is not effective during transient engine operation. On the other hand, when the engine is operating in steady conditions, cycle-to-cycle variations will appear, caused by small differences in the amount of fuel injected and the injection timing. To minimise the effect of these cycle-to-cycle variations, usually several consecutive cycles are measured and averaged, since one randomly chosen cycle may not be representative of the engine's steady operating conditions [56].

In addition to or instead of averaging the cylinder pressures, a mathematical smoothing algorithm can be used. Examples hereof are curve fitting by means of parabolas, higher order polynomials or splines. Another method is to apply a moving-average filter, which averages a few points to every point in the trace. These mathematical algorithms may be regarded as low-pass filters [80].

Payri et al. apply a three-step approach in the processing of cylinder-pressure data [56]. Prior to averaging (step 2) and filtering (step 3), it is suggested to determine the optimal number of cycles to be averaged (step 1). Increasing the number of cycles to be averaged will at first decrease the standard deviation of pressure samples at each crank angle. There is, however, a point at which adding another cycle to those to be averaged, does not add any more information: the standard deviation will not decrease further. Payri et al. found a number of 25 cycles to be optimal, but the optimal number may vary from engine to engine and from operating point to operating point.

A drawback of these algorithms is that these do not physically interpret the data. Rather, they manipulate the data mathematically, introducing the risk of losing information from the measurement. A method that is claimed to not have this drawback, was proposed by Ding et al. [15]. The heat-release analysis is based on the averaged but *unsmoothed* cylinder pressure signal; the procedure is as follows:

1. Separate the closed-cycle pressure signal (after IVC) from the overall pressure trace.
2. Take the average of 15–25 cycles.
3. Calculate the reaction coordinate (Eq. 2.10) from the averaged data.
4. Fit the reaction coordinate with a multiple Wiebe function (Eq. 2.11) using curve fitting techniques.
5. Calculate the pressure and temperature of the cylinder contents, performing a heat release calculation with the fitted (and smoothed) reaction coordinate as input.

When using a third or higher order Wiebe function, calculated parameters such as peak pressure, peak temperature and indicated power appear to converge. The recommendation therefore is to use at least three Wiebe functions to fit the reaction coordinate. The result is a smooth pressure trace and an accurate description of the heat release in the engine.

2.3. Engine performance and combustion analysis

Many applications of cylinder pressure measurement are described in the literature. Examples are engine health assessment [56, 71], online combustion failure detection [40, 54], prediction of emission formation [27, 41], noise control [55], estimation of cylinder trapped mass [75] and the study of ignition timing [26], or cylinder-pressure based engine control [25] to name just a few.

For the purpose of this thesis the most relevant applications are:

1. determination of engine performance indicators;
2. heat release analysis;
3. characterisation of combustion progression;
4. engine faults and diagnosis.

2.3.1. Engine performance analysis

The first three will be addressed in this section. Section 2.4.2 is dedicated to engine faults and diagnosis.

Many important and commonly used engine performance indicators can be derived from cylinder pressures. Among these are cylinder peak pressure, engine torque, indicated work, indicated power and indicated mean effective pressure. The peak pressure and the crank angle at which the peak pressure occurs, give a first indication whether all cylinders are performing equally well.
If the cylinder pressure p is properly synchronised with the crank angle θ, the instantaneous torque M of one cylinder as a function of crank angle can be determined as follows [18]:

$$M(\theta) = (p(\theta) - p_0)\frac{dV(\theta)}{d\theta} \tag{2.2}$$

where $p(\theta)$ is the absolute cylinder pressure and p_0 the crankcase pressure. The term $dV(\theta)/d\theta$, i.e. the derivative of the cylinder volume with respect to crank angle, follows from (known) engine geometry. The instantaneous *engine* torque can be determined by summing the torques of the individual cylinders, taking into account the engine's firing order and, in case of a V-engine, the V-angle.

The cylinder pressure throughout the engine cycle as a function of the cylinder volume can be plotted on a p-V diagram (or *indicator* diagram). The indicated work is the work produced by the gas on the piston for a cycle and corresponds with the enclosed area of a complete engine cycle plotted in an indicator diagram:

$$W_i = \oint p dV \tag{2.3}$$

With W_i known, the *indicated mean effective pressure* can be calculated: IMEP $= W_i/V_d$, where V_d is the cylinder displacement volume.

Another useful performance indicator is the mechanical efficiency. This parameter accounts for power losses due to friction, as well as the power required to drive the inlet and exhaust valves, the engine-driven cooling water pump(s), lubricating oil pump and fuel oil pumps [37]. These power losses, when grouped together, are called friction power P_f. The mechanical efficiency is defined as: $\eta_m = W_e/W_i$, where W_e is the effective work output per cycle, or, equivalent but more practical, as P_b/P_i, where P_b is the effective power or brake power and P_i is the indicated power. The brake power is the usable power delivered by the engine to the load and is normally determined by measuring the output torque and rpm of the engine shaft [28]. The brake power is equal to the indicated power of all cylinders together minus the friction power: $P_b = P_i - P_f$. The indicated power per cylinder $P_i = W_i n_e/2$ for a four-stroke engine, where n_e is the number of engine revolutions per second.

2.3.2. Heat-release analysis

The release of the chemical energy during combustion of the injected fuel is termed the *heat release*. Heat-release analysis is an important part of internal combustion engine research, and, in particular, of diesel engine research. In order to analyze the heat release, often a single-zone combustion model is applied. Following assumptions apply to a single-zone combustion model [18]:

- The cylinder contents and the thermodynamic properties are uniform.
- The combustion is modeled as release of heat.
- The heat release is uniform in the chamber.

Additionally, the gas mixture may be considered to behave as an ideal gas. The relatively simple single-zone models may be preferable to the potentially more accurate multi-dimensional thermodynamic models, since they are less complex, numerically more efficient and normally provide similar results for many parameters [8]. A heat release model for the contents of the engine combustion chamber, modeled as an open system, starts with the first law of thermodynamics, which in differential form, takes the form [20]:

$$dU = \delta Q - \delta W + \Sigma h_i dm_i \tag{2.4}$$

where dU is the (infinitesimal) change in internal energy of the in-cylinder mass, δQ is the heat input, δW is the work output, dm_i is the mass entering the cylinder (flow out of the cylinder is negative) and h_i is the enthalpy of the mass entering or leaving the cylinder.

The heat release is referred to as *net* heat release when the heat transfer from the cylinder contents to its environment is ignored. The net heat release can be determined from the temperature and pressure rise. The *gross* heat release is obtained when heat transfer effects are included. This quantity thus depends heavily on an accurate estimation of the heat 'loss' from the cylinder contents to the cylinder wall, cylinder head and piston crown. Assuming ideal gas behaviour, the following relation for determining the net heat release can be derived from Eq. B.1 [8]:

$$\delta Q_{hr,net} = \delta Q_{hr,gr} - \delta Q_{ht} = \frac{\gamma}{\gamma - 1} p dV + \frac{1}{\gamma - 1} V dp \tag{2.5}$$

where $\delta Q_{hr,net}$, $\delta Q_{hr,gr}$ and δQ_{ht} are the (infinitesimal) net heat release, gross heat release and heat loss, respectively; γ is the ratio of specific heats, c_p/c_v. Eq.2.5 is convenient to use since the terms pdV

and Vdp readily follow from an indicator diagram, or, equivalently, from pressure-versus-volume data. However, the heat release thus calculated is very sensitive to incorrect values of γ. This parameter is not constant but is a function of temperature. It may be approximated using a linear function [20] or a second order polynomial [8].

For combustion analysis, the *rate* of heat release is a commonly used quantity, (see e.g. [28] or [66]). The net apparent heat-release rate is defined as the instantaneous heat released by combustion minus the instantaneous heat-transfer rate (the heat 'loss') from the cylinder contents to its immediate environment. Assuming ideal gas behaviour this amounts to:

$$\text{NAHRR} = \dot{Q}_{comb} - \dot{Q}_{loss} = mc_v\frac{dT}{dt} + p\frac{dV}{dt} \tag{2.6}$$

In order to be able to use Eq. 2.6, the mass of the cylinder contents needs to be known. The in-cylinder mass at any instant after the intake valves close (IVC) and before the exhaust valves open (EVO), is equal to the mass trapped in the cylinder at IVC, plus the mass of injected fuel minus the amount of blowby, i.e. the gas leaking from the combustion chamber past the piston rings into the crankcase. As several studies show, e.g. [44, 50], the blowby rate in normal operation, as a percentage of total air flow through the engine, is of the order of 0.5-1%. This may seem small enough to neglect. Nevertheless, blowby can seriously affect the compression and combustion expansion pressure diagrams [38]. Blowby is discussed in more detail in Section 2.4.2.

It is not straightforward to determine the trapped mass at IVC. The trapped mass may be estimated using the cylinder pressure. If the gas temperature is known, the total mass in the cylinder can be calculated using the ideal gas law. The difficulty is to determine the gas temperature at IVC, which will be considerably higher than the air temperature in the intake manifold. This is a result of heat pick-up when the intake air flows past the hot intake valve, as well as mixing with the remaining combustion gases [64]. Conversely, if the in-cylinder mass is known, the gas temperature can be computed through the ideal gas law since pressure and volume are known [18].

When the gas temperature is known, the instantaneous heat transfer to the walls can be estimated by using correlations as those developed by Woschni [76] or Hohenberg [29]. Both engine researchers developed correlations based on an assumed relationship between the dimensionless Nusselt and Reynolds number for turbulent flow in pipes: $Nu = cRe^{0.8}$. From this equation, correlations for the heat transfer coefficient h can be found, in which h depends on gas temperature, pressure, velocity and cylinder bore. Then, assuming uniform gas temperature and wall temperature, using Newton's law of cooling the instantaneous heat loss (or heat transfer rate) is found:

$$\dot{Q}_{loss} = hA\Delta T = h\sum_i A_i(T - T_{wall,i}) \tag{2.7}$$

where the index i indicates cylinder wall, cylinder head and piston crown. The respective surface temperatures cannot be measured directly in an engine in the field. Instead, these temperatures will have to be estimated. Then, if $\dot{Q}_{loss}$ may be estimated with reasonable accuracy, the *gross* apparent heat release rate, or *instantaneous combustion heat rate*, follows:

$$\text{GAHRR} = \dot{Q}_{comb} = mc_v\frac{dT}{dt} + p\frac{dV}{dt} + \dot{Q}_{loss} \tag{2.8}$$

The main error in the calculated gross heat release data when using a heat release model as described here, is due to uncertainties in the calculated charge-to-cylinder wall heat transfer [8]. Dividing GAHRR by the fuel's effective combustion heat u_{comb}, the mass rate of fuel burnt, or the *combustion reaction rate* ξ on a mass basis, is found:

$$\xi = \frac{\dot{Q}_{comb}}{u_{comb}} = \frac{mc_v\frac{dT}{dt} + p\frac{dV}{dt} + \dot{Q}_{loss}}{u_{comb}} \tag{2.9}$$

The value of u_{comb} needs to be evaluated at the existing temperature.

2.3.3. Characterising combustion

The process of combustion in a diesel engine is extremely complex. In the diesel engine combustion process four separate combustion phases can be identified [28]:

1. Ignition delay: the period between the start of fuel injection and the start of combustion, expressed in units of time (ms) or crank angle degrees.
2. Premixed (rapid) combustion phase: this phase is characterised by a high heat-release rate caused by rapid burning of the fuel that has mixed with air during the ignition delay period.
3. Mixing-controlled combustion phase: the burning rate in this phase is controlled primarily by the mixing process of the fuel vapor with air.
4. Late combustion phase: a small, still unburned, fraction of the fuel continues to burn at a lower rate during the expansion stroke.

The progression of combustion follows from integration of the combustion reaction rate, Eq.2.9. For convenience, the resulting quantity may be made non-dimensional and expressed as a percentage of the total mass of fuel burnt. The *normalised reaction coordinate* or *normalised combustion progression* X is then obtained:

$$X = \int \frac{\xi}{m_{f,0}} dt \tag{2.10}$$

where $m_{f,0}$ is the total mass of fuel burnt. The normalised reaction coordinate equals unity by definition at the end of the combustion. The progression of combustion may also be expressed as the crank angle(s) at which a fraction of the total mass of fuel has been burnt, e.g. 10%, 50% or 90%. The values also follow from integration of Eq.2.9. This parameter is convenient to use since it is independent of engine rpm.

Other useful parameters related to combustion are the start and end of combustion, expressed in crank angle degrees before or after TDC, and the combustion duration, usually expressed in crank angle degrees. The question is what point of the pressure trace should be identified as the start of combustion (SOC). At SOC, there is a sharp increase of the cylinder pressure. Several methods exist to determine the location of the SOC: the pressure recovery point method, the location of 50% of the peak pressure-rise rate, the zero-crossing point of the peak-pressure rise slope, the peaks of second-order pressure derivative traces, and NAHRR change rate traces. In a comparative study [79], it was found that the pressure recovery point produces the most consistent result. Due to the evaporative cooling upon the fuel injection, the cylinder pressure decreases below the motored pressure trace. The pressure is recovered as heat is released from the high-temperature reaction.

If cylinder pressure data are available, the state of the cylinder contents for the closed-cylinder process can be determined at each incremental crank angle step, by using the mass and energy conservation equations, along with the gas state equation. A diesel engine combustion model that assumes a single homogeneous gas in the cylinder and uses crank-angle based data, is called a zero-dimensional crank-angle model [21]. Combustion may be modeled by using phenomenological models of either one zone, which are a compromise of process representation and accuracy, or multiple zones, which offer more detailed representation of the combustion process and better prediction of exhaust gas emissions [2]. An example of the latter is the two-zone diesel engine combustion model developed by Linden [41] in order to predict the formation of nitric oxide (NO). An example of the former is the zero-dimensional crank-angle model developed by Ding [16]. Ding's combustion model approximates the *normalised reaction coordinate* by means of Wiebe functions[1], assuming ideal gas behaviour. Wiebe functions are widely used in engine research as a single-, double-, or multiple-function combustion model for investigating a wide variety of engine processes, including prediction of engine performance and emission formation [23]. The multiple Wiebe function is expressed as

$$\sum_{k=1}^{n} b_k \left(1 - e^{-a\tau^{m_k+1}}\right) \tag{2.11}$$

where τ represents the dimensionless time. Ding [16] applied a nonlinear least squares fitting method in order to determine the parameters a, b and m for different orders k of the Wiebe function.

[1]This function is named after the Russian engineer and scientist Ivan Wiebe (also spelled as Vibe or Vybe).

A zero-dimensional crank-angle model may be combined with a mean-value engine model to simulate engine operation and predict engine performance parameters. This approach allows calculation of in-cylinder parameters that would not be available in case of a pure mean-value approach. Mean-value engine models average engine performance over the whole operating cycle and are based on the assumption that engine processes can be approximated as a continuous flow through the engine [2].

2.4. Fault detection and diagnosis

Engine failure can seriously affect ship's operation and even endanger personnel present in the engine room. Engine reliability, therefore, is of paramount importance. Incipient faults have to be addressed before they lead to engine failure. This section first discusses fault detection and diagnosis (FDD) methods commonly applied in order to enhance diesel engine reliability. Then it zooms in on engine subsystems and components with the aim of identifying healthy versus unhealthy engine behaviour.

2.4.1. FDD methods for diesel engines

As stated in the Introduction, FDD methods are commonly employed to improve diesel engine reliability. In a comprehensive study into FDD methods specifically tailored for marine diesel engines, Lv et al. identified four categories of FDD methodologies [43]:

1. model based;
2. data driven;
3. knowledge based;
4. hybrid (i.e. a combination of the other three)

These categories are discussed next.

Model-based methods include mathematical models that describe the physical and thermodynamical processes taking place in the diesel engine. These methods require that the user have a certain level of knowledge and understanding of the underlying physical principles of the engine. An example is the marine diesel engine failure simulator by Pagan Rubio et al. [54]. In order to model engine components like the air filter, compressor, air cooler, manifold, cylinders, turbine and ducts, the researchers performed numerous test-bench measurements on a high-speed diesel engine at different loads and constant rpm (generator operation), measuring a vast amount of parameters including cylinder pressure and exhaust-gas temperatures. The developed model is able to reproduce the effect of a number of typical failures. Hence, it is possible to recognise the symptoms of a failure before this failure endangers the correct engine behaviour. The simulator has proven to be to able to identify failure symptoms of a diesel engine and build a reliable failure database for diagnostic purposes.

Another example of a model-based method is the thermoeconomic fault diagnosis method by Xu et al. [77], based on the second law of thermodynamics. This method analyses the exergy flow of each engine component with respect to its surroundings. Increased exergy loss is an indicator of component degradation. Due to the functional coupling between the engine's components, this method may not be able to accurately locate the fault, but the result may narrow the search for a faulty component.

In contrast, domain knowledge is unimportant in the case of **data-driven strategies**; these rely mainly on the quality of historical engine data. Feeding operational data to the data-driven model allows the model to identify normal conditions so that any other conditions may be considered abnormal and diagnosed as faults. However, in order to identify and classify specific faults, data on faults is required. Since the amount of studies on fault-prognosis methodologies is limited, the lack of fault data may prove to be an obstacle [74].

Examples of data-driven FDD methods are machine-learning algorithms like artificial neural networks (ANN). Using an ANN, Karatug et al. have developed an engine performance model and proposed a fault-diagnostic approach based on comparing the real and estimated values of engine parameters [36]. First, the measured engine parameters are normalised. Then, the correlation between the normalised variables is determined. Evaluation of these variables allows for diagnosing a combustion-related fault with a decision-making system. The developed fault-decision system applies to three different fault scenarios: anomalous injection timing, piston ring failure and clogged injection nozzle.

According to the authors, minor and major faults can be prevented by the developed fault-diagnostic approach.

In another research project, a data-driven FDD-method has been developed to isolate the damaged injector of an internal combustion engine [51]. The method is based on statistical analysis of the fuel-rail pressure in the time domain as well as an FFT (fast Fourier transform) frequency analysis of the same signal. Using an arrangement of three ANN's, the method extracts the relevant features of the fuel-pressure signal from the injection rail, even when the engine's fuel-pressure regulator compensates the pressure variation caused by a faulty injector. As such, the system is capable of accurately detecting and isolating a damaged injector.

Knowledge-based FDD methods rely on the availability of expert domain knowledge and/or a set of rules to diagnose faults [43]. The systematic approach enables the determination of fault causes and corresponding solutions. In a study performed by Kang et al., a hierarchical level FDD method is proposed, combining domain knowledge of dual-fuel engines with advanced data analysis techniques [35]. The hierarchical levels are 1. the entire engine, 2. subsystems, and 3. individual components or sensors. The method is intended to detect and diagnose abnormal engine conditions based on engine performance curves, using dynamic thresholds to account for varying loads. The researchers argue that it is preferable to use dynamic thresholds rather than OEM limits in order to detect engine abnormalities in an early stage.

Hybrid models combine aspects of different categories of methods. A recent contribution in this field is the introduction of an expert system for the diagnosis of marine diesel engines introduced by Gharib et al. [22]. They developed an expert diagnosis system for marine diesel engines enabling the user to assess abnormal operation and increase the reliability and efficiency of marine diesel engines. Another example of a hybrid model is the framework described by Coraddu et al. [12], which combines physical models with data-driven models in order to determine the dynamic state of a four-stroke diesel engine. For the in-cylinder process a two-zone zero-dimensional combustion model was used. The modelling approach results in accurate, reliable and computationally efficient models.

2.4.2. Engine faults and their effect on cylinder pressure

In order to distinguish healthy from faulty engine behaviour, one should look at the difference between normal (healthy) and actual engine parameters. Deviations from normal behaviour could be indicative of an incipient fault in any of the diesel engine subsystems. Obviously, it is necessary to identify and quantify those engine parameters that indicate healthy versus unhealthy/faulty engine behaviour. It is helpful at this stage to give a formal definition of the term *fault*. One may define a fault as an unpermitted deviation of at least one characteristic property or parameter of the system from the acceptable, usual or standard conditions [17]. The deviation may be quantified either as an absolute value, e.g. the difference between the observed and the reference value of some parameter, or as a relative value, i.e. a percentage of the reference value. A fault may be assumed to occur when the deviating value exceeds a certain limit for a given parameter. The permissible deviation will differ from parameter to parameter and from engine to engine.

According to a study on engine health assessment by applying a digital twin, the overall engine health status and the health of individual cylinders may be quantified over its entire operating envelope by inspecting the following engine parameters [71]:

- brake specific fuel consumption;
- peak cylinder pressure;
- IMEP;
- cylinder exhaust gas temperature.

The study suggests that the exhaust gas temperatures of underperforming cylinders are likely to decrease significantly with respect to those of healthy cylinders. A deviating exhaust gas temperature provides a first indication of the cylinder condition but cannot by itself explain the actual cause of the anomalies. A significant reduction in the IMEP or peak pressure of the underperforming cylinder may also be observed. Underperforming cylinders may also be identified by applying a heat-release analysis based on cylinder pressure measurement [39].

The failure source and the failure manifestation are not a simple one-to-one mapping relationship. On the one hand, one fault source may correspond to multiple fault manifestations; on the other hand, multiple fault sources may correspond to one fault manifestation. Or multiple failure sources may correspond to the cross-coupling phenomenon of multiple failure manifestations [77].

Among the faults that may occur in a diesel engine, there are more than a few that will affect cylinder pressures. Hence, monitoring of the cylinder pressures may reveal these faults. Faults that can affect cylinder pressures, may be divided over the subsystems where they occur. The following is a list of diesel engine subsystems, in which any of the below mentioned faults might occur, which are likely to affect cylinder pressures [31, 32]:

1. **Inlet and exhaust system:** Possible issues are excessive pressure drop in the air filter, leaks in the intake air manifold or exhaust manifold, and high pressure losses in the exhaust ducting.
2. **Cylinders / compression loss:** Typical faults include intake valve seat failure, excessive blowby past piston rings, and improper valve clearance.
3. **Turbocharger:** Faults may involve malfunction of the air compressor or the exhaust gas turbine, both of which can impair charge air delivery.
4. **Air cooler:** Common issues include reduced cooling efficiency and excessive pressure drop across the cooler, both of which affect intake air density and cylinder filling.
5. **Increased friction losses:** This may result from factors such as insufficient lubrication, main bearing wear or insufficient cooling. While not directly linked to individual cylinder faults, increased mechanical friction raises the indicated mean effective pressure (IMEP) required to maintain constant engine output. These effects tend to impact all cylinders uniformly rather than a single cylinder.

In the following paragraphs, the above-mentioned engine subsystems and their possible faults and effects with regard to cylinder pressures are explored further. The equations that can be used to describe and detect the faulty behaviour, are also treated concisely. It is worth noting that different faults can have the same effect, in which case it is necessary to identify more symptoms. In many cases, it is possible to find a unique combination of symptoms that allows unequivocal identification of a specific failure [54]. Additional sensor information to the cylinder pressure data will then be required.

Fuel injection system

Many engine faults, malfunctions and failures have their origin in the high-pressure fuel-injection pump and fuel injectors. Causes may be incorrect injection timing, injector blockage or fuel-injection equipment being out of calibration, or, most commonly, leakage in the delivery valve/nozzle valve [34]. It is of considerable interest, therefore, to detect and diagnose these faults before they lead to failures of the combustion process.

The following method may be used to that end. The difference in pressure between the combustion pressure and the motored pressure can be used for engine health supervision as well as injection control [40]. The motored pressure is assumed to be equal to the measured cylinder pressure and symmetric around TDC until the start of injection. Hence, for crank angles $\theta < \theta_{inj}$:

$$p_{motored}(-\theta) = p_{measured}(\theta) \tag{2.12}$$

The intermediate section, where $|\theta| < |\theta_{inj}|$, is filled by a curved segment according to: $p_{motored} = a|\theta|^{1.5} + b$. From inspection of the pressure difference, the burnt fuel mass and injection angle can be reconstructed. Then, the mass fraction burnt can be approximated by

$$MFB(\theta) \approx \frac{p_{measured}(\theta)}{p_{motored}(\theta)} - 1 \tag{2.13}$$

By comparison with reference values, the proper functioning of the fuel injection system can be monitored, and possible injection faults may be detected.

Inlet and exhaust system

Intake and exhaust systems can have a considerable influence on engine power and torque. The exhaust back pressure in diesel engines with an exhaust-gas driven turbocharger should not exceed the level prescribed by the engine manufacturer. Thus, it is particularly important to avoid high flow resistance in the exhaust system. The pressure drop across the air-intake filter and air cooler, which is proportional to the square of the volumetric intake flow, must also be limited [48].

The air filter must filter dust fractions out of the intake air. A clogged air filter has increased flow resistance; this effect can be described by introducing a constant K that multiplies the nominal (quadratic) flow resistance during normal conditions:

$$\Delta p = K a_{f,nom} \dot{V}^2 \tag{2.14}$$

Here, Δp is the pressure drop across the air filter, $a_{f,nom}$ the nominal proportionality constant, and $\dot{V}$ is the volumetric flow rate of the intake air.

A similar equation applies to the pressure drop of the intake air across the air cooler. In that case, the constant K accounts for the obstruction of the air through the air cooler by e.g. dust deposits. The effect of both failures is that, due to the increased flow resistance, the intake-air manifold pressure will decrease. The same effect can be observed in the case of a leaking air manifold. Exhaust manifold leakage or excessive pressure drop in exhaust ducts also lead to a decrease in intake manifold pressure [54].

Compression loss

Loss of compression may be the result of cracks in the cylinder head, a blown head gasket, a leaking intake or exhaust valve, excessive blowby past the piston rings or cylinder liner due to wear [14]. Obviously, these faults lead to lower peak pressures of the faulty cylinder. Close inspection of the pressure-versus-crank angle trace during the compression phase could reveal that this is due to the loss of compression. The pressure loss due to leakage is determined by the mass flow of gas (or blowby rate) out of the cylinder, which depends on the pressures inside and outside the cylinder. The following generic equation may be used to calculate the mass flow per unit area through an orifice with area A [11]:

$$\frac{\dot{m}}{A} = \frac{p_{in}}{\sqrt{RT}} \Psi \tag{2.15}$$

The value of the dimensionless flow function Ψ is determined by the ratio of the pressures inside and outside of the cylinder (in the crankcase), p_{in}/p_{out}. Assuming isentropic compressible flow, Ψ is a complicated function of the pressure ratio:

$$\Psi = \sqrt{\frac{2\gamma}{\gamma - 1}} \sqrt{\left(\frac{p_{out}}{p_{in}}\right)^{\frac{2}{\gamma}} - \left(\frac{p_{out}}{p_{in}}\right)^{\frac{\gamma+1}{\gamma}}} \tag{2.16}$$

The above formula is valid for non-choking flow. Choking occurs above the critical pressure ratio when the velocity of sound is reached somewhere in the flow path [65]:

$$\frac{p_{in}}{p_{out}} > \left(\frac{\gamma + 1}{2}\right)^{\frac{\gamma}{\gamma-1}} \tag{2.17}$$

In the case of choking Ψ is limited to:

$$\Psi = \sqrt{\gamma \left(\frac{2}{\gamma + 1}\right)^{\frac{\gamma+1}{\gamma-1}}} \tag{2.18}$$

For common values of γ ranging from 1.33 to 1.4, choking occurs when $p_{in}/p_{out} >$1.85 to 1.89. Given this relatively small pressure ratio, choking is expected to occur during most of the compression stage and power stroke. Especially in the case of a turbocharged engine, the ratio of the charge air pressure to the (essentially atmospheric) crankcase pressure may be well above this value during most of the operating conditions. The value of Ψ then is independent on the pressure ratio and equals 0.67 to 0.68. In order to be able to calculate the mass flow out of the cylinder, the area of the orifice needs to be known, which may likely not be the case. However, if the cylinder pressure is known as function of the cylinder volume or crank angle, a value of the orifice's area may be chosen so that the that the calculated pressure agrees best with the measurements.

Turbocharger

The turbocharger directly affects cylinder pressures: the compressor delivers the proper charge pressure of the combustion air and the exhaust-gas driven turbine supplies the required shaft power to drive the compressor. Dust particles may cause abrasive wear and deposits of fine particulate matter can form on the compressor walls in turbocharged engines, reducing compressor efficiency and air mass flow rate [54]. Injecting a cleaning fluid routinely during operation is an effective measure to clean compressor surfaces of deposited fine particulate matter.

The correct working of the turbocharger may be verified by comparing the actual operating point with the compressor and turbine charts. A compressor chart typically shows the pressure ratio and the isentropic compressor efficiency as a function of the (non-dimensional) mass flow for different compressor speeds. The turbine chart typically shows the non-dimensional mass flow and the isentropic turbine efficiency as function of the turbine pressure ratio for different turbine speeds [65].

The characteristic charts for the compressor and the turbine may likely be unavailable. To overcome this problem, Kouremenos and Hountalas used the method of *operation similarity* to reproduce the charts from shop test data [38]. The method requires the following data in order to be able to construct the turbine and compressor charts:

1. pressure before and after the compressor;
2. pressure before and after the turbine;
3. air temperature before and after the compressor;
4. exhaust gas temperature before and after the turbine;
5. rotational speed of the turbocharger.

Not all of the above-mentioned parameters may be available, in which case it will be necessary to estimate the values.

The isentropic efficiency, mentioned previously, is a useful performance indicator of the turbine and the compressor: it is a measure of how efficient the compression or expansion stage is executed in comparison with the idealised adiabatic and internally reversible (isentropic) process. In the case of the compressor, the isentropic efficiency is defined as:

$$\eta_c = \frac{\text{isentropic compressor work}}{\text{actual compressor work}} = \frac{h_{2s} - h_1}{h_2 - h_1} \tag{2.19}$$

The isentropic turbine efficiency is defined as:

$$\eta_t = \frac{\text{actual turbine work}}{\text{isentropic turbine work}} = \frac{h_1 - h_2}{h_1 - h_{2s}} \tag{2.20}$$

In the above equations, h_1 is the specific enthalpy at entrance state, h_2 the specific enthalpy at exit state and h_{2s} the specific enthalpy at exit state for the isentropic process. In both equations, the exit pressures are taken the same in the actual and the isentropic case. This parameter can be found using measured data of inlet and outlet temperature and pressure of both components.

An alternative method for estimating the compressor performance chart is the method by Casey and Robinson [10]. The objective of this method is to calculate the values of the polytropic efficiency and the work coefficient λ for specific values of the flow coefficient ϕ and tip-speed Mach number M; the dimensionless parameters λ, ϕ and M are defined as:

- $\lambda = (h_2 - h_1)/{u_2}^2$, where u_2 is the circumferential speed of the impeller blade tip;
- $\phi = \dot{V}/(u_2 {D_2}^2)$, where D_2 is the impeller tip diameter;
- $M = u_2/a_1$, where a_1 is the inlet speed of sound.

The method allows the performance chart of a centrifugal compressor stage to be obtained from limited data without knowledge of the compressor stage geometry. The equations provide a fully parameterised system of algebraic functions for the performance chart.

2.5. Conclusion

This section concludes the literature review. First, the most important findings are presented. Second, a research gap is discussed. Based on the findings of this chapter the most important conclusions are:

1. **System understanding and implementation**
   It may be challenging to equip an existing engine on board of a ship with permanent instrumentation for continuous cylinder pressure measurement. Ideally, the pressure transducers are flush mounted, but this is likely not possible. Instead, they will have to be mounted on the connection in the cylinder head to the indicator channel, giving rise to pressure fluctuations that are picked up by the sensor. This also has a beneficial effect, however, namely it limits the potential effect of thermal shock.
   Another critical aspect is the synchronisation between the measured crank angle and cylinder pressure. This can be realised by installing a sensor on the engine's flywheel that 'counts' the teeth, together with a sensor for reference. Both the pressure and crank angle signal have to be in phase in order for the data generated to be useful. In order to determine the *absolute* cylinder pressure, an additional pressure sensor may be required for reference. In addition, sufficient data points have to be available, at least one per crank angle degree, but preferably more. Provided that these requirements are met, the system should be able to provide useful data.

2. **Preprocessing cylinder pressure data**
   In order to be able to extract useful information from cylinder pressure measurement, it is a prerequisite to have sufficiently accurate data. Three conditions to achieve this were identified:

   (a) Correct phasing of cylinder pressure with crank angle
   One of the (dynamic) methods described in 2.2.1 should be applied to determine the TDC position, taking into account the thermodynamic loss angle. Thus, it is verified that the synchronisation error between crank angle and cylinder pressure is sufficiently small; literature suggests that 0.2° is the maximum allowable fault. A dynamic TDC determination method appears more suitable than a static one, since the latter involves elaborate measurement on the engine on board, which would be impractical, whereas the former requires interpretation of measured values.

   (b) Correct pressure referencing
   The cylinder pressure must be referenced (pegged) to a known (absolute) pressure. Using the pressure sensor in the engine's intake manifold, if present, would be the obvious choice. Then, the pressure at inlet bottom dead center is set equal to the intake manifold pressure each cycle. Alternatively, one of many numerical algorithms could be applied to determine the pressure offset.

   (c) Smoothing of the pressure signal
   In order to mitigate the adverse effects of inevitable pressure fluctuations and noise during measurement, the pressure trace must be smoothed. Averaging a number of cycles eliminates random noise, but systematic errors will persist. Further smoothing will have to be done by using filtering or curve-fitting techniques, to which purpose several methods are available.

3. **Engine performance and combustion analysis**
   A number of parameters relating to engine (or cylinder) performance and combustion, which can be determined from cylinder pressure data, have been identified. Parameters like IMEP, heat-release rate and (normalised) combustion progression can readily be calculated by analysing the pressure-volume relation, using a one-zone combustion model, together with a model for the heat 'loss'. However, determining the heat flow from the cylinder contents is not straightforward. While there are proven correlations for calculating the heat-transfer coefficient, there is not a general method to determine the cylinder wall temperature. Thus, calculation of the heat flow is accompanied with large uncertainty. This potentially introduces a large error leading to inaccurate calculation of the heat-release rate and derived parameters.

4. **Fault detection and diagnosis**
   Four categories of FDD methods exist that are suitable for diesel engines. Of these, only purely

data-driven methods do not require the user to have domain knowledge. However, using cylinder-pressure data 'without' knowledge does not appear feasible to the author. A (hybrid) combination of a model-based, knowledge-based and data-driven method would appear to be more suitable. A thermodynamic model is required to analyse combustion and a knowledge-based and/or data-driven method in order to detect and assess anomalies.

Faults on component level may be detected by comparing actual engine parameters with parameters taken from the same or a similar engine, like measurements taken at the test bench in the engine factory. Incipient faults that arise during operation may thus be detected; examples are faults in the turbocharger or the fuel injection system, a leakage in the intake or exhaust manifold, or gas leakage from a cylinder through the piston springs or an intake or exhaust valve. Acceptable values of the deviations from the benchmark values will have to be established; there may be some arbitrariness here, if the engine manufacturer does not provide these values.

In addition, it is important to note that different faults may have the same effect on cylinder pressures. In order to allow unequivocal identification of a particular fault, it may be necessary to identify a unique set of symptoms, not only from cylinder pressure data but from other operational engine data as well. It should also be noted that the cylinder pressure may not be the parameter best suited to indicate a potential fault. In the case of the turbocharger it would be more appropriate to analyse rpm and air intake manifold pressure, rather than cylinder pressure.

Research gap

Studies about cylinder pressure measurement mainly concern lab engines, since diesel engines in the field are generally not equipped with such a system. Although there is ample literature about research on the topic of FDD methods for diesel engines, only a few of these studies use cylinder pressure data, as these data are not commonly available. Instead, in most cases readily available engine sensor data are analysed. Therefore, a largely unexplored field is cylinder pressure measurement in support of FDD-methods of marine diesel engines. This may be regarded as a research gap.

Notably, a few studies have considered cylinder pressure data for diagnostic purposes. One such study [53], however, overlooked the essential step of preprocessing, incorrectly assuming that the raw pressure data were already accurate with respect to crank angle alignment and pressure offset. Another study uses cylinder-pressure data to develop a *digital twin* for engine health assessment [71]. Interestingly, they applied a numerical algorithm to determine the pressure offset and the TDC position simultaneously. They also acknowledged that the resulting heat-release curves were inaccurate due to an unspecified error. Payri et al. [56] present an in-depth discussion on preprocessing cylinder pressure signals, including filtering. However, their work is limited to preprocessing alone and does not extend to engine condition monitoring or diagnostic applications.

This suggests that a comprehensive methodology for cylinder pressure analysis, including both data preprocessing and diagnostic interpretation, could make a valuable contribution to engine condition monitoring and fault detection. This thesis aims to address this need by investigating the potential of cylinder pressure measurement to assess engine performance and combustion characteristics, and to enable fault detection and diagnosis in marine diesel engines.

3

Research methodology and measurement system

The three-step Plan of approach of this thesis was outlined in Section 1.3. The first step—the literature review—was presented in the preceding chapter. It identified a key research gap: the limited application of cylinder pressure measurement data for diagnostic purposes in marine diesel engines. This thesis aims to contribute to closing that gap, as its central objective is precisely to explore the diagnostic potential of such data.

This chapter outlines the research methodology used throughout the remainder of this thesis. While the second explicitly stated step in the Plan of approach is the preprocessing of cylinder pressure data, this assumes that a selection of suitable measurement data is already available. However, the prior and implicit step—collecting and selecting the appropriate cylinder pressure datasets—is, while not academically central, essential to the practical execution and reliability of this research.

Accordingly, this chapter begins by presenting the overall research methodology, including data collection and selection (Section 3.1). It then describes the cylinder pressure measurement system installed on HNLMS Groningen in detail (Section 3.2). Lastly, it provides an overview of the Ocean-going Patrol Vessel's main engines (Section 3.3), as certain engine-specific details are crucial for understanding the subsequent analysis and results.

3.1. Research method

Although not strictly part of the research scope, the installation and commissioning of the cylinder pressure measurement system on HNLMS Groningen was largely carried out by the author. As such, it may be considered the zeroth step of this research. The next step involved collecting operational measurement data. Since the commissioning of the system, it has recorded a substantial amount of operational data over a period exceeding two years, including more than ten months of sailing. Several hundred cylinder pressure measurements—each comprising a corresponding dataset—have been collected. Consequently, a selection must be made for detailed analysis.

In line with the identified research gap and the overarching research question, this study primarily focuses on detecting anomalies in engine behaviour. Ideally, such analysis requires a known instance of a fault or failure occurring during system operation. One such case occurred in August 2024, when the crew of HNLMS Groningen replaced the fuel-injection pump of the starboard main engine due to a deviating exhaust gas temperature (see Figure 3.5).

This case is particularly relevant for two reasons. First, it allows for a direct comparison of cylinder pressure data before and after the component replacement. Second, the fuel-injection pump is also the subject of a parallel research effort—the *frontrunner* project—which investigates its operational lifespan, replacing the pump only after failure. Both the frontrunner project and the specific case of the replaced pump are discussed in greater detail in Section 3.3. To evaluate potential degradation of the component over time, and to assess the impact of its replacement, a baseline is required. For this purpose, data from March 2023 are used. At that time, the engines had just completed a major overhaul at the 16,000 running hours mark, the scope of which is also outlined in Section 3.3.

Additionally, during the same period, HNLMS Groningen's hull was cleaned and the vessel became the only ship in its class to be fitted with a Hull Vane—a fixed, wing-like spoiler mounted below the stern. The Hull Vane generates hydrodynamic lift, thereby reducing the ship's resistance through the water. It is intended to lower fuel consumption and emissions, while improving propulsion efficiency. High-speed testing before and after installation on HNLMS Groningen confirmed its positive effect on performance [63], with a 10% reduction in fuel consumption across the full operational profile, peaking at a 16% reduction at 17.5 knots.

Given these modifications, it would not be appropriate to compare data collected before March 2023 with data collected afterwards. The ship lacked the Hull Vane and likely had a more fouled hull, both of which affect the required engine power at a given speed. Moreover, the engine had not yet been overhauled. Therefore, only data collected from March 2023 onward are considered valid for comparison under consistent operating conditions.

For this research, datasets were selected based on identical propulsion control setpoints to ensure comparability. The focus is on analysing cylinder pressure data from the following three periods, all under similar operational conditions:

- **March 2023**: Immediately after completion of the 16,000-hour engine overhaul and the installation of the Hull Vane. The total running hours of starboard main engine
- **August 2024 (pre-replacement)**: Prior to replacement of the fuel-injection pump and fuel injector in cylinder B2 of the starboard engine.
- **August 2024 (post-replacement)**: After replacement of these components.

The next steps, following the collection of raw measurement data from the occasions described above, are as follows:

1. Preprocess the raw data using the approach developed in Chapter 4. This includes accurate alignment of the TDC position, pegging to the correct reference pressure, and appropriate smoothing of the original pressure trace to enable subsequent analysis.
2. Analyse the preprocessed data according to the methodology described in Chapter 5, focusing on performance evaluation, combustion analysis, and fault detection and diagnosis.
3. Present and interpret the results of this analysis, as detailed in Chapter 6.

3.2. Cylinder pressure measurement system of HNLMS Groningen

This section describes the cylinder pressure measurement system installed on HNLMS Groningen. The system provides continuous monitoring of cylinder pressures during engine operation. It is connected to all cylinders of both main engines, enabling individual cylinder pressure measurements in real time. Figure 3.1 illustrates the main components of the system and their integration with the engine. The system relies on three primary input signals: cylinder pressure, crank angle, and a trigger pulse. Additional data—such as engine speed, cylinder exhaust gas temperature, intake manifold pressure, and turbocharger RPM—are supplied by the ship's Integrated Platform Management System (IPMS).

Each engine is equipped with twelve piezoelectric pressure sensors—one per cylinder—mounted via a 6 mm small-bore indicating channel in the cylinder head. The sensors are not directly mounted on the indicating channel but are mounted in an adapter that is screwed onto the cylinder head. These sensors convert the cylinder pressure into an electrical charge, which is subsequently transformed into a voltage signal by a charge amplifier. This analog signal is then digitised by an analog-to-digital (A/D) converter. The digitised pressure signal must still be referenced to a known pressure. In this case this is the intake manifold pressure. This step is further explained in Section 4.2.

Crank angle resolution is achieved using an optical encoder that detects the 360 teeth on the engine flywheel, providing pressure readings at every 0.5° of crankshaft rotation. A trigger bolt mounted on the flywheel passes a dedicated trigger sensor once per revolution, establishing a reference position for accurate crank angle alignment and data synchronisation. While the system continuously buffers pressure data in real time during engine operation, actual recording of this data is event-driven and occurs under one of the following conditions:

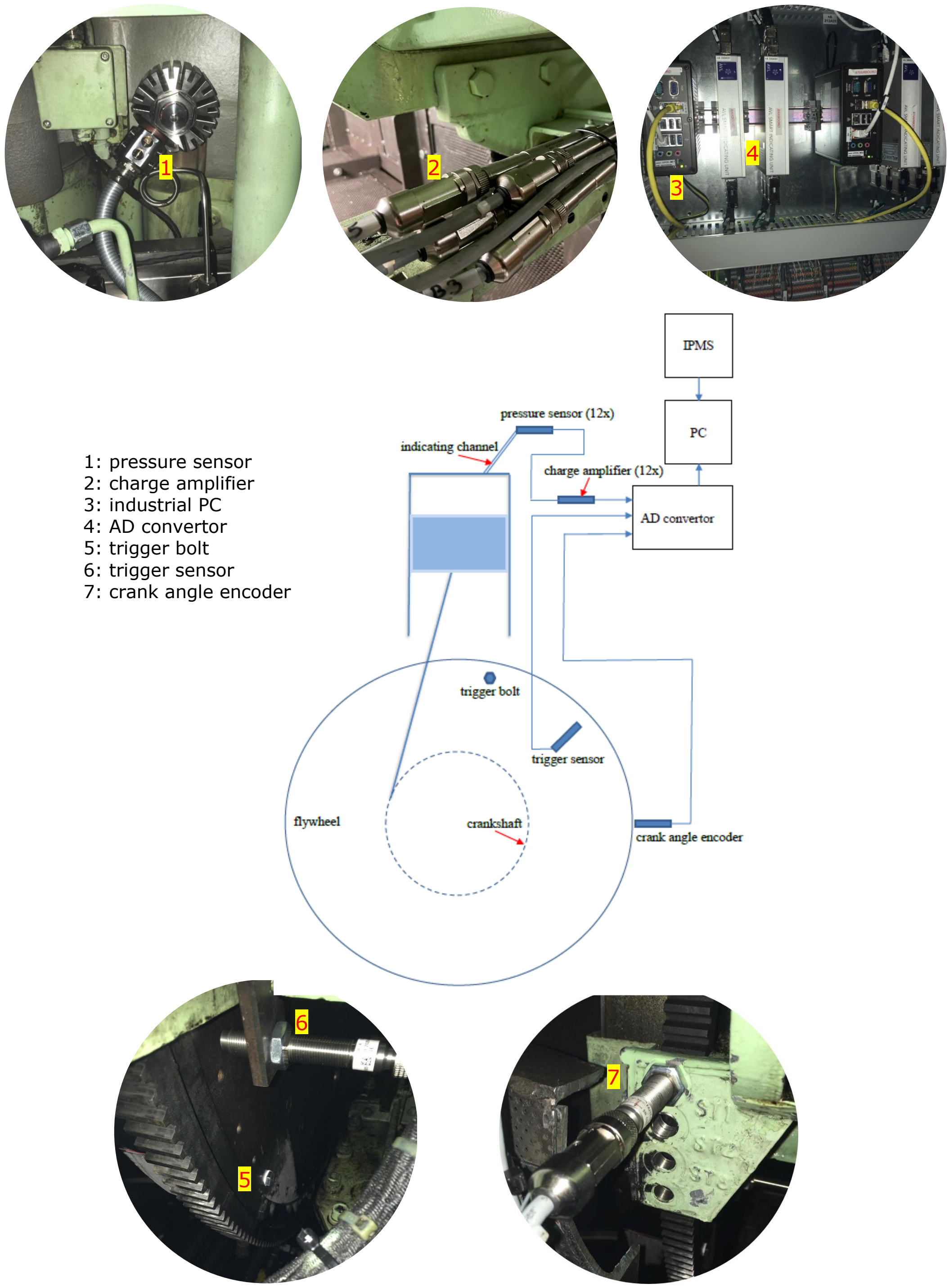

Figure 3.1: Conceptual sketch of the cylinder pressure measurement system of HNLMS Groningen showing the main components

1. Manual initiation by the operator from the ship's technical control room.
2. Automatic initiation at predefined time intervals configured by the operator.
3. Automatic initiation in the event of an engine shutdown, in which case the buffered data from the last 50 engine cycles is saved.

Figure 3.2 presents two typical plots that can be derived directly from cylinder pressure data. The first plot (Figure 3.2a) shows cylinder pressure as a function of crank angle for a selected cylinder and engine cycle. The crank angles corresponding to BDC and TDC are shown in the graph.[1] To generate this plot from the raw measurement data, two preprocessing steps are required: pressure referencing and synchronisation of the pressure signal with the crank angle. These preprocessing steps are discussed in detail in Chapter 4. The graph highlights the peak pressure, p_{max}, and its corresponding crank angle, denoted as apmax.

Figure 3.2b displays the corresponding indicator diagram, i.e., the pressure–volume diagram for the same cycle. The indicated work, W_{i}, is represented by the area enclosed by the curve, which can be computed by integrating the pressure–volume data.

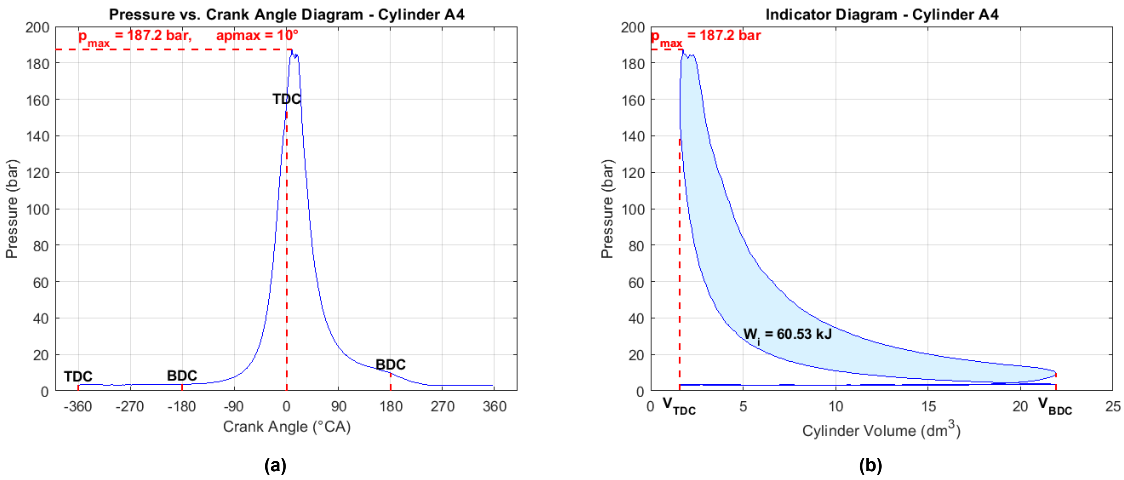

Figure 3.2: Pressure-versus-crank angle diagram and indicator diagram: (a) p-θ diagram, showing p_{max} and apmax, (b) indicator diagram, showing W_{i}.

3.3. Main engine characteristics

This section describes the main characteristics of the Holland-class OPV main engines. These engines are medium-speed, four-stroke, V12, turbocharged marine diesel engines. They were built in 2008 and 2009 and are certified in accordance with IMO Tier I NO_x emission regulations, which have been in effect since 2000. As such, they predate the more stringent Tier II requirements introduced in 2011. Table 3.1 lists the key engine specifications.[2]

The starboard engine rotates clockwise, while the port engine rotates counterclockwise. Figure 3.3 shows a cross-sectional view of the MAN 12V28/33D engine [46]. The left side of the figure illustrates the intake system: fresh combustion air enters the cylinder through two inlet valves, which are supplied by a common intake air manifold serving both cylinder banks. The inlet valves are actuated via a pushrod and rocker arm by the camshaft located to the left of the cylinder.

Also visible on the left side is the high-pressure fuel pump, driven by the same camshaft. Each cylinder is equipped with its own unit-type fuel pump, which includes a solenoid valve. This valve controls both the fuel injection quantity and timing, based on commands from the engine's electronic monitoring and control system. Figure 3.4 shows a detail of the fuel-injection pump and the fuel injector mounted in the cylinder head.

[1] By the convention adopted in this thesis, TDC corresponds with 0° CA. Hence, inlet BDC is at -180°.

[2] The exhaust valve opening (EVO) angle listed in Table 3.1 corresponds with the data provided by the OEM. However, analysis of the $p-\theta$ diagram suggests this value—75° before BDC—is likely incorrect. A more plausible value is approximately 30° before BDC.

The right side of Figure 3.3 depicts the exhaust system. Exhaust gases exit the cylinder through two exhaust valves, which are actuated—again via pushrod and rocker arm—by the camshaft on the right. Each cylinder bank has its own exhaust manifold, which routes the exhaust gases to the turbine of its dedicated turbocharger.

The engine's monitoring and control system plays a critical role in balancing cylinder-to-cylinder performance. In particular, it adjusts injection timing and duration via the solenoid valves in an effort to equalise exhaust-gas temperatures across all cylinders.

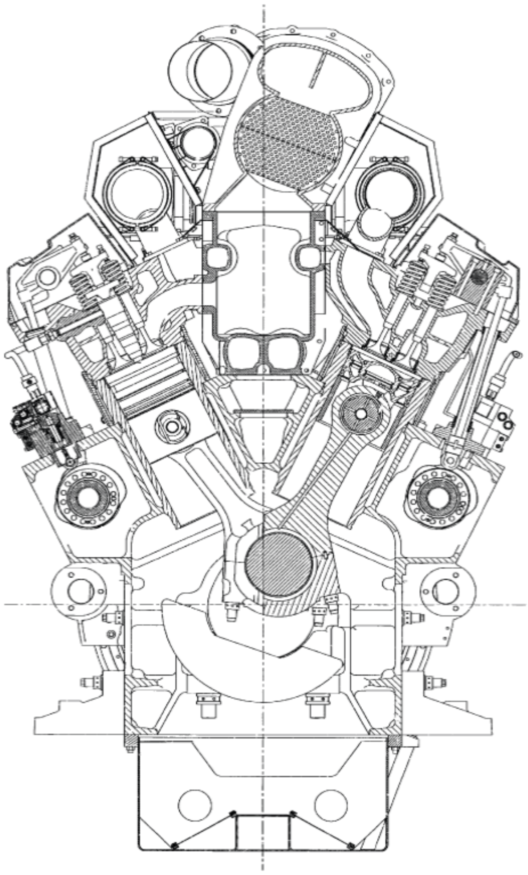

Figure 3.3: Cross section of engine 12V28/33D

Frontrunner project

As part of a research initiative by the Netherlands Defence Academy, the high-pressure fuel pumps of the main engines are no longer being replaced strictly according to the prescribed maintenance schedule. Instead, fuel pumps are only replaced upon failure. Under the original equipment manufacturer's (OEM) guidelines, these components are typically replaced every 8000 operating hours, which schedule is designed to prevent unexpected failures based on the manufacturer's experience. Although this interval is considered conservative and generally effective, the possibility of sudden fuel pump failure can never be fully excluded.

Since these fuel pumps typically exhibit no clear signs of degradation prior to failure, replacement is commonly based solely on accumulated running hours. In principle, individual cylinder exhaust gas temperatures might serve as failure indicators. However, this signal is rendered ineffective due to the presence of an exhaust-gas temperature balancer in the engine. This system equalises cylinder exhaust temperatures by adjusting the fuel injection duration per cylinder, with a maximum adjustment of $\pm 3^{\circ}$ crank angle. The exact start of injection (SOI), however, is proprietary information and is not disclosed by the OEM.

Given the high cost associated with preventive replacement of fuel pumps, this setting presents an ideal opportunity to test the frontrunner concept in practice. In this context, continuous cylinder pressure

Table 3.1: Holland class OPV's main engine characteristics [45][46]

Number of cylinders	12	
Number of revolutions per cycle	2	
Nominal engine power	5400	kW
Nominal engine speed	1000	rpm
Idling engine speed	400	rpm
Bore	280	mm
Stroke	330	mm
Displacement volume	20.32	dm^3
Connecting rod length	640.6	mm
V-angle	52°	
Geometric compression ratio	13.8	
Inlet valve opening (IVO)	69°	before TDC
Inlet valve closure (IVC)	30°	after BDC
Exhaust valve opening (EVO)	75°	before BDC
Exhaust valve closure (EVC)	48°	after TDC
Valve overlap	117°	
Nominal piston speed	11	m/s
Nominal brake mean effective pressure	26.6	bar
Nominal firing pressure	190	bar
Fuel injection pressure	450	bar
Direction of rotation starboard engine	CCW	
Direction of rotation port-side engine	CW	
Firing sequence starboard engine	A1-B4-A4-B2-A2-B6-A6-B3-A3-B5-A5-B1	
Firing sequence port-side engine	A1-B5-A5-B3-A3-B6-A6-B2-A2-B4-A4-B1	

measurement may serve as a valuable diagnostic tool, potentially revealing anomalies related to a faulty injector or a degraded fuel pump.

Case study: Fuel pump replacement

As mentioned in Section 3.1, the replacement of a high-pressure fuel pump on board HNLMS Groningen provides an interesting case study. During a deployment in 2024, the crew observed that the exhaust gas temperature of one cylinder (B2) on the starboard main engine began to deviate noticeably from that of the other cylinders.

As illustrated in Figure 3.5, the exhaust gas temperature of cylinder B2 increasingly diverged from the rest over time. Over the course of several days, the temperature difference continued to grow. Once the deviation exceeded 25 K, and with no indication of stabilisation, the crew decided to replace both the fuel-injection pump and the injector of cylinder B2. Technically, this replacement was not yet required; the engine manufacturer allows for temperature differences up to 100 K. However, the crew opted for a precautionary approach and installed a new fuel pump from the onboard stock.

This event presents a valuable opportunity to investigate whether anomalies in the cylinder pressure data of B2 were detectable, either at the time of the observed temperature deviation or even earlier, before the exhaust gas temperature began to diverge.

Major 16,000-hour overhaul

In 2023, the main engines of HNLMS Groningen underwent a scheduled major overhaul as part of the 16,000-hour maintenance cycle (16k service). During this overhaul, key engine components—including cylinder heads, cylinder liners, fuel injectors, pistons, connecting rods, connecting rod bearings, and main bearings—were replaced. The high-pressure fuel pumps were also removed and tested at the Royal Netherlands Navy's fuel pump testing facility. Following successful testing and approval, all pumps were reinstalled.

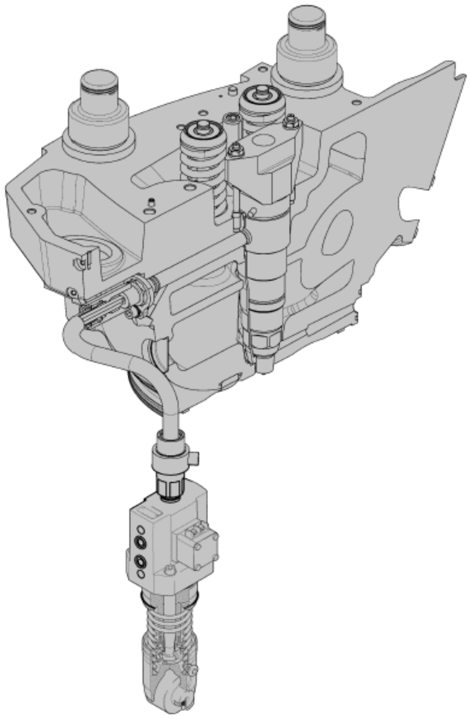

Figure 3.4: Fuel injection system of the V28/33D engine, showing the unit pump assembly. The system consists of a fuel-injection pump with integrated solenoid valve (bottom), a double-walled high-pressure fuel line, and the fuel injector.

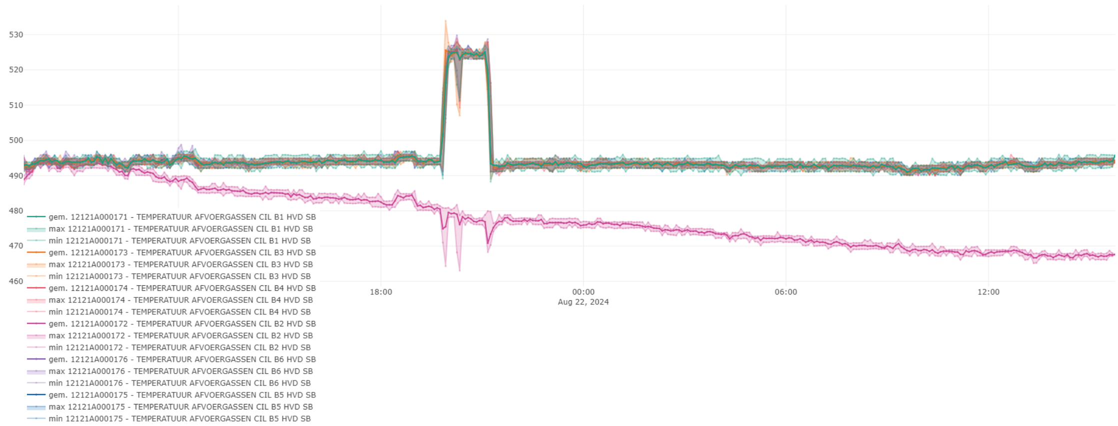

Figure 3.5: Exhaust gas temperatures of all cylinders on the starboard main engine, highlighting the rising deviation of cylinder B2 (pink line) over a period of, roughly, 24 hours.

This approach constitutes a deviation from the OEM's prescribed maintenance procedure, which would typically require full replacement. However, it was permitted under the conditions of the frontrunner project described earlier. Notably, the last complete replacement of all 24 high-pressure fuel pumps took place in November 2021, during the 8,000-hour maintenance interval.

4

Preprocessing cylinder pressure data

This chapter outlines the steps involved in preprocessing the raw data collected by the cylinder pressure measurement system of HNLMS Groningen. To extract meaningful information from the cylinder pressure data, it is essential to first process and manipulate the raw measurements. As detailed in Section 2.2, several preprocessing steps are required before the data can be analysed.

The initial step is to synchronise the pressure signal with the crank angle. This is explained in Section 4.1. This step is necessary because, in the measurement system setup aboard HNLMS Groningen, pressure and crank angle are not automatically aligned with sufficient accuracy, as discussed in Section 3.2. The next step involves referencing the measured pressure to a known value (Section 4.2). This process, commonly known as "pegging," is necessary because piezoelectric pressure sensors do not measure absolute pressure but instead respond to pressure changes. The third step is to smooth the pressure signal (Section 4.3). Smoothing is crucial for obtaining reliable results, particularly for parameters that require pressure differentiation, such as the heat-release rate. The detailed procedures for each of these steps are explained in the following sections.

4.1. Synchronising pressure and crank angle

The cylinder volume depends on the position of the piston and is therefore a function of the position of the crankshaft. In order to be able to construct an indicator diagram or calculate the *IMEP* accurately the cylinder pressure must be related to the cylinder volume and therefore the crank angle. In principle, it suffices to know the exact crank angle of one reference cylinder, since the crank angles of the other cylinders can be inferred from this reference. The top dead center (TDC) position is usually taken as the reference for the crankshaft position. Several parameters are very sensitive to an error in the TDC position. An error of only 1° will lead to incorrect indicator diagrams, as well as major errors in the calculation of performance indicator as indicated work, indicated power or *IMEP* (10%) and total heat release (25%) as well as combustion duration.

4.1.1. Tazerout method (T−s diagram)

In Section 2.2.1 several methods for determining the position of TDC have been compared. Of the compared methods, the method by Tazerout [69] appeared to be the most feasible. This method is based on the thermodynamic analysis of the temperature-entropy (T−s) diagram of a motoring (i.e. non-firing) engine during the compression and expansion stages. In the case of HNLMS Groningen, the cylinder pressure data from a stopping main engine are available, since these data are saved automatically every time the engine is stopped. This feature has been implemented to have the cylinder pressure data available in case of a failure that leads to an engine shutdown. The data from the last 50 cycles will then remain available for later analysis.

Since its publication, the Tazerout method has been proven to provide reliable results for a wide range of internal combustion engines. When the TDC position is well calibrated, the compression and expansion strokes under motoring conditions are symmetric with respect to the peak temperature in the T−s diagram. In the case of an error in the TDC position, a loop appears which has no physical significance. The Tazerout method involves shifting the crank angle until the loop in the T−s diagram appears or disappears. The value by which the crank angle is shifted is called the TDC shift.

In order to be able to construct the T−s diagram, the temperature and entropy values must be calculated using the pressure signal. The temperature can be found using the ideal-gas law, assuming the mass of the in-cylinder gas is constant:

$$T = \frac{pV}{mR} \tag{4.1}$$

where T is the absolute temperature, p the absolute pressure, V the cylinder volume, m the mass of the in-cylinder gases and R the specific gas constant. To calculate the mass, the initial temperature, i.e. the temperature at IVC is required. This temperature is not measured directly but we can reasonably assume that the air temperature in the cylinder at IVC will be slightly higher than that of the air in the intake manifold, which is measured. This is the result of heat transfer from hot engine parts, like the intake valves and the cylinder wall, to the relatively cold intake air. This ”heat pickup” will vary depending on whether the engine is cold or still hot from previous operation. Hence, to analyse the sensitivity of the Tazerout method to variation of the initial temperature, this parameter will be varied.

The entropy can be found starting from the Tds relation, known from thermodynamics: $Tds = dh - vdp$, where ds is the (infinitesimal) entropy change, dh the enthalpy change, v the specific volume and dp the pressure change. With the ideal-gas relations $pv = RT$ and $dh = c_p(T)dT$, where c_p is the specific heat at constant pressure, it follows that the entropy change is given by

$$ds = c_p(T)\frac{dT}{T} - R\frac{dp}{p} \tag{4.2}$$

Integration of Eq. 4.2 provides the entropy value with respect to a reference or initial value s_0 at initial pressure p_0:

$$s = s_0 + \int c_p(T)\frac{dT}{T} - R \ln \frac{p}{p_0} \tag{4.3}$$

Since the entropy is a function of the temperature, as expressed by Eq. 4.3, the shape of the T−s diagram might be sensitive to the method by which the intermediate temperatures are calculated. The assumption of ideal-gas behavior is not necessarily valid at high pressures. Therefore, in addition to using the ideal-gas law, the intermediate temperatures were also calculated using the more accurate Redlich-Kwong equation of state:

$$p = \frac{\bar{R}T}{\bar{v} - b} - \frac{a}{\bar{v}(\bar{v} + b)T^{1/2}} \tag{4.4}$$

The Redlich-Kwong equation is a two-constant equation of state that is frequently used in thermodynamics; $\bar{R}$ and $\bar{v}$ are the universal gas constant and the specific volume on a per mole basis, respectively. The two gas-specific constants (a and b) account for the non-ideal gas behavior. With a and b set to zero, the Redlich-Kwong equation reduces to the ideal gas law. Since the Redlich-Kwong equation is not explicit in temperature, calculating the temperature with this equation requires an iterative procedure. The details of this procedure are described in Appendix A.

4.1.2. Results

The pressure data used are extracted from a measurement taken with a stopping engine. In such an instant, the engine rpm and cylinder pressures decrease with each cycle. Therefore, the pressure data from a single cycle need to be analysed. In order to be able to analyse the pressure data, the signal is first smoothed by means of cubic-spline interpolation, see Section 4.3. Using the smoothed pressure trace and choosing a suitable initial temperature, the intermediate temperatures and the corresponding entropy values are calculated. Then, finally, the T−s diagram can be drawn.

This procedure is repeated for:

- all twelve cylinders, since the outcome may differ from cylinder to cylinder;
- initial temperatures varying from 300 K to 340 K, which are temperatures expected to occur during operation;

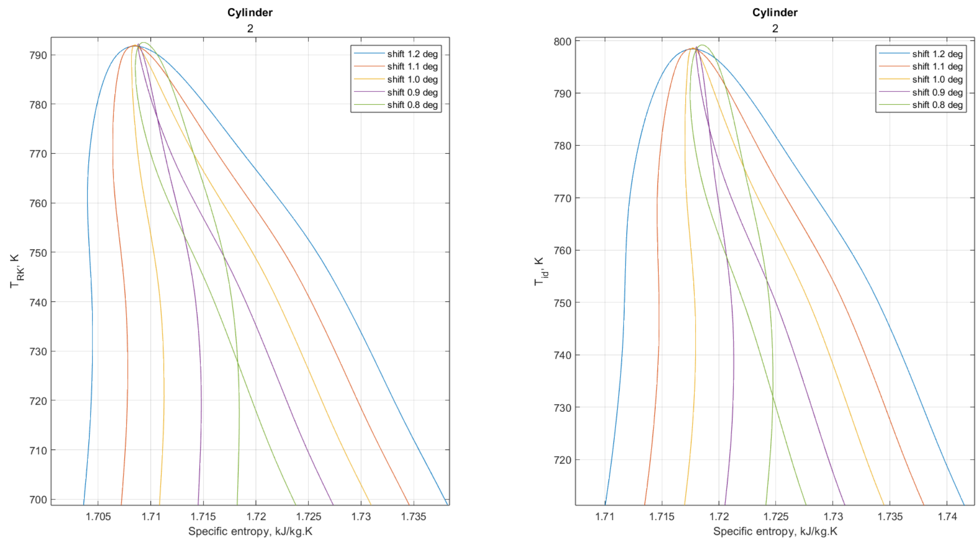

(a) (b)

Figure 4.1: T−s diagram showing a loop at the incorrect TDC shift, temperature calculated by (a) Redlich-Kwong equation and (b) ideal-gas law

- temperature and entropy values calculated by the Redlich-Kwong equation and the ideal-gas law.

Figure 4.1 shows the resulting T−s diagram for an arbitrary cylinder (cylinder 2 of the A-bank) and an initial temperature of 300 K. Figure 4.1a shows the resulting graph when using the Redlich-Kwong equation; Figure 4.1b shows the result when using the ideal gas law. Both graphs show a loop for a TDC shift of 0.8° (green line) and 0.9° (purple line), which disappears at 1.0° (yellow line). Although the values of both temperature and entropy differ slightly for both graphs, the TDC shift for which the loop disappears is the same for both methods. In addition, for the initial temperatures checked (300-340 K), the value does not affect the outcome.

Table 4.1: TDC shift per cylinder $(^{\circ})$, $\mu = 0.9$, $\sigma = 0.074$

cylinder	1	2	3	4	5	6
A-bank	0.9	1.0	0.9	0.9	0.8	0.8
B-bank	0.9	0.9	0.8	1.0	0.9	1.0
mean (μ)	0.90					
stdev (σ)	0.074					

There is, however, a (small) difference between the individual cylinders. Table 4.1 shows the TDC shifts for all cylinders. The mean value $\mu = 0.9°$. The values of all cylinders differ from the mean value by no more than 0.1°. The standard deviation $\sigma = 0.074°$.

Figure 4.2 shows the probability density function for the (discrete) TDC shift values of all cylinders. Also drawn is the probability density function of a normal distribution with the same mean and standard deviation. Assuming that the TDC shift is normally distributed around μ, the probability that all the TDC shift values are in the interval $[\mu - \sigma, \mu + \sigma]$ is 0.68, and in the interval $[\mu - 2\sigma, \mu + 2\sigma]$ is 0.95; these values are generally applicable to a normal distribution. Hence, we can say with 95% confidence that the actual TDC shift lies within the interval [0.75, 1.05].

4.2. Pressure referencing

This section describes the methods used in this thesis to convert the pressure change measured by the piezoelectric sensors to an absolute pressure. This is done by referencing (or *pegging*) the cylinder pressure to a known external pressure, or alternatively, by applying a numerical method to determine the correct pressure offset.

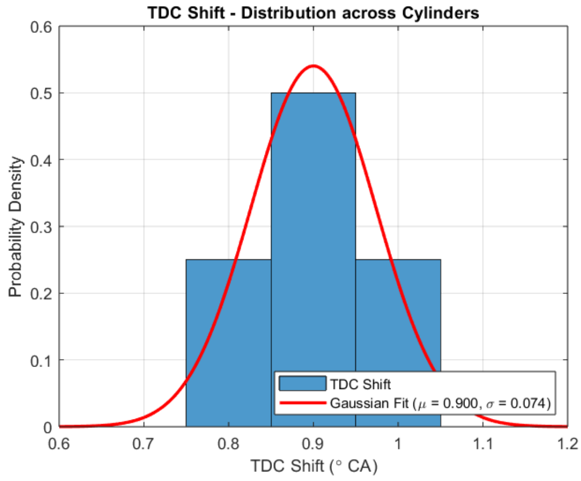

Figure 4.2: Probability density of TDC shift across cylinders, including the best-fit Gaussian curve based on sample mean and standard deviation.

4.2.1. Intake manifold pressure

In Section 2.2.2, several methods have been compared to reference the cylinder pressure to a known value. There, it was concluded that the most suitable method would be to equate the cylinder pressure at inlet bottom dead center (IBDC) with the (absolute) intake manifold pressure. This conclusion appears valid for a laboratory engine, but does not necessarily apply to an engine on board of a ship. Therefore, we now investigate whether the intake manifold pressure is suitable for our purpose. In fact, this pressure is measured and recorded in the case of HNLMS Groningen with an update rate of 1 Hz. A typical cylinder pressure measurement involves recording the pressure during 25 cycles (50 crankshaft revolutions), which takes 3 to 7.5 s, depending on the actual engine rpm.

During one measurement, the pressure at IBDC for all cycles is equated to the intake manifold pressure at the start of the measurement. This is done automatically by the cylinder pressure measurement system's data acquisition functionality. The intake manifold pressure is measured as gauge pressure, thus as pressure relative to the atmosphere. In order to convert this relative pressure to an absolute pressure, 1 bar, the assumed atmospheric pressure, is added to the relative value. The resulting pressure is the cylinder pressure that is recorded. During the measurement, the intake manifold pressure should essentially be constant in order for this method to be valid.

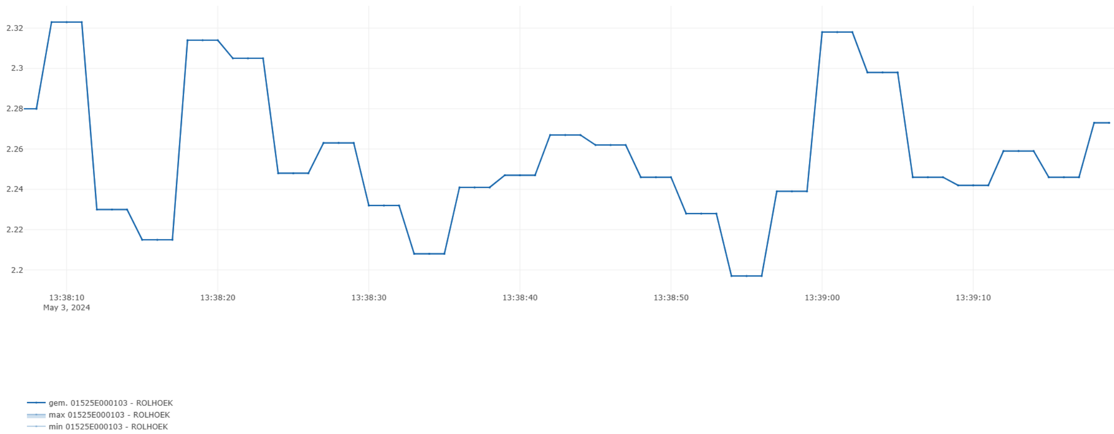

Figure 4.3: Effective intake manifold pressure at moderate sea state, pressure in bar(g)

Figure 4.3 shows a typical intake manifold pressure when sailing with moderate sea state. The pressure can be seen to fluctuate with an amplitude of the order of magnitude of $0.05 - 0.1$ bar. This fluctuation appears small enough to regard the pressure as constant.

In contrast, Figure 4.4 shows the intake manifold pressure when sailing in a rough sea. Now, the pressure fluctuates with an amplitude of more than 1 bar. The pressure can be seen to drop from 2.4 bar(g)[1] to 1.2 bar(g) and rise again to 2.4 bar(g) in just a few seconds. This is the result of the rolling and/or pitching movement of the ship, which causes the engine rpm, the fuel mass flow, the turbocharger rpm and, as a consequence, the intake manifold pressure to fluctuate considerably.

Under these circumstances, during one measurement the intake manifold pressure may increase or decrease significantly and, consequently, the cycle-to-cycle cylinder pressures. Fluctuations of this magnitude may therefore be considered too high for this method of pressure referencing. Therefore, these circumstances require a more robust method. That is the topic of Section 4.2.2

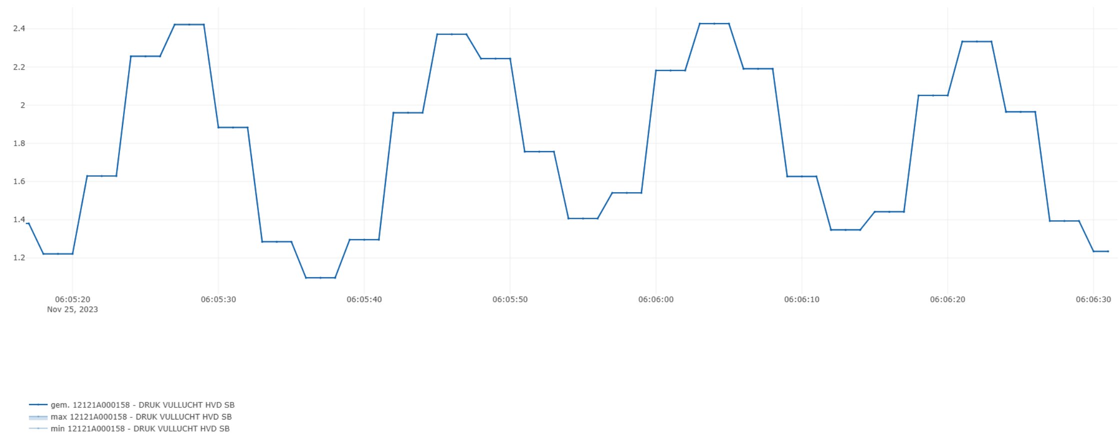

Figure 4.4: Effective intake manifold pressure at heavy sea state, pressure in bar(g)

4.2.2. Linear least-squares method

When the intake manifold pressure is too unsteady to be used as reference, the pressure offset may be determined from the recorded pressure data. The *linear least-squares method* (LLSM) presented here is a multiple regression method that fits the pressure trace during the compression stage to a polytropic curve for a given polytropic exponent. This method was proposed by Tunestal e.a. [72] and Zhang e.a. [78].

First, it is assumed that the measured pressure p_m differs from the true pressure p by an unknown, constant pressure offset Δp:

$$p = p_m - \Delta p \tag{4.5}$$

The true (absolute) pressure is assumed to follow a polytropic compression curve from the moment the inlet valves are closed (IVC) until the start of injection (SOI):[2]

$$pV^n = C \tag{4.6}$$

Here, n is the assumed polytropic exponent and C an unknown constant. Eq. 4.5 and 4.6 combine to give

$$p_m = \Delta p + CV^{-n} \tag{4.7}$$

Eq. 4.7 applies to all measured pressures during the analysed compression phase. Thus, the

[1]The unit bar(g) indicates the gauge pressure, thus the pressure relative to the atmosphere.

[2]The exact crank angle at which the fuel injection starts belongs to the intellectual property of the engine manufacturer and is thus unknown. However, for the purpose of determining the pressure offset, this is not a problem because, as it turns out, it is sufficient to analyse the period from 100° to 40° before TDC, which is well before SOI.

following equation applies:

$$\begin{bmatrix} p_{m,i} \\ \cdot \\ \cdot \\ \cdot \\ p_{m,f} \end{bmatrix} = \Delta p + C \begin{bmatrix} V_i^{-n} \\ \cdot \\ \cdot \\ \cdot \\ V_f^{-n} \end{bmatrix} = \begin{bmatrix} 1 & V_i^{-n} \\ \cdot & \cdot \\ \cdot & \cdot \\ \cdot & \cdot \\ 1 & V_f^{-n} \end{bmatrix} \begin{bmatrix} \Delta p \\ C \end{bmatrix} \tag{4.8}$$

where index i indicates the initial and f the final value. In matrix notation, Eq. 4.8 can be written as:

$$\boldsymbol{y} = \boldsymbol{\Phi\theta} \tag{4.9}$$

where $\boldsymbol{y}$ is the vector of measured cylinder pressures (the dependent variables), $\boldsymbol{\Phi}$ the matrix with 1's in the first column and V^{-n} in the second (the independent variables), and $\boldsymbol{\theta}$ the vector of unknown parameters Δp and C, which are to be determined. The least-squares solution $\hat{\boldsymbol{\theta}}$ of Eq. 4.9 is given by:

$$\hat{\boldsymbol{\theta}} = \left(\boldsymbol{\Phi}^T\boldsymbol{\Phi}\right)^{-1} \boldsymbol{\Phi}^T\boldsymbol{y} \tag{4.10}$$

The solution $\hat{\boldsymbol{\theta}}$ of Eq. 4.10 is the combination of Δp and C that minimises the sum of the squares of the residuals, i.e. the difference between the values of p_m and $(\Delta p + CV^{-n})$. This procedure can be repeated for different values of n; this will produce different pressure offsets.

Validation: determining pressure offsets for different polytropic exponents

To validate the linear least-squares method described above, it is first tested on pressure data from the stopping engine and, second, on data from the engine at full load. In the case of the stopping engine, the intake manifold pressure is known to be atmospheric and virtually constant. Hence, the calculated pressure offset should essentially be zero.

The polytropic exponent n depends on the temperature and composition of the in-cylinder gas. It is not known a priori which value of n best describes the actual compression phase. Therefore, the procedure is repeated here for different values of the polytropic exponent: n is varied from 1.33 to 1.4 in steps of 0.01; for each n the pressure offset Δp and the constant C are calculated that best satisfy Eq. 4.8. The value of n that results in a pressure offset closest to zero would be the optimal choice.

The resulting pressure offset is shown in Figure 4.5 (a) as a function of n for the stopping engine. The scattered dots represent the calculated values of the individual cylinders for a given n; the line connects the mean pressure offset values of all cylinders for varying n. The value n = 1.38 gives a mean pressure offset that is practically equal to zero with a standard deviation of 0.01 bar. Thus, n = 1.38 would be the value of choice. Figure 4.5 (b) shows the pressure offset for the engine at full load. Choosing a polytropic exponent of 1.37 gives the pressure offset closest to zero; the standard deviation is 0.067 bar. The intake manifold pressure at the time of this measurement was seen to fluctuate mildly between 2.77 and 2.86 bar(g). Hence, the uncertainty is $\pm$ 0.05 bar, a value that is reflected by the standard deviation. Consequently, any value for n between 1.36 and 1.37 could be equally valid.

Figure 4.6 (a) shows the compression curve according to the polytropic model of cylinder A1 of the stopping engine. The section shown is the part that is used to determine the pressure offset, which is from 100° to 40° before TDC. This is well after IVC en well before SOI. Here, n = 1.38 has been implemented with a pressure offset equal to zero. It can be seen that the polytropic curve practically coincides with both the measured and smoothed pressure curves. Figure 4.6 (b) shows the small difference between these curves, zooming in on a small part of the graph. The difference between the smoothed pressure and the polytropic curve is on the order of less than 0.02 bar, which is small enough to be neglected. This confirms that n = 1.38 is an appropriate choice for this particular measurement.

Now, the previous step is repeated for the engine under load. A polytropic exponent of n = 1.37 is chosen, as previously motivated. The result is shown in Figure 4.7. Again, the polytropic compression curve agrees well with the curves of the measured and the smoothed pressure. Zooming in on a small part of the graph reveals that the difference between the smoothed pressure and the polytropic curve is smaller than 0.1 bar, which is sufficiently accurate for the purpose of this thesis.

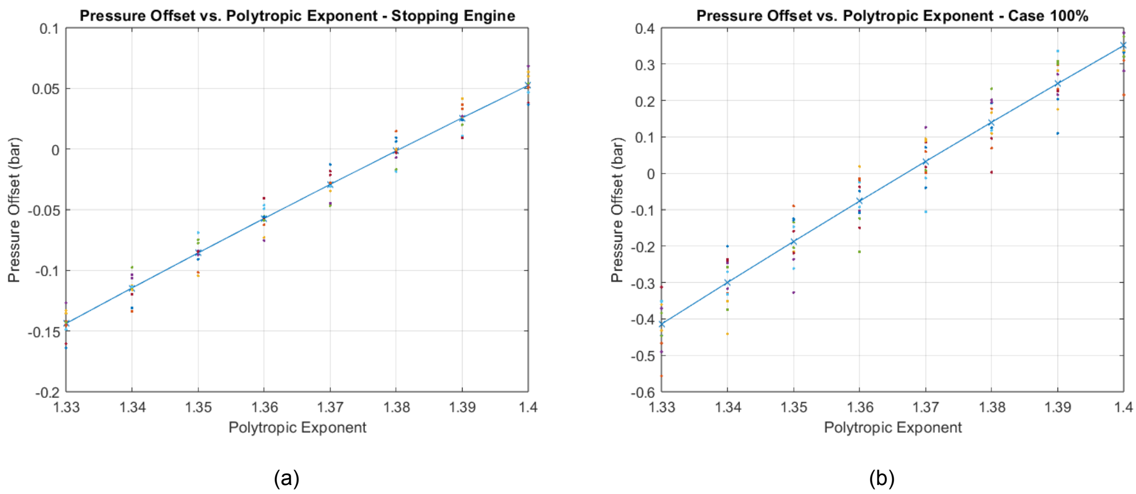

Figure 4.5: Pressure offset versus polytropic exponent calculated with linear least-squares method:
(a) stopping engine: n =1.38 gives correct pressure offset of 0 bar
(b) engine at 100% load: n =1.36-1.37 gives correct pressure offset of ~0 bar.

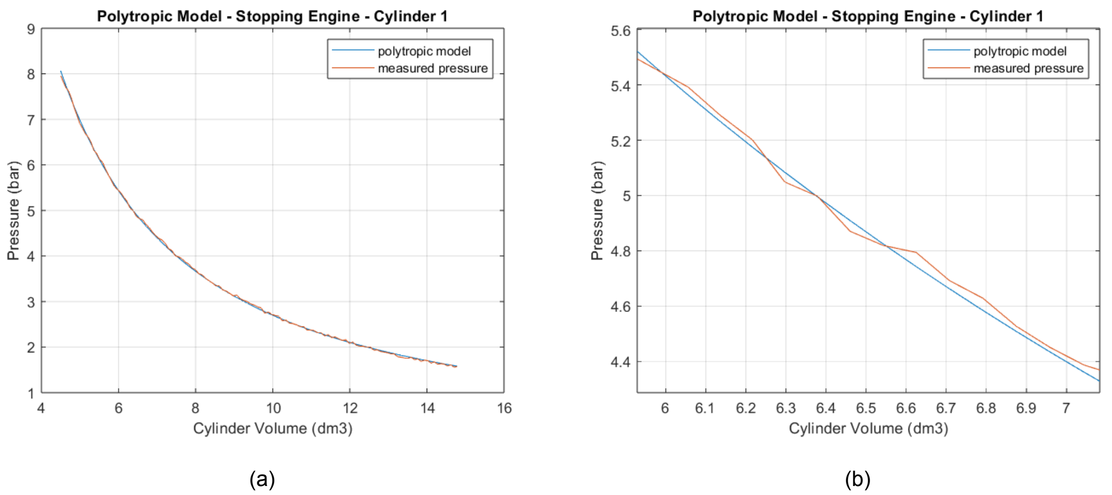

Figure 4.6: Polytropic pressure-volume diagram vs. trace of measured pressure; (a) part of p-V diagram used for LLSM, (b) zoom shows good agreement between measured pressure and polytropic model.

Validation: test of robustness

A second validation test assesses the robustness of the method. An intentional pressure offset is introduced in advance to simulate the effects of (1) rough sea conditions and (2) a malfunctioning intake manifold pressure sensor. The first test case is performed by adding 1.5 bar to the measured cylinder pressures of the engine at full load. This would be a worst-case scenario of the effect of the sea state on the intake manifold pressure, as demonstrated by Figure 4.4. Second, 2.8 bar is subtracted from the measured pressure. This test represents the scenario of a defect pressure sensor in the intake manifold. Then, the reference pressure would become zero instead of 2.8 bar(g). Both forced errors should be undone using the linear least-squares method.

Figure 4.8 (a) shows the results of the first test, i.e. the pressure offset versus polytropic exponent for the additive error of 1.5 bar. Comparing Figure 4.5 (b) with 4.8 (a), it is apparant that the calculated pressure offsets for a given polytropic exponent differ by 1.5 bar, which is the desired result. The sign of the pressure offset is in agreement with Eq. 4.5: the pressure offset Δp is to be subtracted from the measured pressure. The same conclusion holds for the case of subtracting 2.8 bar: the difference between the pressure offsets in Figure 4.5 (b) and 4.8 (b) now is 2.8 bar. Now, the negative sign of the pressure offset indicates that 2.8 bar is to be added to the original pressure.

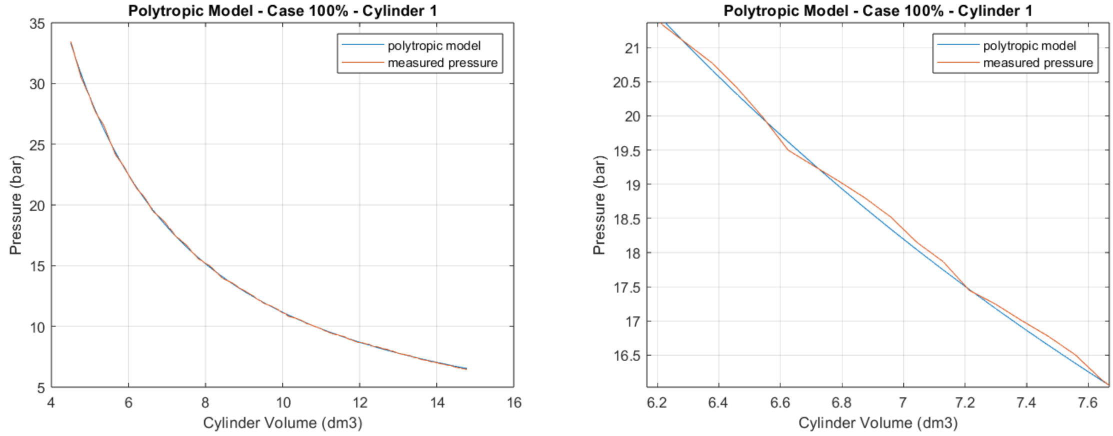

(a) (b)

Figure 4.7: Pressure-volume diagram of compression phase of engine at 100% load; (a) part of curve used for linear least-squares method, (b) zoom shows close agreement between polytropic model and trace of measured pressure.

The validation tests support the conclusion that the linear least-squares method implemented here is a suitable alternative to the preferred method of pegging at IBDC. LLSM appears to be a reliable and robust method. It provides satisfactory results when appropriate values of n are used: for the engine under investigation here $n = 1.37$ for the engine under load and $n = 1.38$ for the unloaded or stopping engine.

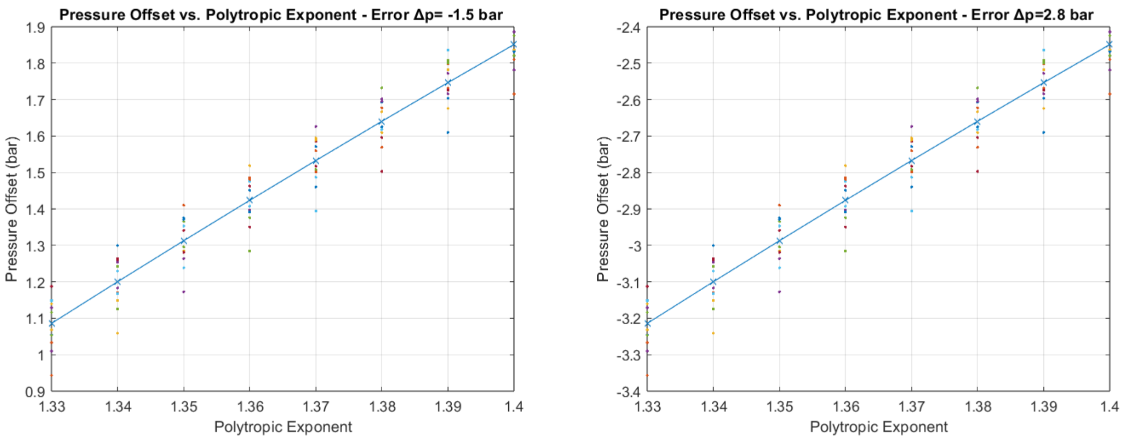

(a) (b)

Figure 4.8: Pressure offset versus polytropic exponent calculated with linear least-squares method for erroneous cylinder pressure, engine at full load: (a) additive error due to sea state (1.5 bar) (b) subtractive error due to defect sensor (2.8 bar)

4.3. Smoothing the pressure signal

Smoothing represents the final stage in the preprocessing of the cylinder pressure signal. As outlined in Section 2.2.3, it is a crucial step in preparing diesel engine pressure data for analysis, as it reduces high-frequency noise and improves the reliability of derived combustion parameters. It serves the following purposes:

1. Smoothing reduces rapid fluctuations in the pressure signal, which are often caused by sensor behaviour or external disturbances.
2. It improves the accuracy and consistency of performance parameters derived from the pressure

trace, such as peak pressure and the crank angle at which it occurs.

3. It enables more reliable computation of pressure derivatives, which are essential for metrics such as heat release rate. Since numerical differentiation amplifies noise, smoothing helps reduce errors in these calculations.

A two-step approach is employed in the final stage of preprocessing the cylinder pressure data. First, the pressure traces are averaged,[3] followed by a smoothing operation applied to the averaged trace.

4.3.1. Cycle averaging

Cylinder pressure measurements from multiple engine cycles are averaged to reduce the influence of random noise. Following the recommendations of Payri et al. [56], 25 consecutive cycles are used for this purpose. However, this approach is only applicable under steady-state operating conditions, i.e., when engine speed is constant and load fluctuations are negligible during the measurement period, which typically takes 3 to 5 seconds. In the case of the stopping engine described in Section 4.1.2, where the TDC shift is evaluated, or when heavy sea states induce significant engine oscillations, this step is not carried out.

Besides averaging many cycles of one cylinder, researchers sometimes average the pressures across several or all cylinders of an engine. This is, however, not applicable when analysing cylinder-to-cylinder variations or identifying anomalies specific to individual cylinders.

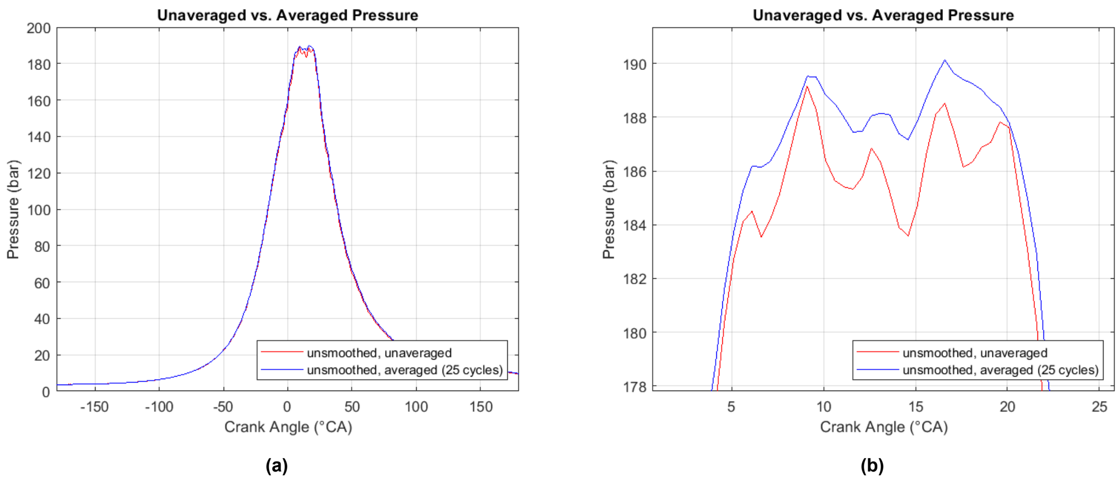

Figure 4.9: Effect of averaging on the pressure trace

Figure 4.9a displays the p-θ graph of a single arbitrary cycle (red) and the averaged pressure trace over 25 cycles (blue). Overall, there is little difference between the individual and the averaged pressure trace. However, during the combustion phase, particularly from just before peak pressure until approximately 20° ATDC, the averaged curve shows less-pronounced spikes, as Figure 4.9b shows. Notably, the crank angle where peak pressure occurs (apmax) differs significantly between both curves: 9°ATDC for the unaveraged trace versus 17°ATDC for the averaged trace. Apparently, cycle-to-cycle variations cause this large difference. This is a result of the relatively flat, nearly isobaric, nature of the pressure curve during the combustion stage shown.[4] Consequently, apmax may not be a reliable parameter for characterising combustion.

The impact of averaging the original pressure trace on its derivative, the rate of pressure rise, is now examined. To begin, an appropriate differentiation method is selected. Several approaches exist for calculating the derivative of a discrete signal sampled at equal time intervals. The following three common methods are evaluated:

1. Backward difference method: $f'(x_i) \approx \big(f(x_i) - f(x_{i-1})\big)/h$
   A first-order method using the current and previous sample. This is the method used in Simulink's Derivative block.

[3]Throughout this text, the term average refers to the arithmetic mean, i.e., the sum of all values divided by the number of items.

[4]This may be regarded as a justification for the isobaric stage in the idealised Diesel and Seiliger cycle.

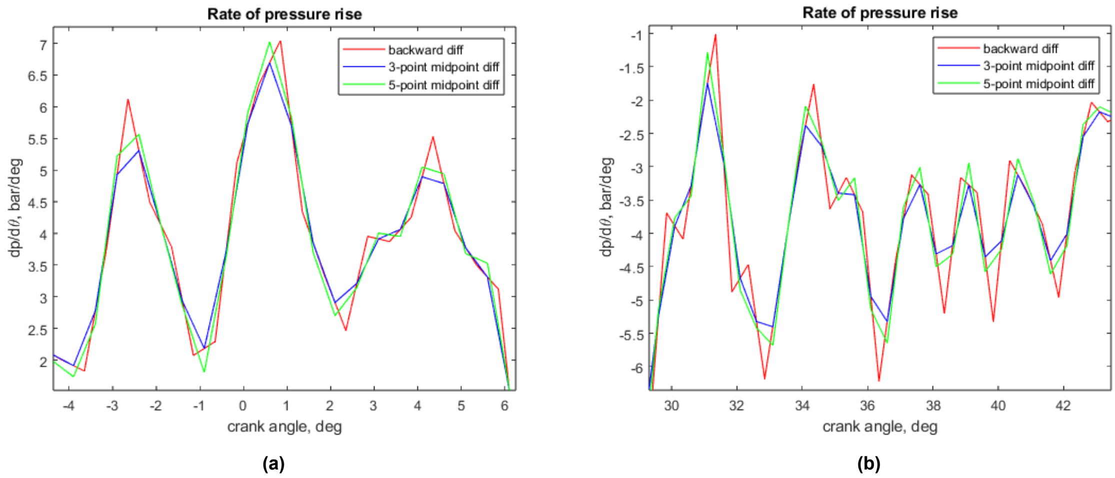

Figure 4.10: Rate of pressure rise calculated by three different differentiation methods

2. Three-point midpoint difference: $f'(x_i) \approx \big(f(x_{i+1} - f(x_{i-1})\big)/2h$
   A second-order method that averages the forward and backward differences.
3. Five-point midpoint difference: $f'(x_i) \approx \big(-f(x_{i+2}) + 8f(x_{i+1}) - 8f(x_{i-1}) + f(x_{i-2})\big)/12h$
   A fourth-order method providing higher accuracy by considering more neighboring points.

The optimal differentiation method minimises noise amplification. Figure 4.10 presents segments of the derivative of pressure with respect to crank angle, $dp/d\theta$, computed using the three differentiation methods. Figure 4.10a shows the graph just after SOC, where the cylinder pressure rises rapidly. The curves derived using the backward difference method (red) and the five-point midpoint method (blue) exhibit the highest amplitude of visible oscillations. In the subsequent combustion phase shown in Figure 4.10b, when the pressure is decreasing ($dp/d\theta < 0$), this trend persists. Overall, the backward difference method amplifies the noise to the highest extent: the curve displays a pronounced sawtooth pattern, while the five-point midpoint curve is marginally smoother. The three-point midpoint method produces a slightly smoother signal still with reduced high-frequency fluctuations, thereby producing the least noisy derivative. Consequently, the three-point midpoint method is selected as the preferred differentiation technique.

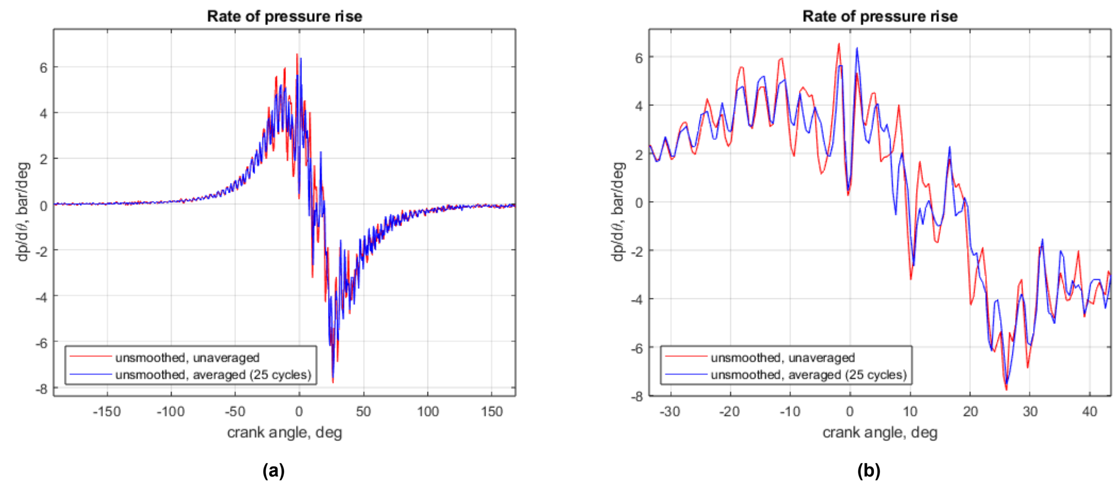

Figure 4.11: Rate of pressure rise for unaveraged and averaged pressure trace

Next, the effect of averaging on the derivative of the pressure trace is analysed. As shown in Figure 4.11a, the impact of averaging appears limited—particularly during the compression phase and the late stages of combustion, where the difference between the unaveraged (red) and averaged (blue) curves is negligible. However, toward the end of compression and throughout the combustion phase up to approximately 40°ATDC, the red curve exhibits more pronounced spikes compared to the blue, as highlighted in Figure 4.11b.

Notably, high-frequency, *non-random* noise remains clearly visible in the signal. This noise exhibits a periodicity of 3°CA, which, at the measurement engine speed of 1000 rpm, corresponds to a frequency of approximately 2 kHz. The likely source of this noise is acoustic resonance within the indicating channel, as discussed in Section 2.2.3. To demonstrate that this frequency aligns with a typical acoustic resonance mode, Eq. 2.1 is applied. Using γ =1.35, T =800 K, a channel diameter of 6 mm, a length of 25 cm, and an estimated resonance chamber volume of 1 cm^3 at the sensor mounting location, the equation yields a predicted resonance frequency of approximately 1 kHz. This is of the same order of magnitude as the observed 2 kHz frequency, indicating that acoustic resonance likely is the underlying cause. The presence of this remaining noise shows the necessity for the next step in the smoothing procedure.

4.3.2. Spline-based smoothing

The averaged pressure trace is further processed using a cubic smoothing spline, which approximates the data with a piecewise cubic polynomial. The underlying mathematical framework is detailed in Appendix C. A central feature of this method is the smoothing parameter $p \in [0, 1]$, which dictates the balance between smoothness and fidelity to the original data. Lower values of p yield a smoother curve by allowing greater deviation from individual data points, while higher values produce a closer fit to the data at the expense of reduced smoothness.

As demonstrated by Zhong et al. [80], cubic smoothing splines are particularly effective for both steady-state and transient cylinder pressure signals. The method effectively suppresses high-frequency noise while preserving the essential features of the pressure curve. This approach has been shown to maintain the integrity of key trends in the data, filtering out unwanted fluctuations.

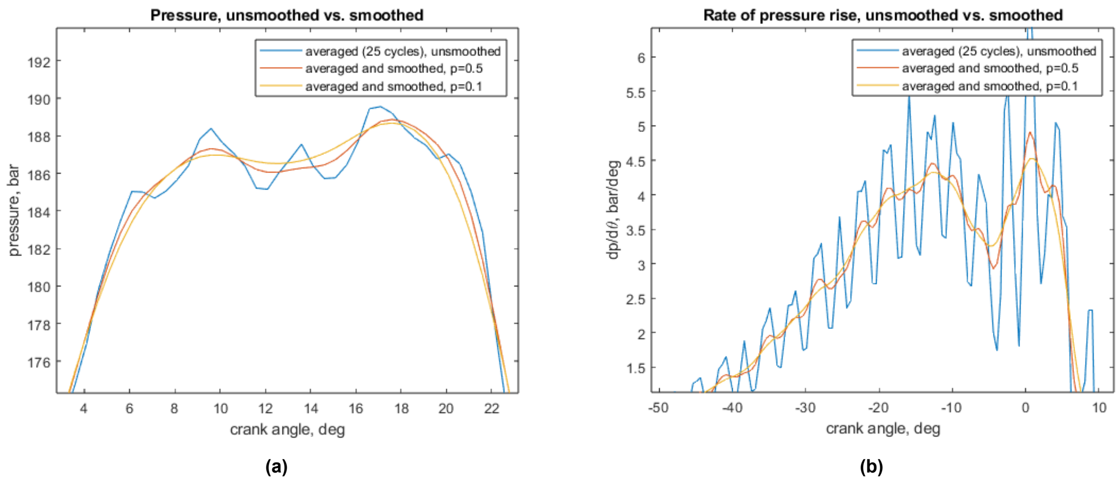

Figure 4.12: Pressure (a) and the rate of pressure rise (b) plotted versus crank angle, unsmoothed versus smoothed, with smoothing parameters 0.5 and 0.1.

The cubic spline smoothing method is applied to a set of averaged cylinder pressure traces from an arbitrary engine cycle to demonstrate its effect. To illustrate the influence of the smoothing parameter p, values of 0.5 and 0.1 are used. Figure 4.12 presents segments of the resulting pressure traces and their corresponding rates of pressure rise. In the left figure, the unsmoothed averaged pressure trace is shown in blue, alongside the smoothed curves in red (p = 0.5) and orange (p = 0.1). Both smoothed curves closely approximate the original trace. As expected, the curve with p = 0.5 adheres more closely to the unsmoothed data but is slightly less smooth than the curve with p = 0.1.

Figure 4.12b displays the rate of pressure rise, $dp/d\theta$, corresponding to the three pressure traces. The oscillations visible in the unsmoothed signal may again be attributed to acoustic resonance within the indicating channel. With a smoothing parameter of p = 0.5, these high-frequency components largely remain present (red curve). In contrast, the curve smoothed with p = 0.1 (orange) is substantially smoother and appears to follow the central trend of the oscillations in the unsmoothed signal. This suggests that $p = 0.1$ offers a good compromise, effectively smoothing the derivative signal while still preserving the underlying characteristics of the original pressure trace.

5

Performance, combustion and fault analysis

This chapter outlines the methodology developed for the analysis of cylinder performance, combustion characteristics, and fault detection. Section 5.1 describes how cylinder pressure measurements are used to derive certain performance indicators. Then, Section 5.2 presents a methodology for quantifying the heat release within the cylinder during the combustion process. The chapter concludes with Section 5.3, which focuses on the detection and diagnosis of engine faults based on deviations in combustion and performance metrics.

5.1. Engine and cylinder performance analysis

In this section, a detailed analysis is conducted using three key parameters that offer direct insight into individual cylinder performance:

1. Peak pressure and its corresponding crank angle
2. Compression pressure
3. Indicated Mean Effective Pressure (IMEP) and indicated work (W_i)

If not mentioned otherwise, these parameters are extracted from averaged and smoothed pressure traces by applying the methods described in Section 4.3, effectively suppressing measurement noise while preserving the underlying physical phenomena.

5.1.1. Peak pressure and angle of peak pressure

The peak pressure p_max is the highest instantaneous pressure reached within the combustion chamber during a cycle. The corresponding crank angle, apmax, provides information about the phasing of combustion. Large deviations in p_max across cylinders can indicate uneven combustion, injector malfunctions, or differences in amount of injected fuel. Similarly, shifts in apmax can signal abnormal combustion timing or detonation. The use of these parameters is demonstrated now using operational cylinder pressure data.

Figure 5.1 presents a bar plot comparing various representations of peak pressure obtained from a 25-cycle cylinder pressure measurement. Data from six cylinders (B bank) are displayed. For each cylinder, the two leftmost bars represent the highest and lowest peak pressures recorded across all individual cycles. As shown, these can differ by more than 10 bar. The third bar shows the average of the peak pressures from the individual cycles, which is slightly higher than the fourth bar: the peak pressure derived from the averaged pressure trace.

The three rightmost bars correspond to the peak pressures obtained from the averaged and subsequently smoothed pressure traces, with varying smoothing parameters. These values are consistently lower; notably, smaller smoothing parameters (p) result in lower peak pressures. The close agreement among the five rightmost bars indicates a strong correlation, suggesting that the choice among these specific peak pressure definitions has minimal impact on the overall assessment.

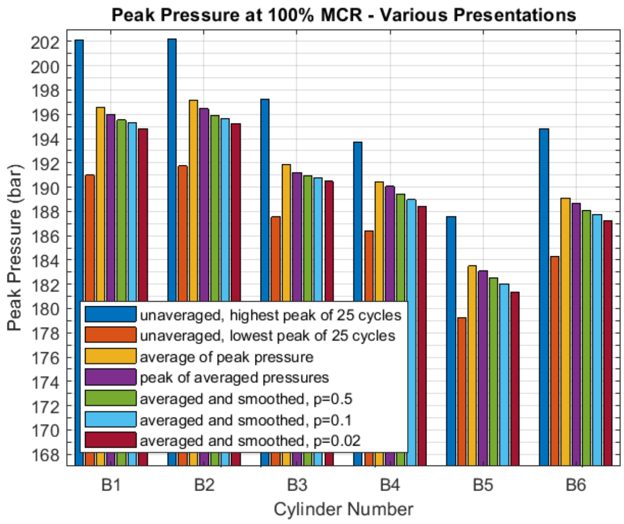

Figure 5.1: Different ways of presenting peak pressures of a cylinder bank (six B-bank cylinders).

Figure 5.2a illustrates the cylinder-to-cylinder variation of the mean peak pressures across all 12 cylinders. The data reveal a substantial spread: the difference between the highest and lowest average peak pressure is approximately 14 bar. This level of variation could be indicative of several factors, including normal manufacturing tolerances, uneven combustion conditions, or potential mechanical or fuel system imbalances. However, at this stage, it is unclear whether such a discrepancy falls within the expected range for this engine or if it signals an underlying anomaly. A broader dataset, including repeated measurements under varying conditions, is required to draw meaningful conclusions.

Complementing this, Figure 5.2b presents the cycle-to-cycle variation of peak pressure for a single, arbitrarily selected cylinder, based on a 25-cycle recording. In this case, the peak pressures span a range of approximately 12 bar from the lowest to the highest observed value. Similar magnitudes of cycle-to-cycle variation are observed across all cylinders, suggesting that this variability is characteristic of the engine under the given operating conditions.

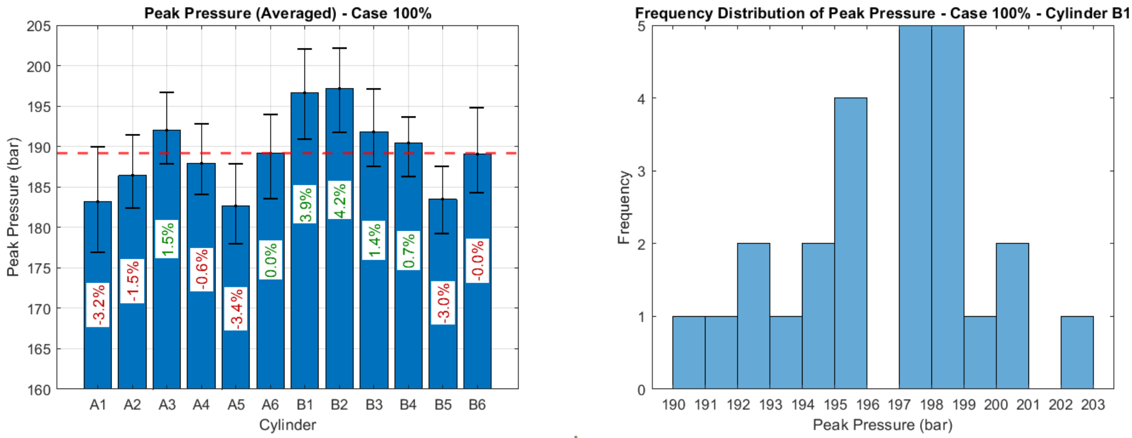

(a) (b)

Figure 5.2: (a) Mean peak pressure per cylinder (25-cycle average); (b) Frequency distribution of peak pressure.

Next, the angle of peak pressure is examined. Figure 5.3 presents the frequency distribution of the crank angles at which maximum pressure occurs (apmax), effectively illustrating the cycle-to-cycle variation in the timing of the combustion peak.

Notably, the distributions differ significantly between cylinders. In Figure 5.3a, the angles of peak pressure are distributed over a narrow range of approximately 3°CA, indicating relatively consistent peak timing across cycles. In contrast, Figure 5.3b shows a much broader distribution—spanning about 13°CA—suggesting a high degree of variation in the peak pressure angle for that cylinder.

As discussed in Section 4.3.1, this broader spread does not necessarily indicate poor combustion quality, nor does it directly imply issues with injection timing or ignition. Instead, it reflects the quasi-isobaric nature of the combustion process in this specific operating point. In such cases, the pressure remains nearly constant over a range of crank angles during peak combustion, making the exact crank angle at which maximum pressure occurs less physically meaningful.

Therefore, relying on the angle of maximum pressure as a diagnostic indicator can be misleading. This analysis supports the conclusion that apmax is not a reliable parameter for assessing cylinder performance, particularly under conditions where the pressure peak is broad and flat.

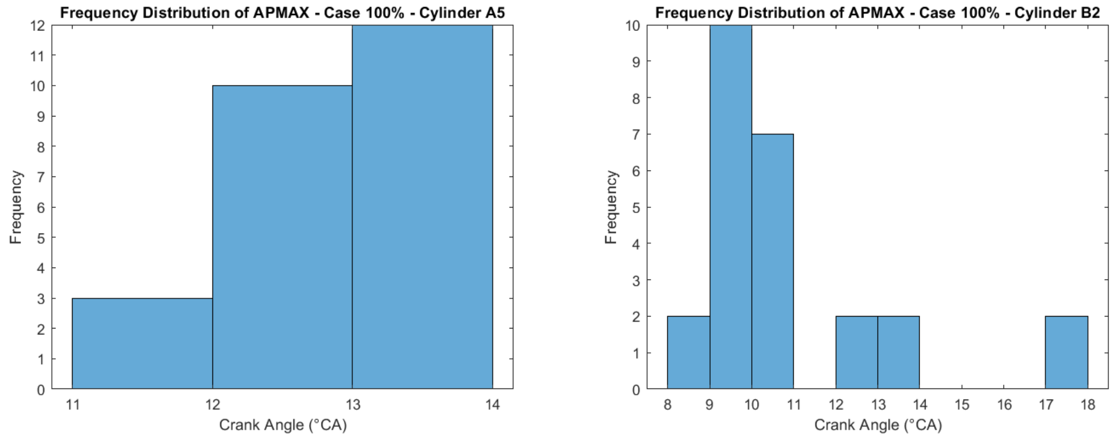

(a) (b)

Figure 5.3: Frequency distribution of angles of maximum pressure of (a) cylinder A5, and (b) cylinder B2.

5.1.2. Compression pressure

Compression pressure is typically evaluated near top dead center (TDC) of the compression stroke, specifically just before the start of injection (SOI). It serves as an important indicator of the engine's ability to compress the intake air, and is influenced by several mechanical and thermodynamic factors, including valve sealing quality, piston ring condition, cylinder wall wear, and intake air conditions (such as pressure and temperature). For consistency and comparability, compression pressure is usually extracted at a fixed crank angle prior to fuel injection. This approach avoids variability caused by changes in combustion timing and allows for comparisons across cylinders or over time. Since the precise timing of SOI is proprietary information held by the engine manufacturer (OEM), the measurement is decoupled from injection timing and instead referenced to a fixed crank angle during the compression stroke. This ensures that the metric remains usable even when SOI is unknown or variable.

Figure 5.4 illustrates both the cylinder-to-cylinder variation and cycle-to-cycle variation of the compression pressure. Specifically, Figure 5.4a displays the compression pressure measured at three crank angles before TDC (45°, 30°, and 20° BTDC) across all cylinders. Also shown is the mean compression pressure at 20° BTDC, providing a benchmark for comparison. These data help assess uniformity in compression behaviour across cylinders and may reveal excessive gas leakage from the cylinder.

Figure 5.4b presents the frequency distribution of the compression pressure at 15° BTDC for a single, arbitrarily chosen cylinder. This reveals the cycle-to-cycle variation in compression pressure, which can be affected by transient effects, measurement noise, or other slight differences from one cycle to another.

At this stage, it remains unclear whether the observed differences in compression pressure—both across cylinders and between cycles—are within the expected margin for this engine, whether they indicate meaningful deviations due to, e.g., wear, leakage, or if they are the result of load variation during the measurement. A larger dataset and further analysis would be needed to determine whether these variations are significant.

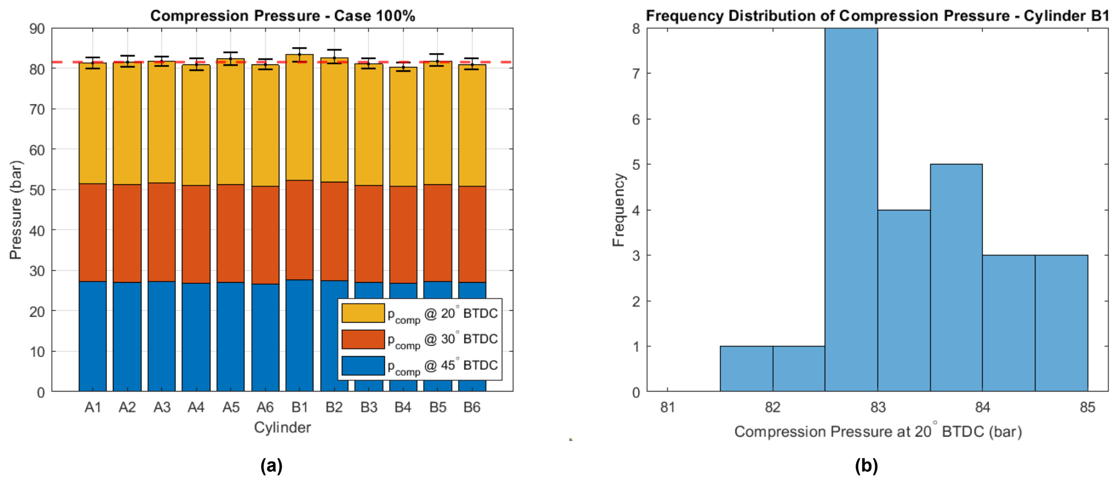

Figure 5.4: Compression pressure - cylinder-to-cylinder and cycle-to-cycle variation: (a) compression pressure at three crank angles, showing the minimum and maximum value; (b) Frequency distribution of compression pressure.

5.1.3. Indicated Mean Effective Pressure (IMEP)

The *indicated mean effective pressure* (IMEP), introduced in Section 2.3.1, is a key engine performance parameter that quantifies the *indicated work* output per cycle, normalised by the engine's *displacement volume* V_d. It is defined as:

$$\text{IMEP} = \frac{W_\mathrm{i}}{V_\mathrm{d}} = \frac{1}{V_\mathrm{d}} \oint p(\theta)\, dV \tag{5.1}$$

Here, W_i denotes the indicated work, $p(\theta)$ is the cylinder pressure as a function of crank angle θ, and dV represents the infinitesimal change in cylinder volume due to piston motion. The integration is carried out over a complete engine cycle (720° CA).

IMEP is typically expressed in **bar** and can be interpreted as the hypothetical constant pressure that, if applied uniformly during the expansion stroke, would produce the same work output as that obtained from the actual pressure trace.

In this work, IMEP is used instead of the indicated work W_i, as it facilitates comparison between different engines by accounting for variations in displacement volume. While W_i is specific to a particular engine geometry, IMEP is a normalised metric, making it more universally applicable in performance benchmarking and diagnostics. Furthermore, IMEP is sensitive to both combustion efficiency and mechanical condition, and is therefore widely used in engine health monitoring [54].

To calculate IMEP from measured data, the indicated work W_i must first be determined by numerically integrating the pressure-volume data over a full cycle. For the discrete data sampled at uniform crank angle intervals (0.5° CA), this is done here using the trapezoidal rule:

$$W_\mathrm{i} \approx \sum_{i=1}^{n-1} \frac{1}{2} \left(p_i + p_{i+1}\right) \left(V_{i+1} - V_i\right) \tag{5.2}$$

where:

- p_i and V_i are the pressure and corresponding volume at crank angle index i,
- n is the total number of data points across one complete engine cycle.

To convert the result to IMEP in bar, the calculated W_i (in joules) is divided by the displacement volume V_d (in m^3) and multiplied by 10^5.

Figure 5.5 shows IMEP calculated over 25 cycles for each of the 12 cylinders. Subfigure 5.5a illustrates the cylinder-to-cylinder variation in IMEP, calculated from the averaged and smoothed[1] pressure

[1] For the evaluation of IMEP, the degree of smoothing has minimal impact. Due to the nature of integration, short pressure spikes are effectively mitigated, resulting in IMEP values that are virtually identical whether based on smoothed or unsmoothed pressure traces.

traces over 25 engine cycles. Especially the B-bank exhibits notable differences: cylinders B1, B2 and B3 show relatively high IMEP, whereas cylinders B5 and B6 underperform. This trend aligns with the peak pressure variation shown earlier in Figure 5.2a, suggesting a consistent pattern in performance imbalance across cylinders.

Figure 5.5b presents the cycle-to-cycle IMEP distribution for one arbitrarily selected cylinder over 25 cycles. The spread, ranging from approximately 27.5 to 32 bar, is considerable and highlights the variability in combustion performance even within a single cylinder.

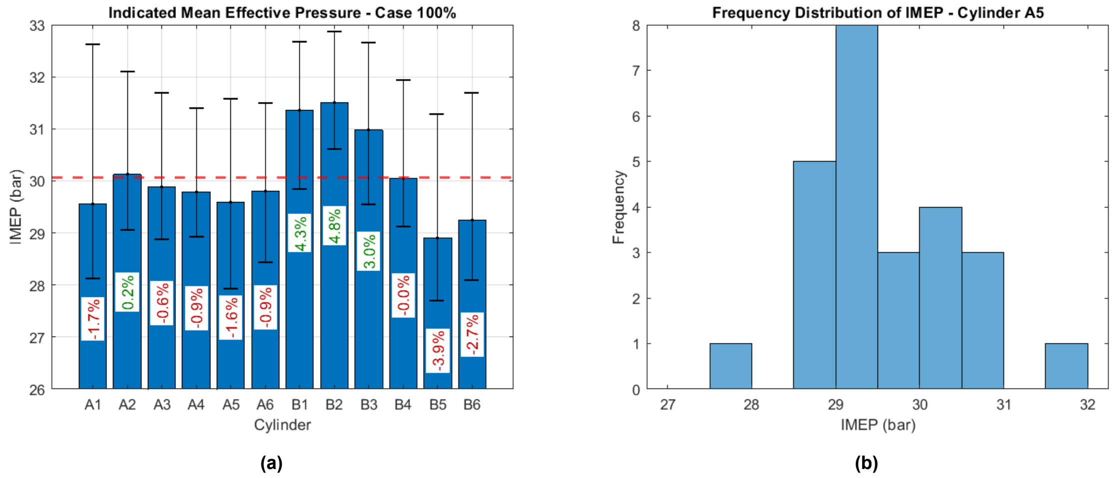

Figure 5.5: Indicated mean effective pressure (IMEP): (a) cylinder-to-cylinder variation, based on mean values over 25 cycles; (b) frequency distribution for a single cylinder.

5.2. Combustion model

Several parameters may be used to quantify combustion, as described in Section 2.3. The *net* apparent heat release rate (NAHRR) and the *gross* apparent heat release rate (GAHRR) are useful parameters that quantify the instantaneous heat that is released by the combustion of the injected fuel. The GAHRR is directly proportional to the burn rate of the fuel (see Eqs. 2.8 and 2.9) and is calculated from the NAHRR by adding the instantaneous heat-transfer rate.

As discussed in Section 2.5, the calculation of the heat-transfer rate is subject to considerable uncertainty. This is primarily due to the strong dependence of the heat-transfer rate on the cylinder-wall temperature, a parameter that cannot be measured directly. Consequently, the use of the GAHRR, as well as the derived *normalised combustion progression*, may introduce significant inaccuracies. Nevertheless, it should be quite feasible to include a heat-transfer submodel. It would require the following steps:

1. Determine the gas temperature T_{gas} using a thermodynamic equation of state, based on the estimated initial mass and temperature of the cylinder contents at IVC.
2. Estimate the heat-transfer coefficient h, typically based on empirical correlations.
3. Estimate the surface temperature T_{wall} of the (1) cylinder wall, (2) cylinder head and (3) piston crown.
4. Compute the instantaneous heat loss, i.e. the total heat transfer rate as the sum of $hA(T_{\text{gas}} - T_{\text{wall}})$ for the three components, where A is the (instantaneous) surface area exposed to the in-cylinder gases.

To derive GAHRR and the corresponding fuel mass metrics, the following additional steps are necessary:

5. Determine GAHRR by adding the calculated heat loss to the NAHRR.
6. Obtain the fuel mass burn rate by dividing GAHRR by the lower heating value (LHV) of the fuel.
7. Integrate the fuel burn rate over time to determine the cumulative mass of fuel burnt.

8. Update the total in-cylinder mass by adding the mass of fuel burnt to the initial gas mass at each integration step.

It should be noted that many of the above steps involve rough estimations of highly uncertain parameters. Therefore, incorporating a heat-transfer model does not inherently enhance the accuracy of the simulation. It does, however, substantially increase the model's complexity. To avoid this drawback, the NAHRR is adopted here as the primary metric for quantifying the net energy released during combustion. The methodology is detailed in Section 5.2.1. The implementation of the combustion model in MATLAB® - Simulink® is presented in Section 5.2.2.

5.2.1. Calculation of net heat release

The net apparent heat release rate (NAHRR) on a per-crank-angle-degree basis is calculated using the following expression:

$$\text{NAHRR}(\theta) = \frac{\gamma}{\gamma - 1}\frac{pdV}{d\theta} + \frac{1}{\gamma - 1}\frac{Vdp}{d\theta} \tag{5.3}$$

where γ is the ratio of specific heats, defined as c_p/c_v. Eq. 5.3 is derived by applying the first law of thermodynamics to the cylinder contents after IVC, under the assumption of ideal gas behaviour. The derivation is provided in Appendix B.

For cylinder-to-cylinder comparison, a constant value of γ may be used, as proposed by Liu and Dumitrescu [42]. A value of $\gamma = 1.35$ is typically appropriate, as it is close to the average of the values during the compression and expansion strokes. Conveniently, when using Eq. 5.3 with a constant γ, there is no need to determine the temperature of the in-cylinder gas.

The (absolute) cylinder pressure p is known from measurement and $dp/d\theta$ follows from differentiation of the pressure with respect to the crank angle θ. Derived from engine geometry, the cylinder volume V depends on θ through the following relationship:

$$V(\theta) = \frac{V_\text{d}}{\epsilon - 1} + \frac{V_\text{d}}{2}\left(1 + \text{L/R} - \cos\theta - \sqrt{(\text{L/R})^2 - \sin^2\theta}\right) \tag{5.4}$$

Here, V_d is the cylinder displacement volume, ϵ the volumetric compression ratio, and L/R the ratio of connecting rod length to crank radius. For the HNLMS Groningen's main engines, these values are taken from Table 3.1. The derivative of V with respect to the crank angle, $dV/d\theta$, is given by

$$\frac{dV}{d\theta} = \frac{V_\text{d}}{2}\left(\sin\theta + \frac{\sin\theta\cos\theta}{\sqrt{(\text{L/R})^2 - \sin^2\theta}}\right) \tag{5.5}$$

The terms V and $dV/d\theta$ evaluated by the respective Eqs. 5.4 and 5.5 are then be substituted in Eq. 5.3 in order to evaluate NAHRR.

As an example, Figure 5.6 shows a graph of NAHRR versus θ of a random engine cycle of the 12V 28/33D engine. The four combustion stages, as described in Section 2.3.3, are discerned in the graph. The inflection points in the NAHRR trace are the defining points of the transition between the combustion stages 2-3-4 [42]:

1. Ignition delay: immediately after the start of the fuel injection (SOI), the NAHRR is negative because of the evaporative cooling effect of the injected fuel droplets.
2. Premixed combustion: the rapid rise of NAHRR starting at the minimum and ending at the inflection point.
3. Diffusive combustion: the phase between the two inflection points where NAHRR peaks.
4. Late combustion: the descending part of the graph until NAHRR is virtually zero.

When all terms in Eq. 5.3 have been evaluated, this differential equation may be integrated to give the *cumulative apparant heat release* as a function of the crank angle:

$$Q_\text{net}(\theta) = \int_\text{SOC}^{\theta} \text{NAHRR}(\theta)d\theta \tag{5.6}$$

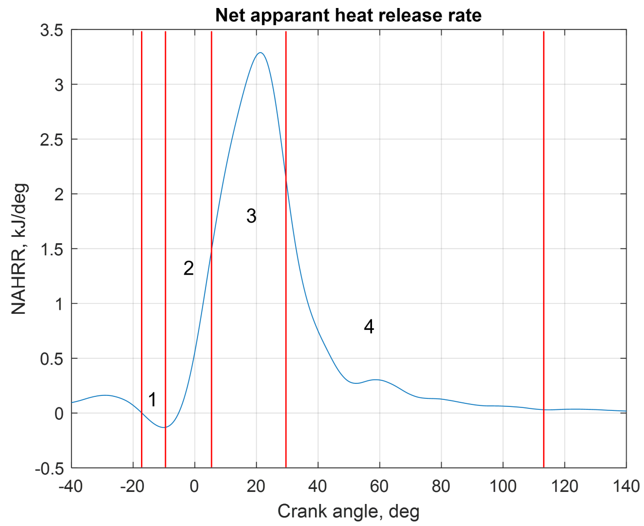

Figure 5.6: Net apparant heat release rate showing different combustion stages: (1) ignition delay, (2) premixed combustion, (3) diffusive combustion, (4) late combustion

By definition, $Q_{\text{net}}(\theta) = 0$ at the start of combustion (SOC). The cumulative apparent heat release at the end of combustion (EOC) is the *net total heat release*:

$$Q_{\text{net,tot}} = Q_{\text{net}}(\text{EOC}) = \int_{\text{SOC}}^{\text{EOC}} \text{NAHRR}(\theta) d\theta \tag{5.7}$$

Figure 5.7a shows Q_{net} versus θ for an arbitrary cylinder and engine load. The two graphs shown represent Q_{net} derived from both the smoothed and unsmoothed pressure trace; the graphs appear to agree well. Figure 5.7b zooms in on a small portion of the graph near the origin and shows a local minimum of the smoothed curve, which suggests that the combustion starts here. Then, Q_{net} is defined to equal zero, here at -4°. The unsmoothed curve highlights the highly irregular nature of the data, indicating that this definition of SOC is somewhat arbitrary. For instance, choosing 0° as SOC would be equally justifiable given the steep rise in the graph immediately thereafter. A reasonable conclusion is that identifying the exact start of combustion in the cylinder, based on these cylinder pressure measurements, is unfeasible. However, this phenomenon does not appear to affect the value of Q_{net} significantly.

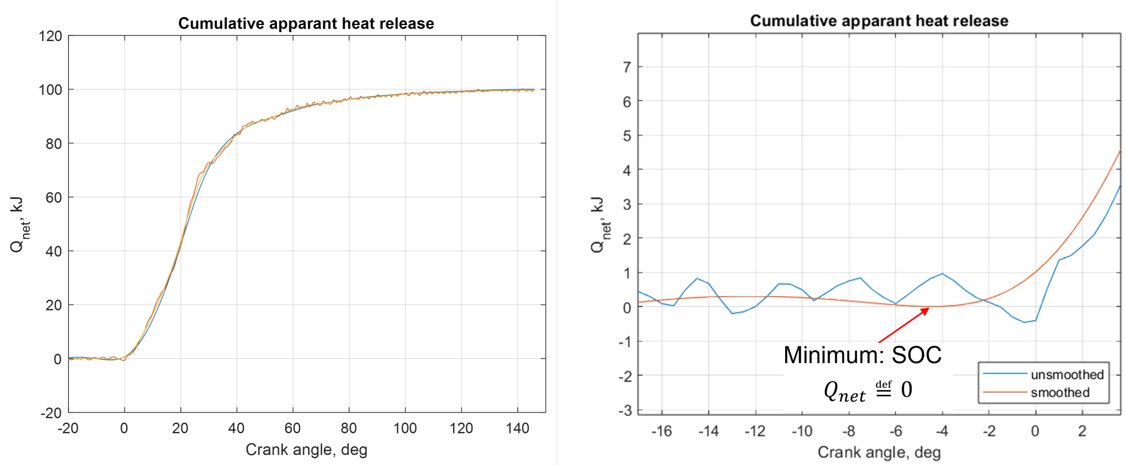

(a) (b)

Figure 5.7: Cumulative apparent heat release Q_{net}

The cumulative apparent heat release enables a cylinder-to-cylinder comparison of the total energy released during combustion. Figure 5.8 visualises the crank angles corresponding to specific cumulative heat release values for the engine operating at 100% MCR load: 10 kJ (Q10), 25 kJ (Q25), and so on. Up to 75 kJ, the curves remain relatively flat, though minor variations are apparent. In particular, cylinders A5 (5) and B5 (11) appear to exhibit a delayed start of combustion. For cylinder B5, this delay persists throughout the combustion process. Most notably, the 100 kJ threshold is reached more than 10 crank angle degrees later than in the other cylinders, indicating a retarded heat release profile.

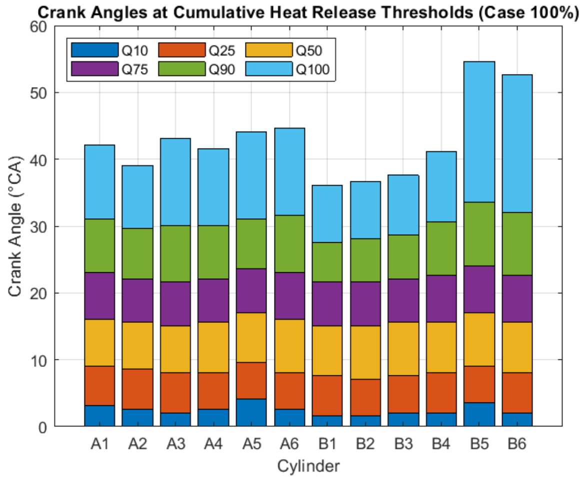

Figure 5.8: Crank angles corresponding to cumulative heat release thresholds (Q10, Q25, Q50, Q75, Q100) for each cylinder, highlighting cylinder-to-cylinder variations in combustion phasing.

The fraction of the net energy release from SOC up to a specific crank angle θ, ERx, is defined as the ratio of the net cumulative heat release to the total heat release:

$$\text{ERx} = \frac{Q_{\text{net}}(\theta)}{Q_{\text{net,tot}}} \tag{5.8}$$

The *normalised energy release* ERx is a similar quantity to the commonly used MFB (percentage mass of fuel burnt, see Section 2.3.3). By definition, both dimensionless quantities ERx and MFB take on values ranging from 0 at SOC to 1 (100%) at EOC. The latter quantity is based on the GAHRR and requires a heat-transfer model, wheras the former, based on the NAHRR, does not. Essentially, the ERx curve describes the chemical energy (or heat) release of an engine cycle as a function of the crank angle, after subtracting the heat loss to the surroundings.

Figure 5.9a presents the normalised net heat release as a function of crank angle for an example cylinder. This curve effectively illustrates the progression of the combustion process, indicating the cumulative energy released during the expansion stroke. Key combustion milestones are marked where the normalised heat release reaches 10%, 50%, 90%, and 95%, denoted as ER10, ER50, ER90, and ER95, respectively. These are visually highlighted with vertical red lines at crank angles of 2.1°, 16.6°, 36.6°, and 46.6°.

Combustion is largely complete by approximately 80° crank angle, beyond which the energy release becomes negligible. This representation provides insight into the timing and duration of the combustion event within the cylinder.

The second part of Figure 5.9b compares the crank angles corresponding to specific energy release points (e.g., ER10, ER25, ER50) across all cylinders. This comparison reveals cylinder-to-cylinder variations in combustion phasing. Most notably, cylinder A5 shows a delayed energy release relative to the other cylinders. While this deviation could suggest a potential anomaly—such as delayed ignition, injector irregularity—it may also fall within the normal statistical variation observed in multi-cylinder engines. Such comparisons are useful for identifying cylinders with atypical combustion behaviour and can inform further diagnostics or targeted maintenance actions.

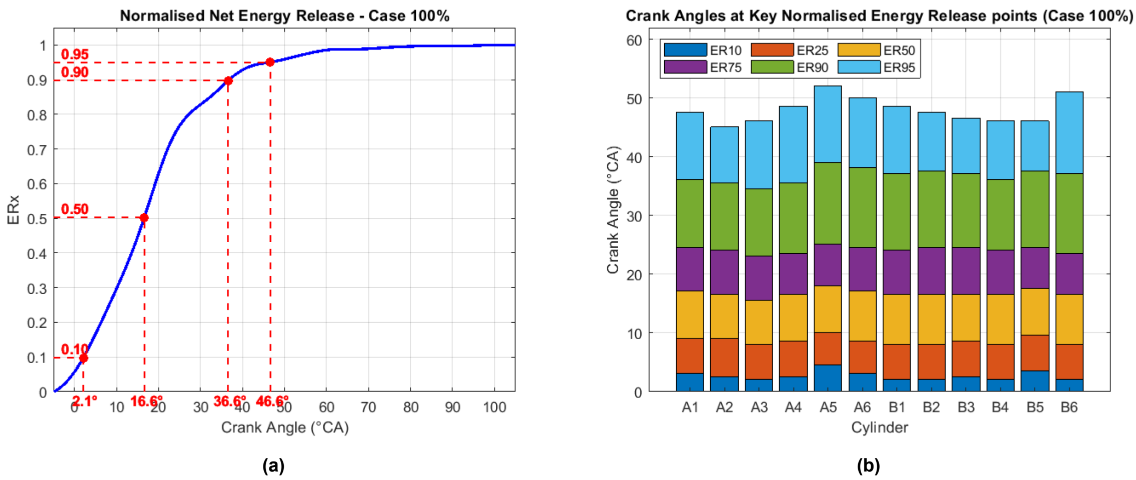

Figure 5.9: Normalised net heat release at 100% MCR. (a) Cumulative energy release curve for a representative cylinder, highlighting key combustion milestones (ER10, ER50, ER90, ER95). (b) Comparison of crank angles corresponding to specific energy release levels across all cylinders, illustrating cylinder-to-cylinder variation in combustion phasing.

5.2.2. Simulink® model

The calculation of the parameters NAHRR and Q_{net} is performed using the MATLAB® - Simulink® model shown in Figure 5.10.[2] The model has two inputs:

1. The angular velocity ω (omega) of the crankshaft (rad/s), equal to $2\pi n/60$ where n is the recorded engine speed (rpm) at the time of the measurement.
2. A set of measured cylinder pressures (Pa).

All units used in this model are fundamental SI-units, e.g. J, J/s or W. More convenient units as kJ/° crank angle or kW are the result of post-processing. The crank angle θ (theta) is calculated by integration of ω. The integrator also fulfils the task of synchronising the pressure with the correct crank angle. This is done by assigning the proper initial value to the integrator, using the TDC shift determined by the method explained in Section 4.1. The function block "cylinder volume" calculates V as a function of θ using Eq. 5.4. Rather than differentiating the cylinder volume, the term dV/dt is calculated using the function block "dV/dt". This analytical function uses Eq. 5.5, multiplying the term $dV/d\theta$ by $d\theta/dt$, or ω. The multiplicators K1 and K2 represent the terms

$$K_1 = \frac{1}{\gamma - 1}, K_2 = \frac{\gamma}{\gamma - 1}$$

from Eq. 5.3. The term dp/dt, or the rate of pressure rise (RoPR), is produced by the differentiator block "dp/dt", which computes the time derivative of the cylinder pressure. This parameter represents the rate at which the cylinder pressure increases during combustion, and is typically measured in pressure per unit of crank angle (e.g., bar/°CA). A higher RoPR indicates a more rapid combustion process, caused by a larger amount of fuel being burned in a shorter time. This can lead to increased engine power output but may also result in higher thermal and mechanical stresses on engine components.

The model output is:

1. The net apparent heat release rate NAHRR (J/s).
2. The cumulative apparent heat release Q_{net} (J).
3. The indicated work W_i (J).

The output NAHRR (in J/s) results from adding the terms $K_1 V dp/dt$ and $K_2\, p\, dV/dt$.[3] Output Q_{net} (in J) is the result of integrating NAHRR. By definition, $Q_{\text{net}} = 0$ at SOC. However, the exact moment

[2] The model is time-based rather than angle-based. This allows for the model to be extended with a (time-based) heat transfer model at a subsequent stage, if so desired.

[3] In order to express NAHRR in the more convenient unit of kJ/°CA, the value must be divided by ω. This is done during post-processing in order to keep the Simulink model as concise as possible.

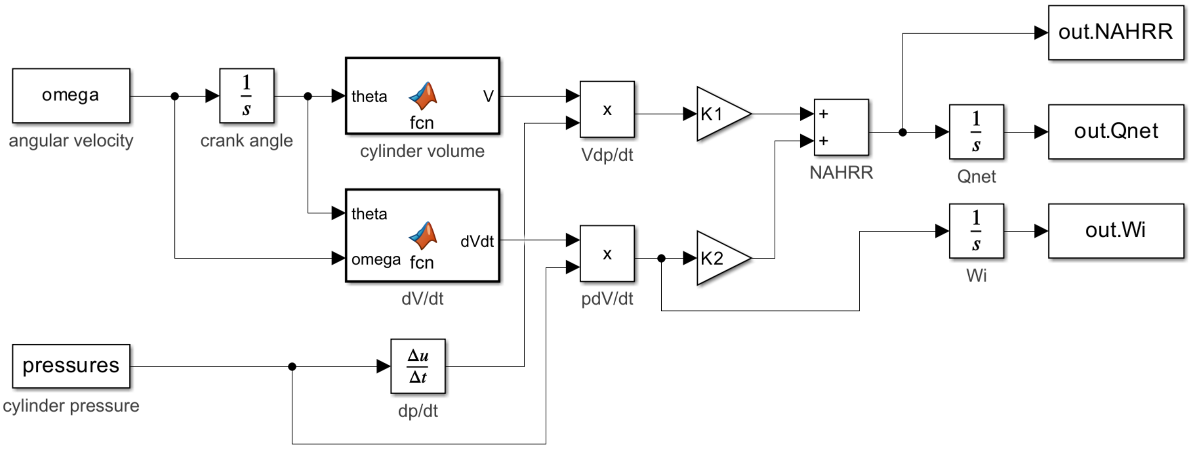

Figure 5.10: Simulink model for determining NAHRR and Q_{net}

or crank angle of SOC is not known a priori. Hence, the integrator "Qnet" is arbitrarily given an initial value of 0 at the start of the simulation, resulting in a certain offset at SOC. After the simulation, the initial value may then be adjusted with the correct offset. Starting with the new, correct initial value, the simulation can then be repeated to give the correct Q_{net}.

In addition, the model computes the indicated work by integrating the term pdV/dt. The indicated work W_{i} is defined as $\oint pdV$ (Eq. 2.3) for a whole engine cycle (i.e., 720°CA). Accordingly, the final output of the integrator block "Wi" corresponds to the total indicated work W_{i}.

Once both the net total heat release, $Q_{\text{net,tot}}$, and the indicated work, W_{i}, are known, the *thermodynamic efficiency* of the cycle can be evaluated. This metric quantifies how effectively the engine converts the chemical energy of the fuel—after accounting for heat losses (as represented by the net heat release)—into useful work. The thermodynamic efficiency, η_{td}, is defined as:

$$\eta_{\text{td}} = \frac{W_{\text{i}}}{Q_{\text{net,tot}}} \tag{5.9}$$

This definition is consistent with the thermodynamic treatment of internal combustion engines, as outlined by Klein Woud [37]. Determining the *effective efficiency* or the *indicated efficiency* would additionally require the evaluation of mechanical losses and heat transfer effects; this is not done here.

The efficiency η_{td} can be computed on a per-cylinder basis to assess the relative performance of individual cylinders. Significant deviations in η_{td} between cylinders may indicate issues related to combustion quality, injector performance, or cylinder-specific losses.

As previously discussed, the current model does not include a heat-transfer submodel. Consequently, it eliminates the need to calculate the temperature and composition of the in-cylinder gas mixture, as well as the need for uncertain estimations of surface temperatures of the cylinder wall, cylinder head, and piston crown.

5.3. Fault detection and diagnosis

This section outlines the diagnostic methodology employed to detect and identify specific faults based on cylinder pressure measurements. The approach combines manufacturer guidelines with independent diagnostic criteria to evaluate engine condition and cylinder-specific performance.

Diagnostic thresholds and reference conditions

The first step in the diagnostic process involves consulting the operational guidelines provided by the original equipment manufacturer (OEM). According to these guidelines, the nominal peak pressure at nominal engine load is 190 bar, with an allowable deviation of up to 7 bar from the mean across individual cylinders. Similarly, for exhaust gas temperatures, a maximum permissible deviation of 100 °C from the mean of all cylinders is specified [45].

For performance parameters not explicitly addressed by the OEM, supplementary standards must be applied. Hountalas [30] proposes a general diagnostic rule allowing a maximum deviation of ±3%

from a ”reference engine” — typically an engine in a verified nominal condition, such as that observed during a factory acceptance or test bench trial.

In this study, the reference point is established using data from HNLMS Groningen immediately following a major engine overhaul and scheduled maintenance carried out in March 2023, after approximately 16,000 operating hours. This post-maintenance condition is assumed to represent nominal engine performance, and thus serves as a benchmark against which subsequent measurements can be evaluated. Comparisons with later data sets allow for the detection of deviations in cylinder performance, which may indicate the development of mechanical wear, injector faults, or other system anomalies.

Monitored parameters and diagnostic strategy

The following parameters are evaluated to assess cylinder-level performance and combustion quality:

- Peak pressure, averaged over the measured cycles.[4]
- Compression pressure at fixed crank angles before TDC.
- Indicated mean effective pressure (IMEP).
- Combustion characteristics: net total heat release $Q_{\text{net,tot}}$, and crank angles corresponding to characteristic intervals of net cumulative energy release (e.g., Q10, Q50, Q90).
- Thermodynamic efficiency, defined as $W_{\text{i}}/Q_{\text{net,tot}}$.

Comparative analysis across cylinders enables identification of abnormal behaviour indicative of potential mechanical issues or deviations in fuel delivery. As the focus of this work is the fuel injection system, deviations in compression pressure are of secondary interest. If, however, an anomaly in peak pressure is detected, it may result either from combustion irregularities or from gas leakage (e.g., via valves, piston rings, or liner wear). To differentiate between these causes, compression pressure is also assessed. If compression pressure remains within the expected range, the root cause is more likely related to combustion — potentially implicating injector or fuel-injection pump malfunction, incorrect fuel quantity, or timing deviation.

Influence of operating conditions and sea-state

It is important to acknowledge the potential influence of external conditions during measurement. Due to vessel motion, minor fluctuations in engine load may occur even within the short duration (3–5 seconds) required to acquire 25 consecutive engine cycles per cylinder. These dynamic effects may partly explain the cycle-to-cycle variations observed earlier in Section 5.1.

Therefore, if a parameter exceeds the $\pm$3% diagnostic threshold, further investigation is required to determine whether the deviation reflects a genuine fault or is a consequence of transient load variation due to sea-state. In such cases, a correlated rise or fall in multiple parameters (e.g., peak pressure, IMEP, and total energy release) across all cylinders may indicate a global load change, rather than a cylinder-specific issue.

Diagnostic outcome

The analysis of various indicators extracted from cylinder pressure measurements taken at different times is aimed at the early detection and identification of emerging faults, particularly in the fuel injection system. By combining OEM tolerances with data-driven comparisons to a known-good reference state, this method provides a framework for onboard condition monitoring and informed preventative maintenance decisions.

[4] The crank angle of peak pressure is not considered a reliable diagnostic indicator, as motivated in Section 5.1.

6 Results

In this chapter, the methodology outlined in the preceding chapters is applied to operational data collected from HNLMS Groningen. As described in Chapter 3, the performance of the engine and its individual cylinders is assessed on three distinct occasions. First, immediately following a major overhaul conducted in the first quarter of 2023 at approximately 16,000 operating hours. Two subsequent data sets are then examined for comparison: one acquired in August 2024 during a transit period—prior to the replacement of a fuel injection pump, around 3400 running hours later—and another obtained following the installation of the new pump. This three-point comparison enables an analysis of the engine's condition and performance over time, including the effects of maintenance interventions.

Section 6.1 presents and analyses the parameters related to overall engine performance, offering insight into trends and deviations at cylinder level. This is followed by Section 6.2, which focuses on parameters associated with combustion behaviour, particularly the net-energy-release characteristics. Finally, Section 6.3 evaluates the results in the context of the fault detection and diagnosis (FDD) framework introduced earlier.

6.1. Performance analysis results

This section presents the results of the engine performance analysis. The methodology outlined in Section 5.1 is applied to the measurement data obtained from the vessel at sea. As outlined previously, particular attention is given to starboard main engine and, specifically, cylinder B2, due to the replacement of its fuel-injection pump. The performance of this cylinder is compared to that of the other cylinders across the three measurement occasions. Nonetheless, as deviations may also occur in other cylinders, all cylinders are considered in the analysis.

During each of the selected measurements, the vessel was operating at the same propulsion control setting: a virtual propeller shaft speed of 200 rpm, which corresponds to an actual propeller shaft speed of 223 rpm and a diesel engine speed of 967 rpm.[1] Although external conditions such as wind and sea state inevitably vary, this approach ensures that operating conditions are as consistent as possible across the different measurements.

The performance parameters (1) peak pressure, (2) compression pressure, and (3) indicated mean effective pressure (IMEP) are evaluated for all cylinders using averaged and smoothed cylinder pressure traces. This enables cylinder-to-cylinder comparison and the identification of abnormal operating behaviour.

Peak pressure

Figure 6.1 presents the peak pressures for all cylinders, averaged over multiple engine cycles. Included in the graph is:

1. A red dotted line representing the overall mean peak pressure, calculated as the average of the peak pressures across all cylinders.

[1] The maximum propulsion control setting is 230 rpm, corresponding to the maximum engine speed of 1000 rpm.

2. The percentage deviation from this overall mean for each cylinder, where green indicates a positive deviation and red bars a negative one.
3. The maximum and minimum peak pressures per cylinder, indicated by an I-shaped marker.

For Case 1 and 3, the average peak pressures are based on 25 engine cycles for every cylinder, while Case 2 is based on 9 cycles.[2] Case 1 (Figure 6.1a) represents the condition immediately following the major engine overhaul, whereas Case 2 (Figure 6.1b) corresponds to the state of the engine approximately 17 months later, shortly before the replacement of the fuel-injection pump in cylinder B2. Case 3 (immediately after the replacement) is shown in Figure 6.1c.

In Case 1, cylinder B2 exhibited the highest peak pressure of all cylinders. By Case 2, its peak pressure had decreased significantly, falling below the average value. In the first dataset, cylinders A1, A5, and B5 appear to underperform relative to the other cylinders. In Case 2, cylinder B1 displays a notably higher peak pressure, while cylinders A3, A5, and B5 show below-average performance.

In Case 3, following the replacement of the fuel injection pump, cylinder B2 appears to have regained its original high-performance state, producing the highest peak pressure. At the same time, peak pressures across the remaining cylinders are reduced. Of particular note is cylinder B5, whose peak pressure declined further.

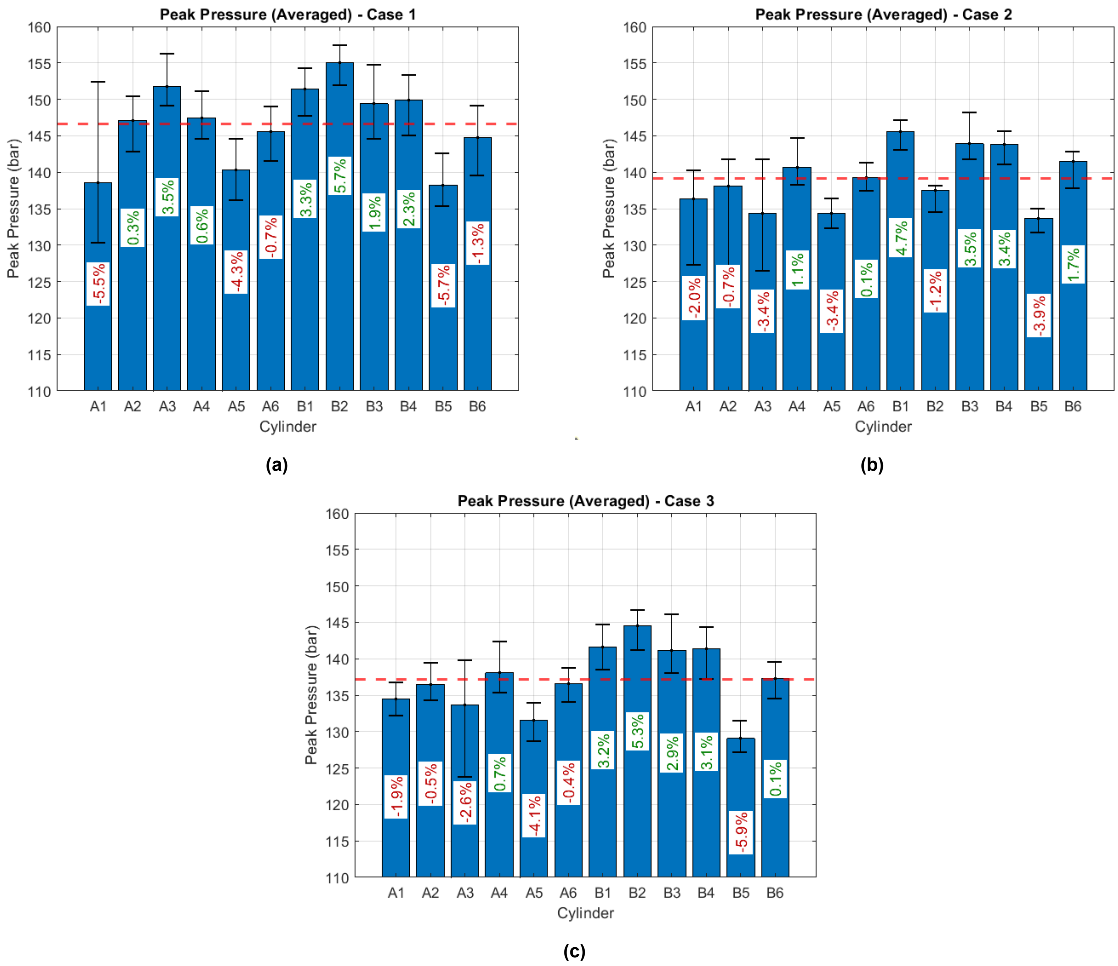

Figure 6.1: Cylinder-to-cylinder variation of peak pressures averaged over multiple engine cycles for each cylinder: (a) Case 1, based on 25 cycles, shortly after overhaul. (b) Case 2, based on 9 cycles, just before fuel-injection pump change. (c) Case 3, based on 25 cycles, right after fuel-pump change.

[2]While 25 cycles were originally recorded for all cases, the data for Case 2 were partially corrupted: the pressure signals for all B-bank cylinders were misaligned with the crank angle across all cycles. This issue was corrected by manually phase-shifting the pressure traces relative to a reference cylinder from the A-bank. Each B-bank cylinder required a different shift per cycle, with the misalignment increasing progressively over the measurement window. Details of this procedure are presented in Appendix D.

Compression pressure

The compression pressures for Cases 1, 2, and 3 are shown in Figure 6.2, measured at crank angles of 45°, 30°, and 20° before top dead center (BDTC). Also shown is the mean value of the compression pressure at 20° BDTC. While some variation in compression pressure is observed between cylinders, it is not considered significant, as the deviations remain within ±3%. The I-shaped markers atop each bar represent the minimum and maximum pressure values at 20° BTDC. Notably, the B-bank cylinders in Case 3 exhibit greater variation. It is unclear whether this reflects a genuine physical difference or is the result of measurement error.

The purpose of including this parameter is to help identify, or rule out, possible causes of anomalies in the cylinder pressure trace. In particular, low compression pressure may indicate leakage past the piston rings or through the intake or exhaust valves, which would affect the overall pressure during the cycle.

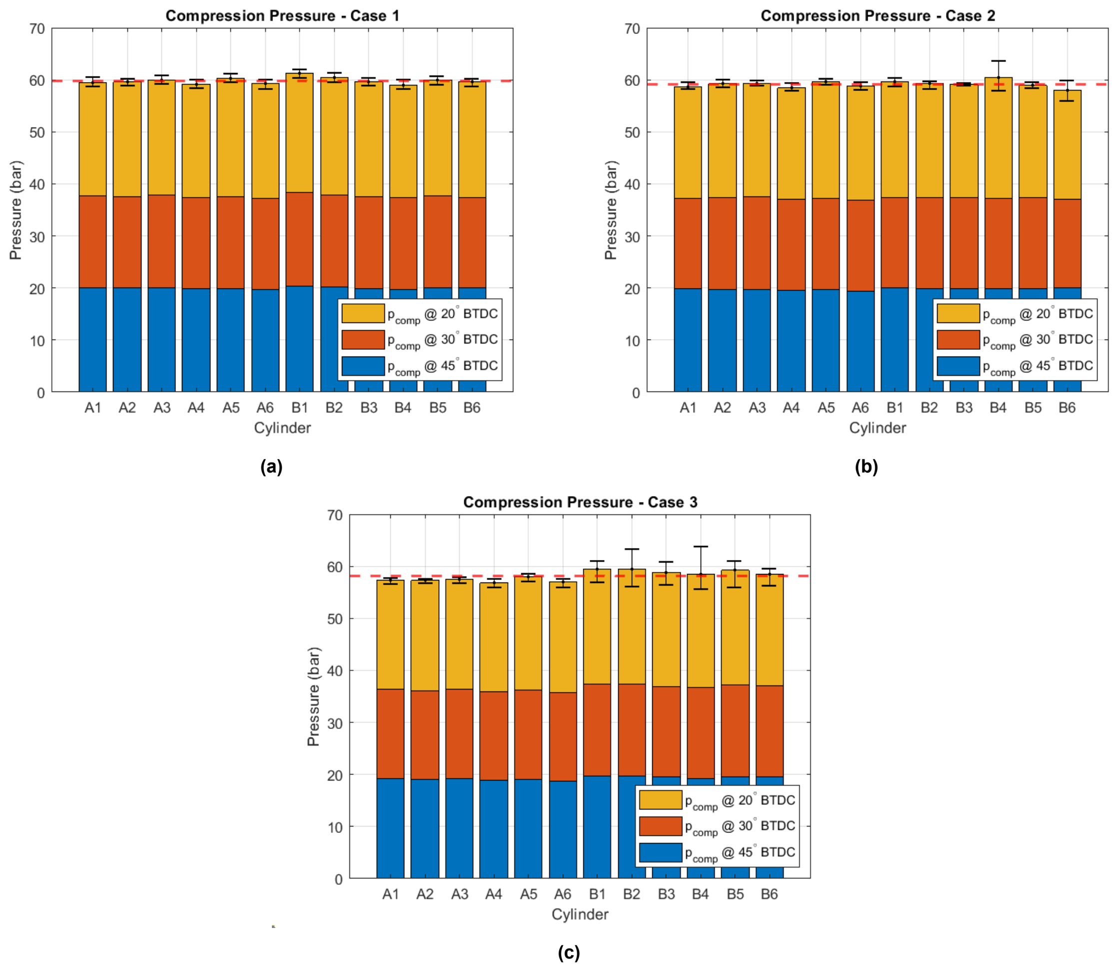

Figure 6.2: Cylinder-to-cylinder variation in compression pressure for all cylinders, with the red line indicating the average compression pressure at 20° BTDC. (a) Case 1: no notable anomalies; (b) Case 2: cylinder B4 shows elevated variation; (c) Case 3: the entire B-bank exhibits above-average variation.

Indicated mean effective pressure (IMEP)

The IMEP, defined by Eq. 5.1, is the third performance parameter considered in this analysis. It is directly proportional to the work output and power contribution of individual cylinders. Figure 6.3 illustrates the cylinder-to-cylinder variation in IMEP across the three cases. The values presented are cycle-averaged IMEP figures, with the mean IMEP across all cylinders also shown to facilitate comparison. Initially, cylinders B1, B2, and B3 exhibit notably higher IMEP values than the others, whereas B5 and B6 appear to underperform. The A-bank displays a relatively uniform performance. In Case 2, cylinder B2 shows a notable reduction in IMEP, consistent with the observed drop in exhaust gas temperature. This decrease in load appears to have been offset by increased contributions from the other cylinders in the B-bank.

In Case 3, following the installation of a new fuel injection pump, the IMEP of cylinder B2 is restored to a level more than 3% above the average. The overall distribution in Case 3 closely resembles that of Case 1, with cylinders B5 and B6 continuing to underperform, compensated by stronger performance from B1 and B2. Notably, the low peak pressure values observed in cylinders A1, A3, and A5 are not reflected in their corresponding IMEP values. This suggests that the diagnostic value of peak pressure as an indicator of cylinder performance is limited.

Notably, in Case 3, the mean IMEP across all cylinders (21.9 bar) is 4% lower than in the other two cases (22.8 bar), indicating that the engine is operating at a 4% lower load overall, although the propulsion control setting is the same. This is likely due to more favourable weather conditions.

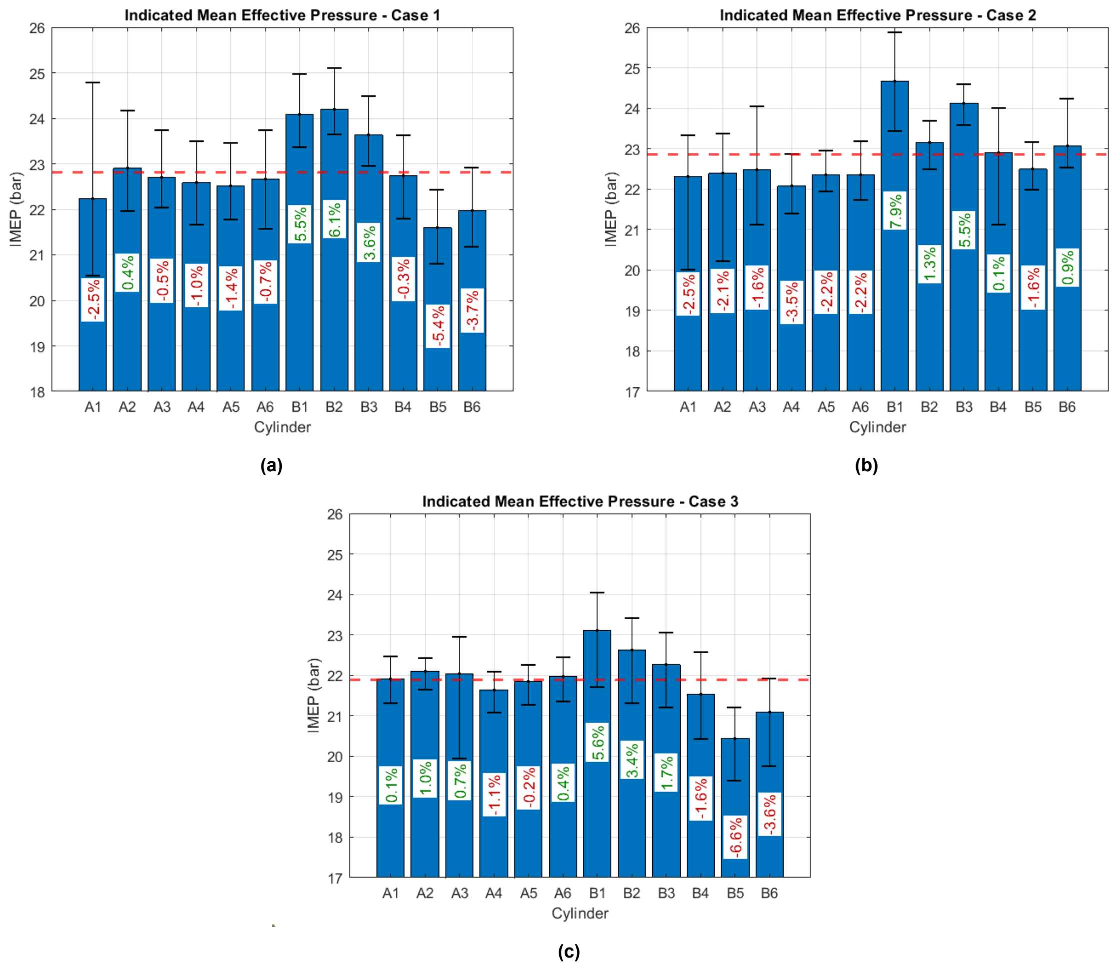

Figure 6.3: Cylinder-to-cylinder variation of cycle-averaged IMEP: (a) Case 1, (b) Case 2, (c) Case 3.

6.2. Combustion analysis results

This section presents the results of the combustion analysis, based on combustion characteristics quantified by the following metrics: (1) net total heat release, (2) crank angles corresponding to characteristic points of the cumulative net heat release (e.g., 10 kJ, 25 kJ, 40 kJ), and (3) thermodynamic efficiency.

Net total heat release

The net total heat release $Q_{\text{net,tot}}$, based on the *net apparant heat release rate*, from all cylinders, is the first combustion-related parameter to be examined for the three cases. Figure 6.4 illustrates how $Q_{\text{net,tot}}$, defined by Eq. 5.7, varies across the cylinders. The resulting trends closely resemble those observed in the IMEP distribution across the cylinders (Figure 6.3). As before, the A-bank exhibits relatively uniform values, while cylinders B1 and B2 initially show elevated energy release, and B5 and B6 underperform. Prior to the replacement of its fuel injection pump, cylinder B2 displayed a noticeable drop in heat release, which appears to have been compensated by the other cylinders on the B-bank.

The two quantities, $Q_{\text{net,tot}}$ and IMEP, appear to be strongly correlated, which is expected: a higher energy input generally results in a greater indicated work output. It is noteworthy that the mean value of $Q_{\text{net,tot}}$ across all cylinders increased from 82.5 kJ in Case 1 to 84 kJ in Case 2, representing a 1.8% increase, while the IMEP remained constant between the two cases. This observation suggests that the overall thermodynamic efficiency decreased by approximately the same proportion during that period.

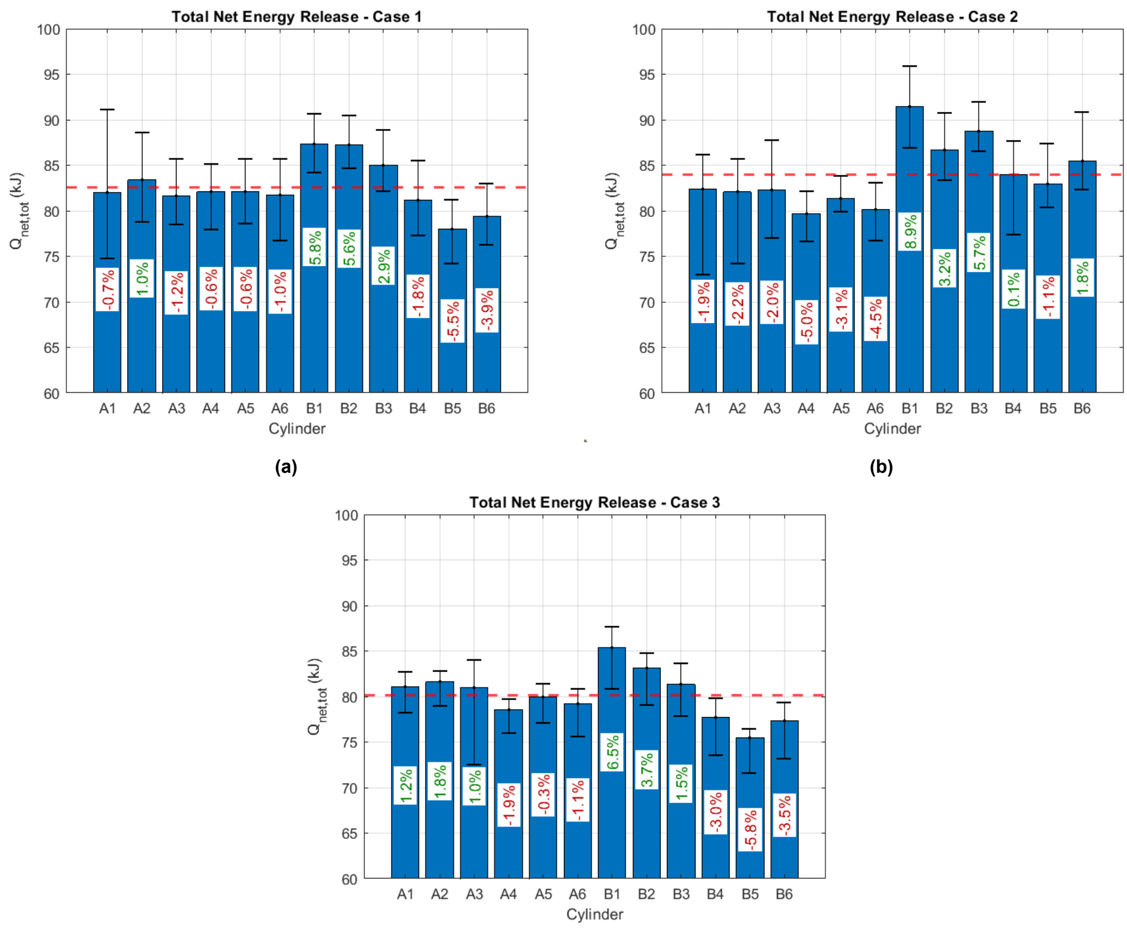

(c)

Figure 6.4: Cylinder-to-cylinder variation of total net energy release: (a) Case 1, (b) Case 2, (c) Case 3

Cumulative net heat release

Figure 6.5 shows the cumulative energy release levels across all cylinders, illustrating cylinder-to-cylinder variation in combustion phasing. Shown are the respective lines corresponding to an energy release of 10 kJ (Q10), 25 kJ (Q25), 40 kJ (Q40), and so on. Initially (Case 1), cylinders A1, A5, and B5 stand out because of the relatively late energy release values. The differences between the individual A-bank cylinders are small compared to the B-bank cylinders. In particular, B5 shows distinct peaks at Q75 in Cases 1 and 3, suggesting that the late combustion phase extends significantly longer than other cylinders. Overall, it is B5 that stands out in its cylinder bank.

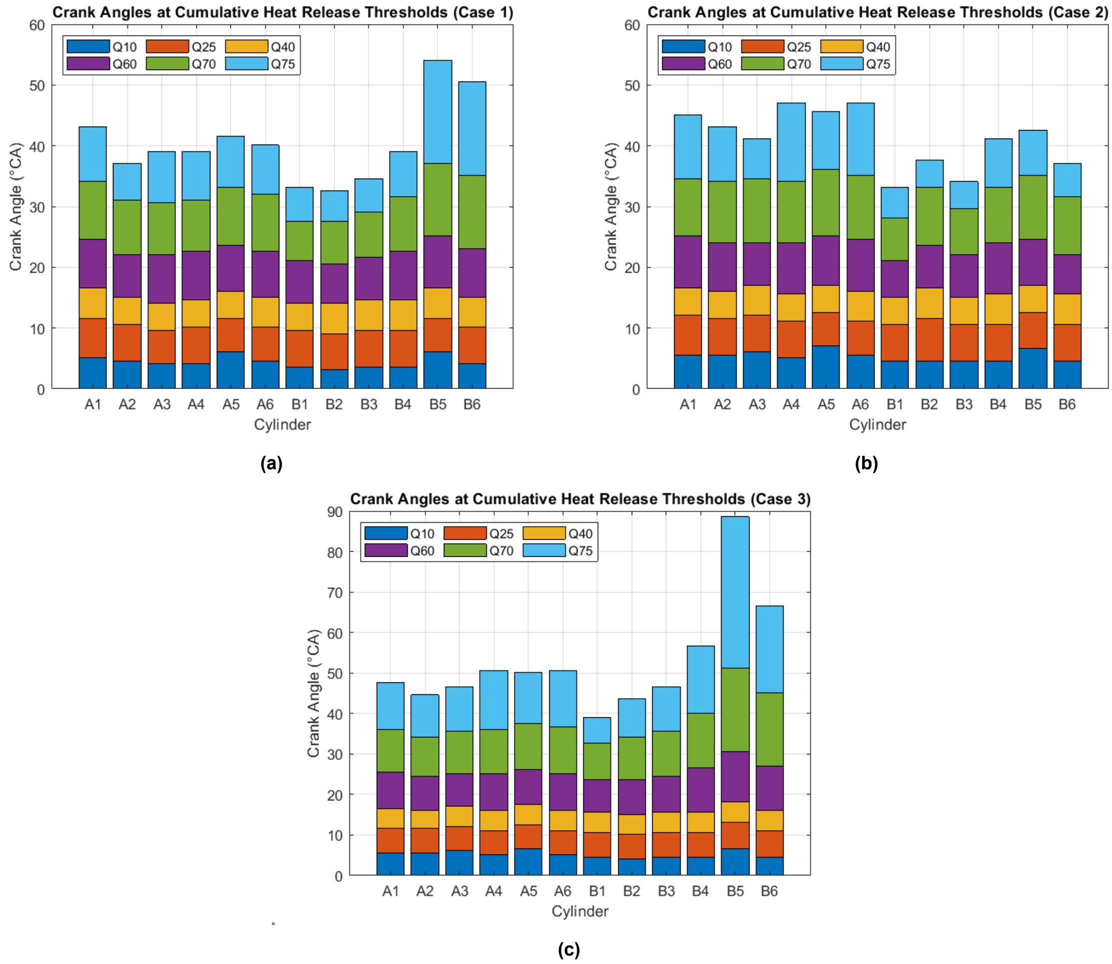

Figure 6.5: Cylinder-to-cylinder variation in cumulative net heat release for: (a) Case 1, (b) Case 2, and (c) Case 3. The lines indicate the crank angles at which each cylinder reaches specific cumulative heat release values—10 kJ (Q10), 25 kJ (Q25), and so on—highlighting differences in combustion phasing between cylinders.

Thermodynamic efficiency

Figure 6.6 presents the thermodynamic efficiencies (η_{td}) of all cylinders for the three cases examined. Deviations from the mean are expressed as relative percentage differences with respect to the average η_{td} value. In Case 1, the differences between cylinders appear minor. Cylinder A1 shows a slight deficit of -1.8%, which, being within a 3% margin, is not considered significant.

In Case 2, the thermodynamic efficiencies of all B-bank cylinders decrease noticeably, following a 2% drop in η_{td} for cylinder B2. This results in a 1.5% reduction in the overall mean thermodynamic efficiency. After the replacement of B2's fuel-injection pump (Case 3), its η_{td} increases by approximately 1.4%. Overall, the variations between cylinders remain small (less than 3%), making it difficult to draw firm conclusions regarding the condition of the fuel-injection system.

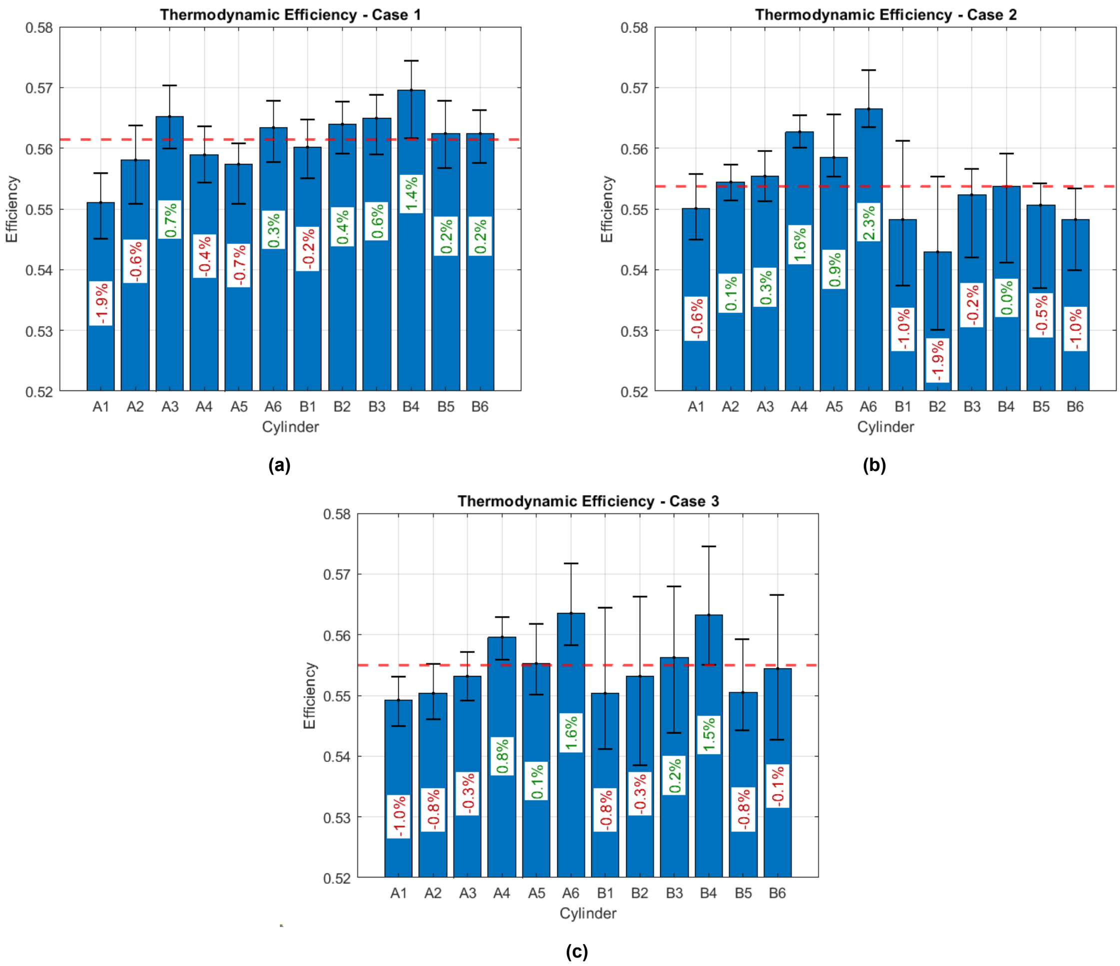

Figure 6.6: Cylinder-to-cylinder variation of thermodynamic efficiency: (a) Case 1, (b) Case 2, (c) Case 3.

6.3. FDD results

This section presents the results of the fault detection and diagnosis on a per-cylinder basis. As outlined in Section 5.3, both the engine OEM's criteria and a general threshold of 3% allowable deviation for any individual cylinder relative to the others are applied.

We begin by examining the **peak pressures**. Strictly speaking, the OEM guideline, which specifies a maximum allowable deviation of 7 bar from the mean, applies only under nominal conditions (i.e., 100% MCR). One might expect that cylinder-to-cylinder variation would diminish at lower loads. However, a comparison of Figure 5.2a (100% load) and Figure 6.1a (~75% load) reveals that the differences remain similar. Therefore, we continue to apply the OEM guideline under the part-load conditions of Cases 1, 2, and 3.

Based on these criteria, cylinders A1, B2, and B5 would be classified as non-compliant in Case 1.

In Case 2, all cylinders meet the criterion and are considered to be operating satisfactorily. In Case 3, cylinders B2 and B5 again fall outside the acceptable range. Ironically, cylinder B2 would have to be rejected both before and after the replacement of its fuel-injection pump—yet not at the time the decision was made, which was based on a deviating exhaust gas temperature. Hence, strictly adhering to the OEM guidelines regarding peak pressure does not appear to be the most prudent approach.

The next parameter under consideration is the **compression pressure**. As outlined in Section 6.1, compression pressures were examined at fixed crank angles of 45°, 30°, and 20° BTDC. The inter-cylinder variation remained within a 3% tolerance range. This indicates that there is no appreciable leakage (blowby) past the piston rings[3] or through the intake or exhaust valves.

Next, we consider the **IMEP**. According to the $\pm 3\%$ criterion, five out of six cylinders on the B-bank would be classified as non-compliant in Cases 1 and 3, as shown in Figure 6.3. In Case 2, however, cylinder B2 falls within the acceptable range. Based on this metric, there is no indication of a malfunction in its fuel-injection system. Rather, cylinder B5 stands out due to underperformance, likely causing other B-bank cylinders, particularly B1 and B2, to compensate by delivering slightly higher load. This suggests a load imbalance rather than a fault in B2 itself.

The first combustion parameter under consideration is the **total net heat release**, $Q_{\text{net,tot}}$. Although in Case 2 three A-bank cylinders deviate by more than 3% from the mean, the overall variation within the A-bank remains approximately 3%. In contrast, the B-bank exhibits a variation exceeding 10%, indicating a notable imbalance in combustion performance. Most notably, cylinder B1 appears to compensate for the underperformance of cylinder B5.

The second combustion parameter considered is the **net cumulative heat release**, specifically the crank angles corresponding to characteristic intervals of the cumulative heat release curve. The observed variations suggest that combustion in cylinder B5 occurs relatively late compared to the others. However, it would be difficult to define a definitive rejection criterion based on this metric, as the acceptable range of variation is not clearly established.

Lastly, the **thermodynamic efficiency** is examined. Overall, the values exhibit minimal variation. In all cases, cylinder-specific efficiencies remain within a range of $\pm 3\%$ of the mean. Therefore, based on this metric, no corrective action would be considered necessary.

Conclusion

The observed trends suggest that cylinders B1 and B2 have been compensating for the underperformance of cylinder B5, and to a lesser extent, B6. The crew's decision to replace the fuel-injection pump and injector of cylinder B2, triggered by its increasingly deviating exhaust gas temperature (see Fig. 3.5), is understandable. It is possible that these components were indeed beginning to degrade, although not yet to the extent that immediate replacement was necessary.

However, based on the evaluated parameters quantifying cylinder and combustion performance, there is no conclusive evidence to justify the rejection of the fuel-injection pump and injector of cylinder B2. On the contrary, the data consistently indicate that cylinder B5 is significantly underperforming. This is reflected in its lower peak pressure, reduced IMEP, decreased total net energy release, and delayed combustion. Importantly, these issues are not attributable to poor compression, suggesting that the combustion process itself is impaired, likely due to inadequate fuel delivery. Given these findings, it would be prudent to examine the condition and functionality of the fuel-injection pump and injector of cylinder B5.

[3] As discussed in Section 2.3.2, a blowby rate of 0.5–1% of total air flow is considered normal.

7 Conclusions and recommendations

This chapter presents the main conclusions of this thesis and provides recommendations based on the findings of this research. In Chapter 1, the central research question was formulated as follows:

> *How can a cylinder pressure measurement system of a naval vessel's main engines be used effectively for the analysis of engine performance, combustion, and fault detection and diagnosis?*

To address this question, several subquestions were formulated and investigated throughout the thesis. These subquestions are answered concisely in Section 7.1, followed by a final answer to the central research question. Section 7.2 then presents recommendations for practical implementation, along with suggestions for future research to further improve the usefulness and effectiveness of cylinder pressure measurement in naval applications.

7.1. Conclusions - answers to research questions

This section lists the conclusions of this thesis in the form of answers to the research subquestions posed in Section 1.2. Then, an answer to the main research question is provided.

1. **What are the key components and operating principles of a cylinder pressure measurement system?**

   The primary components of a *permanent* cylinder pressure measurement system include pressure sensors, usually of the piezoelectric type—one for every cylinder—mounted in the cylinder head; charge amplifiers (one per sensor); an A/D converter; and a data acquisition system. Piezoelectric pressure transducers do not measure absolute pressure but respond only to changes in pressure. To relate the pressure to an absolute value requires an additional sensor. For this purpose, the pressure sensor in the intake manifold is typically used.

   Crank-angle measurement and trigger mechanisms are also essential, usually mounted on the camshaft and/or crankshaft. The system generates discrete data sampled at fixed crank-angle intervals, which can then be processed and analysed.

2. **What are the technical and operational requirements for implementing such a system on the main engines of a naval vessel?**

   A critical requirement is the capability for continuous cylinder pressure measurement and automated recording, in contrast to traditional intermittent methods where an operator manually measures each cylinder in sequence. This conventional approach is time-consuming and less reliable due to varying engine conditions during acquisition. In contrast, an automated system continuously samples and buffers pressure data from all cylinders simultaneously. Data *recording* is event-driven, e.g., triggered manually by the operator, at pre-defined time intervals, or automatically in case of a sudden engine shutdown. For reliable comparison of measurements over time, it is critical that data be collected under comparable engine conditions, such as similar loads, speeds, and environmental factors. This can be integrated into regular operational procedures, for example, during (daily) turbocharger flushing, which typically occurs at high engine load and provides a consistent reference condition.

From a technical integration standpoint, it is essential that the system be compatible with the engine. When the system is installed as a retrofit and is not supplied by the engine OEM, it may not be fully compatible with the engine's existing layout. This was the case on HNLMS Groningen, where a custom synchronisation solution had to be developed. The original camshaft-mounted position sensor could not be used, because this signal is not accessible outside the engine management system. Instead, a metal bolt was installed on the flywheel to serve as a trigger for an inductive sensor, providing a crank-angle reference once per revolution. In addition, a crank angle encoder was installed to ensure accurate timing correlation between the crankshaft position and the pressure signal.

3. **How does the marine environment affect the accuracy and reliability of cylinder pressure measurements?**

   A key advantage of the implemented system is its capability to perform continuous cylinder pressure measurements while at sea, with each data acquisition requiring only a few seconds. In contrast, sequential cylinder pressure measurements may take up to a half hour per engine, during which time engine load may fluctuate due to changing wind and sea conditions. By significantly reducing measurement duration, the system minimises the impact of such variations, improving the accuracy and reliability of the collected data. Furthermore, the system enables the collection of a sufficient number of measurements to support trend analysis over time.

   However, under rough sea conditions, even brief measurements can be affected by fluctuations in engine parameters, as demonstrated in Section 4.2. In particular, variations in intake manifold pressure during data acquisition may compromise measurement accuracy if not properly accounted for. Furthermore, when comparing measurements taken at similar or identical propulsion control settings but at different times, differences in weather and sea state can result in significantly different engine loads. In general, higher sea states impose greater loads on the engine, leading to increased cylinder pressures and derived performance parameters. Interpretation of such data must consider these external influences to avoid misdiagnosis.

4. **What preprocessing steps are required to convert raw cylinder pressure data into usable formats for analysis?**

   As described in Chapter 4, the first step involves ensuring that the pressure signal is correctly aligned with the crankshaft position by accurately determining the TDC position. The method adopted in this work employs a temperature–entropy diagram of the stopping engine to identify TDC. The second step is to reference the cylinder pressure to a known pressure, which, in this case, is the intake manifold pressure recorded by the ship's automation system. In situations where the manifold pressure fluctuates significantly or the pressure sensor is faulty, an alternative method is required. For such cases, a linear least-squares approach is used to determine the appropriate pressure offset.

   The final step in the preprocessing procedure is the smoothing of the pressure signal. Initially, pressures may be averaged to reduce both random noise and cycle-to-cycle variation. However, averaging alone does not eliminate non-random noise, necessitating an additional smoothing step. In this work, a cubic spline method is employed for this purpose. This not only smooths the original pressure trace but also ensures that the derivative of the pressure signal is suitably smooth, which is essential for accurate combustion analysis.

5. **What useful performance indicators can be derived from cylinder pressure data?**

   The most useful cylinder performance indicators identified in this study are the indicated mean effective pressure (IMEP), compression pressure, and, to a lesser extent, the peak pressure p_{max}. The compression pressure and p_{max} can be readily extracted from cylinder pressure data. The IMEP requires integration of the pressure–volume diagram across the engine cycle. Comparing the respective values of these performance indicators across the different cylinders provides insight into the relative performance and condition of each cylinder. It is important to note that p_{max} and IMEP are not necessarily well correlated: as this study has shown, a cylinder exhibiting a high p_{max} compared to others does not automatically produce a high IMEP, and conversely, a low p_{max} does not necessarily indicate a low IMEP. In this context, IMEP is the more informative metric, as it directly reflects the net work output of the cylinder. The distinction between IMEP and p_{max} is important to keep in mind, as in practice, such as during engine factory acceptance tests, only peak pressures are often recorded, rather than the full cylinder pressure trace.

The crank angle at which the peak pressure occurs (APMAX) was also evaluated in this study. However, this parameter exhibited such high variability under normal, steady operating conditions, that it was deemed less suitable for diagnostic purposes.

6. **In what ways can cylinder pressure data provide additional value or insights beyond traditional performance parameters (e.g., fuel consumption, engine load, and power output)?**

   Parameters like fuel consumption and engine load or power typically reflect the overall engine performance, representing the combined effect of all cylinders. In contrast, cylinder pressure measurement has the advantage of enabling performance evaluation on a per-cylinder basis. Specifically, a low p_{max} may be caused by inadequate compression due to, e.g., leakage. If poor compression can be ruled out, a low p_{max} and/or low IMEP is more likely related to combustion problems, narrowing down the range of potential causes.

   Comparing the pressure-based performance indicators may identify imbalances, inefficiencies, or anomalies such as misfiring in specific cylinders, issues that may not be evident from aggregate parameters like fuel consumption or overall power output. Furthermore, when measured continuously, cylinder pressure measurement provides real-time feedback on engine condition, enabling proactive diagnostics and predictive maintenance.

7. **How can cylinder pressure data be used to characterise the combustion process in marine diesel engines?**

   Cylinder pressure data forms the basis for analysing combustion-related parameters. This thesis has focused on (the rate of) net heat release, as well as thermodynamic efficiency. These parameters are derived from the pressure trace and provide insight into the combustion process.

   The *gross* heat release rate, which is directly proportional to the rate of fuel burnt, is a useful combustion parameter but requires the incorporation of a heat transfer model to account for energy lost to the cylinder walls. Such models introduce significant uncertainty and can compromise the accuracy of the results. For this reason, this thesis has focused solely on the *net* heat release rate, which can be determined directly from the pressure data without the need for heat transfer modelling.

   The net heat release rate, and its integral, the net energy release, provide insight into combustion phasing. This thesis has introduced a way for visualising the progression of the net energy release, by displaying cumulative energy release values at various crank angles for all cylinders. This approach clearly reveals cylinder-to-cylinder differences. Absolute values of net energy release (in kJ) were chosen over normalised (non-dimensional) values, as normalisation may obscure underperforming cylinders and hinder accurate diagnostics. In addition, this thesis has examined the thermodynamic efficiency which quantifies how effectively the net *total* released energy (Q_{net}) is converted into work. Deviations in this parameter may indicate suboptimal combustion timing: if combustion occurs too early or too late relative to the piston's position, pressure may not act optimally on the piston, reducing work output.

8. **Can a malfunctioning fuel-injection system be detected through cylinder pressure analysis?**

   The analysis conducted in this thesis has identified several anomalies that may indicate a malfunctioning fuel injection system, particularly in relation to combustion behaviour. Cylinder underperformance is characterised by reduced values of net total energy release and/or thermodynamic efficiency. These anomalies typically coincide with late combustion phasing and low IMEP. Importantly, these findings were not accompanied by any irregularities in compression behaviour, allowing compression-related issues to be ruled out as the underlying cause. This is a promising result, highlighting the potential of cylinder pressure analysis as a diagnostic tool for detecting fuel injection faults.

However, it is important to acknowledge that no components examined in this study were confirmed to have failed. As such, while the results support the feasibility of the proposed fault detection and diagnosis methodology, they are not conclusive. Validation would require confirmed fault cases or evidence of component damage to definitively assess the method's effectiveness.

9. **How does pressure-based fault detection compare in accuracy and timeliness to other diagnostic methods?**

   Traditionally, exhaust gas temperature is used to detect fuel-injection malfunctions. This thesis examined a specific case involving a potentially faulty fuel-injection pump and/or injector, initially flagged due to a deviating exhaust gas temperature. Several pressure-derived performance and combustion indicators were applied to assess this case. Although some deviations were observed, no conclusive evidence linked them directly to a specific fault in the injection system.

   Interestingly, the exhaust gas temperature of the cylinder in question remained within OEM-specified limits, suggesting that the suspected fuel-injection pump may have been replaced prematurely. Post-replacement testing of the pump across three test points showed low flow at medium speed; however, due to the absence of defined rejection criteria, this result was inconclusive. However, after the component was replaced, exhaust gas temperatures across cylinders were well aligned.

   Despite its widespread use, exhaust gas temperature appears to be a limited diagnostic indicator. In this case, it indicated an issue in a different cylinder than the one identified via cylinder pressure analysis. This discrepancy highlights a key limitation: at moderate fault levels, exhaust gas balancing systems may mask injection-related issues, making fault localisation difficult. Moreover, exhaust gas temperature alone cannot reliably distinguish between compression- and combustion-related anomalies—something pressure-derived parameters are better suited for.

   While metrics like peak pressure and IMEP are helpful for assessing general engine performance, they do not pinpoint specific faults such as valve leakage or excessive blowby. These are more effectively detected through deviations in compression pressure. However, the conclusions drawn here remain indicative; definitive validation of pressure-based diagnostics requires the presence of known, verifiable faults to validate the diagnostic insights drawn from pressure data.

Answer to the main research question

Based on the findings of this study, it may be stated that a cylinder pressure measurement system can be used effectively to analyse engine performance, combustion, and fault detection and diagnosis (FDD) in naval main engines, provided that a structured methodology is applied. this methodology consists of the following key components:

1. **Preprocessing of raw cylinder pressure data**
   To ensure accuracy and consistency, the raw pressure signal must be preprocessed. This involves synchronising cylinder pressure with crank angle, determining the correct pressure offset, and applying averaging and smoothing techniques to reduce noise and improve signal quality.
2. **Analysis of performance and combustion parameters**
   Following preprocessing, several performance and combustion-related parameters can be derived. Performance indicators include the indicated mean effective pressure (IMEP), peak pressure, and compression pressure. Combustion-related indicators include the total net heat release, thermodynamic efficiency, and the crank angles at which specific thresholds of heat release are reached.
3. **Fault Detection and Diagnosis (FDD)**
   Cylinder-to-cylinder comparison of these parameters may reveal anomalies, which can be used to identify possible faults. Rejection criteria should be defined based on manufacturer (OEM)

guidelines—though these may require adaptation—and, since the OEM has only specified criteria for peak pressure and exhaust gas temperature, supplemented by operational experience. A structured approach to diagnosis involves determining whether the root cause lies in compression (e.g., valve leakage) or combustion (e.g., injector malfunction).

In conclusion, it may be stated that the findings of this study are promising in terms of the potential and added value of cylinder pressure measurement. It will, however, require actual faults to validate the rejection criteria.

7.2. Recommendations

The following recommendations aim to further enhance the usefulness for the Royal Netherlands Navy (RNLN) of this measurement method and the analysis of the data it provides.

1. **Setup and operational use of a permanent cylinder pressure measurement system**

    - Conduct regular checks of the cylinder pressure measurement system.

      Due to the complex and sensitive nature of the system, it cannot be expected to operate reliably for prolonged periods, e.g., for the duration of a mission, without active supervision. The system has demonstrated recurring malfunctions that have disrupted data collection and analysis. Hence, the system requires regular oversight to ensure proper functioning, and cannot simply be installed and left unattended. In the author's opinion, routine checks should include:

      (a) Performing a measurement and verifying that the pressure traces for all cylinders and cycles are properly aligned.

      (b) Confirming that the recorded pressure at inlet bottom dead center corresponds to the intake manifold pressure, as expected by default.

      (c) Ensuring that measurements are being stored according to the predefined time intervals.

    - Automate data collection and analysis.

      At present, these processes are highly labour-intensive and require specialised engineering skills and in-depth knowledge of engine behaviour, qualifications held by a limited number of already overextended personnel within the RNLN and the Ministry of Defence. This dependency poses a significant risk to the successful adoption and long-term viability of this technically advanced system. The methodology proposed in this thesis offers a practical solution to automate the preprocessing and analysis of cylinder pressure data, thereby reducing reliance on scarce human expertise and enabling more consistent and more frequent use of the system.

    - Establish clear ownership of the system and its data.

      This recommendation is closely tied to the two previous points. Presently, ownership is not clearly defined, which creates the risk that the system will not be properly maintained, regularly used, or that the data will go unanalysed. Onboard engine specialists are responsible for the engines, but not for stand-alone measurement systems like this one. Moreover, they lack the time and qualifications required for the system-specific maintenance tasks, including dismounting sensors and adapters for engine overhauls, reinstalling them afterward, and assess whether the system is functioning properly, or perform troubleshooting.

      From an operational standpoint, user access is also a concern. Initially, the system was conveniently integrated with the Integrated Platform Management System (IPMS). However, after an IPMS update this link was not restored, making the software more difficult to access. This increased threshold discourages regular use by the crew.

    - Establish a database of engine faults and damage cases, along with associated symptoms.

      Although this study has resulted in a preliminary framework for anomaly detection at the cylinder level, the limited number of observed fault cases prevents a full validation of its effectiveness. Preferably, a comprehensive database should correlate specific fault types with characteristic deviations in cylinder pressure signals, ideally at various stages of development. However, the construction of such a database would require a broad range of cylinder-level malfunctions—an undesirable scenario from an operational standpoint.

- If possible, use flush-mounted pressure sensors.
  Using long, small-bore indicating channels introduces acoustic waves within the channel, which become superimposed on the measured pressure signal. This non-random noise must be removed—typically through smoothing or filtering—before calculating combustion-related parameters that rely on the pressure derivative. However, these signal processing steps can lead to a loss of important information. In contrast, flush-mounted sensors eliminate the need for indicating channels and thus avoid introducing such acoustic disturbances, reducing the need for aggressive filtering and preserving more of the original signal integrity. This may require modifications to the cylinder heads, which could be impractical or infeasible for engines already in service.

2. **Preprocessing**

   - Develop and adopt a method for determining TDC position in a loaded engine.
     The method employed in this thesis is applicable only in non-firing conditions and assumes a uniform TDC shift across all cylinders and cycles. When pressure data are not accurately synchronised with crank angle, and if the TDC shift varies between cylinders and/or cycles, a more robust and flexible method is needed. A linear least-squares method, similar to the one used for determining pressure offset, may offer a viable solution.

3. **Cylinder pressure analysis**

   - Exercise caution when considering the crank angle of peak pressure (apmax) as a performance indicator.
     This parameter exhibits significant variability both across cylinders and between engine cycles, even under normal engine conditions. This limits the parameter's reliability for anomaly detection. Superficial or hasty analysis may therefore lead to misinterpretation and erroneous conclusions.

   - The use of peak pressure as an anomaly indicator is not recommended.
     While peak pressure correlates reasonably well with IMEP, it is not a reliable indicator by itself. IMEP is a more robust parameter for anomaly detection purposes.

   - Investigate compression pressure when anomalies in IMEP are detected.
     This helps to either identify or rule out leakage as a potential source of the anomaly.

   - Report on maintenance tasks that may influence cylinder pressures.
     The engineer analysing cylinder pressure data should be fully informed about the engine's maintenance status. As we have seen, certain maintenance activities can significantly impact the pressures within individual cylinders. An example is the replacement of a fuel pump or injector, as demonstrated in this thesis. Other interventions that may affect cylinder pressures include adjusting valve clearance, replacing a piston, or changing piston springs. Furthermore, as shown, replacing a fuel pump in one cylinder can influence the pressures not only in that cylinder but also in others.

Suggestions for further research

The cylinder pressure measurement system on HNLMS Groningen provides ample opportunity for new research. Some suggestions are:

- Compare and evaluate different dynamic methods of TDC determination (see Section 2.2.1); determine which of these methods is most accurate. This is particularly relevant, because it was observed that the cycle-to-cycle synchronisation varied significantly during certain measurements. For these instances, a method is required that determines TDC for firing cylinders.

- Compare different smoothing or filtering methods with regard to the pressure signal. Evaluate whether and to what extent each method affects the combustion-related parameters.

- With regard to heat transfer from the cylinder: there is a large uncertainty in the values of the heat transfer coefficient h as well as the cylinder wall temperature (ref. Eq. 2.7) during combustion. This uncertainty impacts the calculated instantaneous heat transfer rate and, as a consequence, the heat release rate. It would be interesting to determine the influence of the parameters that make up the value of h and the assumed cylinder wall temperature on the heat-release rate. How would this relate to the net heat release parameters determined in this thesis?

- When the opportunity arises, it would be interesting to verify whether there is a difference in measured cylinder pressures and derived parameters before and after engine overhaul, or before and after engine modification.[1]

- As described in Section 2.3.1, the indicated power can be derived from cylinder pressure data. When, in addition, the engine's torque would be measured, the engine's friction power and mechanical efficiency can be determined. This provides insight in the specific engine losses. Alternatively, the propeller shaft torque may be used, together with (known/assumed) gear box losses, to calculate the engine's mechanical efficiency and friction losses.[2]

[1]The OPV's engines will be modified during the planned mid-life upgrade scheduled from 2025-2028. Most significantly, the charge-air coolers of all engines will be replaced.

[2]In June 2025, HNLMS Groningen is performing maneuvering trials to determine the influence of the Hull Vane. During these tests the propeller shafts will be equipped with accurate torque sensors. This would be a good opportunity for the suggested research.

A

Redlich-Kwong equation of state

In Section 4.1, the Redlich–Kwong equation was introduced as a more accurate alternative to the ideal gas law. This equation of state was originally proposed in a 1949 paper, where the authors stated: *"An equation of state containing two individual coefficients is proposed which furnishes satisfactory results above the critical temperature for any pressure"* [60]. While acknowledging that the theoretical basis for their model is "by no means rigorous," Redlich and Kwong justified its use on the grounds that it provides a high degree of accuracy through relatively simple means. As a result, the Redlich-Kwong equation has become widely adopted in Thermodynamics. The remainder of this section outlines how the Redlich–Kwong equation can be applied to various gases.

The Redlich–Kwong equation is an empirical, two-constant equation of state that improves upon the (two-constant) van der Waals model, particularly at higher pressures [49]. It is expressed as:

$$p = \frac{\bar{R}T}{\bar{v} - b} - \frac{a}{\bar{v}(\bar{v} + b)T^{1/2}} \tag{A.1}$$

where:

- constants a and b account for the non-ideal behaviour of gases;
- $\bar{R}$ denotes the universal gas constant, 8314 J/kmol$\times$K.
- $\bar{v}$ is the specific volume in m^3/kmol.

With a and b set to zero, Eq. A.1 reduces to the ideal gas law. The constant a accounts for the attractive forces of the individual molecules in the gas; constant b is a correction for the non-negligible volume of the molecules. Both a and b can be evaluated in terms of the critical pressure p_c and critical temperature T_c of the gas, using the fact that following mathematical conditions apply to the critical point:

$$\left(\frac{\partial^2 p}{\partial \bar{v}^2}\right)_T = 0, \left(\frac{\partial p}{\partial \bar{v}}\right)_T = 0 \tag{A.2}$$

Physically this means that in a p–V diagram, the critical isotherm (i.e., the isotherm that passes through the critical point) has an inflexion point and a horizontal tangent at the critical point. Applying these conditions to Eq. A.1 results in three equations with three unknowns: a, b and $\bar{v}_c$. Solving these equations gives the following result for a, b and $\bar{v}_c$ in terms of critical pressure and temperature:

$$a = \frac{1}{9(\sqrt[3]{2} - 1)} \frac{\bar{R}^2 T_c^{2.5}}{p_c} \tag{A.3}$$

$$b = \frac{\sqrt[3]{2} - 1}{3} \frac{\bar{R}T_c}{p_c} \tag{A.4}$$

$$\bar{v}_c = \frac{1}{3} \frac{\bar{R}T_c}{p_c} \tag{A.5}$$

Eqs. A.3 and A.4 provide a means to calculate the Redlich-Kwong parameters a and b for gases with known critical properties. Table A.1 lists these constants, along with the molar mass and critical point data, for several substances commonly encountered in combustion engine analysis.

Table A.1: Molar mass, critical point and Redlich-Kwong constants of several substances

Gas	M (kg/kmol)	T_c (K)	p_c (bar)	a (J m^{3}K$^{0.5}$/kmol^2)	b (m^3/kmol)
Air	28.97	132.6	37.36	1.602×10^6	0.02557
Carbon dioxide	44.01	304	73.9	6.444×10^6	0.02963
Water	18.02	647.3	220.9	1.426×10^7	0.02111
Nitrogen	28.01	126	33.9	1.553×10^6	0.02677

For a gas mixture, the Redlich-Kwong constants a and b are found using the following procedure. For an n-component gas mixture the value of a is calculated using

$$a = \sum_{i=1}^{n} \sum_{j=1}^{n} y_i y_j a_{ij} \tag{A.6}$$

where y_i and y_j are the respective mole fractions of components i and j. The coefficients a_{ij} of the cross terms can be related to the properties of the pure components by the assumption: $a_{ij} = \sqrt{a_i a_j}$ [60].[1] The value of b follows with

$$b = \sum_{i=1}^{n} y_i b_i \tag{A.7}$$

Temperature determination: fixed-point iteration method

In Section 4.1, the in-cylinder gas temperature was determined using the Redlich-Kwong equation of state (Eq. A.1). Because this equation is not explicit in temperature, the gas temperature cannot be directly solved from Eq. A.1. Instead, a numerical algorithm, known as fixed-point iteration (see e.g. [9]), is applied to calculate the temperature. The steps involved in this iterative approach are discussed below.

First, for convenience, Eq. A.1 is written as

$$p = C_1 T - C_2 T^{-1/2} \tag{A.8}$$

introducing constants $C_1 = \bar{R}/(\bar{v} - b)$ and $C_2 = a/(\bar{v}(\bar{v} + b))$. Second, Eq. A.8 is written as

$$T = \frac{p}{C_1} + \frac{C_2}{C_1} T^{-1/2} \tag{A.9}$$

Then, an initial value T_0 for the temperature must be estimated. This value must be reasonably close to the actual temperature to ensure that the algorithm converges. To this end, one may apply either the ideal gas law or the Van der Waals equation, which are both explicit in temperature. The initial value thus obtained, T_0, is then substituted in the right-hand side of Eq. A.9 to give the second approximation, T_1, which is then substituted in the same manner to give T_2. This procedure is repeated until $|T_n - T_{n-1}| < \xi$, where ξ is the specified tolerance, or until the specified maximum number of iterations has been reached.

[1] Redlich and Kwong, in their original paper [60], described the use of a geometric mean as "somewhat arbitrary," noting that another form of mean could be equally valid.

B

Definition and derivation of NAHRR

In Section 5.2.1, the *net apparent heat release rate* (NAHRR) was introduced as the primary metric for quantifying heat release during combustion. It was defined in Eq. 5.3. This section provides a step-by-step derivation of that expression, starting from the First Law of Thermodynamics. The differential form of the First Law for an open system is:

$$dU = \delta Q - \delta W + \sum h_i \, dm_i \tag{B.1}$$

Here:

- dU is the infinitesimal change in internal energy of the in-cylinder gas;
- δQ is the net heat added to the system;
- δW is the work done by the system;
- h_i is the specific enthalpy of the entering or exiting mass;
- dm_i is the mass entering or leaving the cylinder (*positive for inflow*, *negative for outflow*).

To proceed, we apply the following assumptions:

1. The combustion heat is represented by the gross apparent heat release:

   $$\delta Q_{\text{hr,gr}} = h_f \, dm_f$$

   where h_f is the lower heating value (LHV) of the fuel, and dm_f is the incremental mass of the fuel injected.
2. The net heat input δQ is replaced by the heat loss to the surroundings, denoted δQ_{loss}, which is positive when heat flows *out of* the cylinder.
3. The work done by the gas is modeled as:

   $$\delta W = p \, dV$$

4. Assuming ideal-gas behaviour, the change in internal energy is given by:

   $$dU = mc_v \, dT$$

Substituting these expressions into Eq. B.1, we obtain:

$$\delta Q_{\text{hr,gr}} - \delta Q_{\text{loss}} = p \, dV + mc_v \, dT \tag{B.2}$$

Assuming the in-cylinder gas behaves as an ideal gas, the equation of state is:

$$pV = mRT$$

Taking the total differential of the ideal gas law:

$$p\,dV + V\,dp = mR\,dT \tag{B.3}$$

Solving Eq. B.3 for dT and substituting into Eq. B.2 yields (canceling m):

$$\delta Q_{\text{hr,gr}} - \delta Q_{\text{loss}} = p\,dV + \frac{c_v}{R}(p\,dV + V\,dp) \tag{B.4}$$

Using the definition $\gamma = c_p/c_v$ and the ideal-gas relation $R = c_p - c_v = (\gamma - 1)c_v$, we find:

$$\frac{c_v}{R} = \frac{1}{\gamma - 1}$$

Substituting this into Eq. B.4:

$$\delta Q_{\text{hr,gr}} - \delta Q_{\text{loss}} = p\,dV + \frac{1}{\gamma - 1}(p\,dV + V\,dp)$$

or:

$$\delta Q_{\text{hr,gr}} - \delta Q_{\text{loss}} = \frac{\gamma}{\gamma - 1}p\,dV + \frac{1}{\gamma - 1}V\,dp \tag{B.5}$$

This matches Eq. 2.5 introduced earlier.

Finally, dividing both sides by the crank angle increment $d\theta$ and defining the net apparent heat release rate on a crank-angle basis as:

$$\text{NAHRR}(\theta) = \frac{\delta Q_{\text{hr,gr}} - \delta Q_{\text{loss}}}{d\theta}$$

we obtain the final expression:

$$\text{NAHRR}(\theta) = \frac{\gamma}{\gamma - 1}p\frac{dV}{d\theta} + \frac{1}{\gamma - 1}V\frac{dp}{d\theta} \tag{B.6}$$

This equation allows the net apparent heat release rate to be calculated directly from the pressure trace, conveniently eliminating the need to estimate heat losses.

C
Cubic spline smoothing method

This section outlines the cubic smoothing spline method used throughout this thesis for processing and denoising cylinder pressure signals. The technique was originally introduced by Reinsch [61] and has since become a well-established tool in numerical data analysis. It provides a way to balance how closely the function follows the noisy data against the smoothness of the resulting curve.

To reduce the influence of measurement noise in the cylinder pressure signal, a cubic smoothing spline is applied to the averaged pressure trace. The technique constructs a smooth function $f(x)$ by fitting a piecewise cubic (third-degree) polynomial to the observed data. Unlike cubic-spline interpolation, which passes exactly through all data points, smoothing splines aim to approximate the data while controlling the curvature of the resulting function.

The smoothing spline is the solution to a variational problem: among all twice continuously differentiable functions $f \in C^2[x_0, x_n]$, find the one that minimises:[1]

$$p \sum_{i=1}^{n} \big(y_i - f(x_i)\big)^2 + (1-p) \int_{x_0}^{x_n} \big(f''(x)\big)^2 \, dx \tag{C.1}$$

where:

- (x_i, y_i) are the measured data points; x_i indicates the crank angle, y_i is the measured cylinder pressure;
- $f(x)$ is the smoothing spline to be determined;
- $f''(x)$ is the second derivative of f, which measures its curvature;
- $p \in [0, 1]$ is a smoothing parameter that determines the trade-off between closeness to the data and smoothness of the function.

The first term in Eq. C.1—the *error term*—aims to minimise the sum of squared differences between the function $f(x)$ and the measured data points y (i.e., the cylinder pressure). The second term—the *roughness term*—penalises curvature, thereby promoting smoothness in the fitted function.

By applying the Euler-Lagrange equation to Eq. C.1, Reinsch demonstrated that the solution to the optimisation problem is a function $f(x)$ composed of piecewise cubic polynomials defined on each subinterval:

$$f(x) = a_i + b_i(x - x_i) + c_i(x - x_i)^2 + d_i(x - x_i)^3, \quad x_i \le x < x_{i+1} \tag{C.2}$$

Using cubic polynomials ensures that $f(x)$, $f'(x)$ and $f''(x)$ are continuous at their common endpoints. The smoothing parameter p controls the trade-off between fidelity to the data and the smoothness of the resulting curve. When $p = 1$, the minimisation reduces to an interpolation problem where $f(x_i) = y_i$ for all i. At the other extreme, when $p = 0$, the minimiser is the function with minimal curvature—a straight line. Intermediate values of p result in a compromise: high-frequency noise is suppressed while essential signal features are preserved.

[1] In his original paper [61], Reinsch incorporated relative weights for the errors, $y_i - f(x_i)$, with these weights determined by the standard deviation of the measured data points y_i. The built-in MATLAB function *csaps* supports the inclusion of such weights. In addition, *csaps* allows specifying a weight function (vector) for the roughness penalty term. Here, the weight function is omitted; it is set to one across all data points.

D
Manual correction of corrupted pressure trace

As discussed in Section 6.1, the pressure trace for Case 2 exhibited significant corruption: all B-bank cylinder pressure signals were misaligned with respect to the crank angle. Figure D.1 illustrates this issue for cylinder B2 showing raw, unsmoothed pressure data across 25 engine cycles.

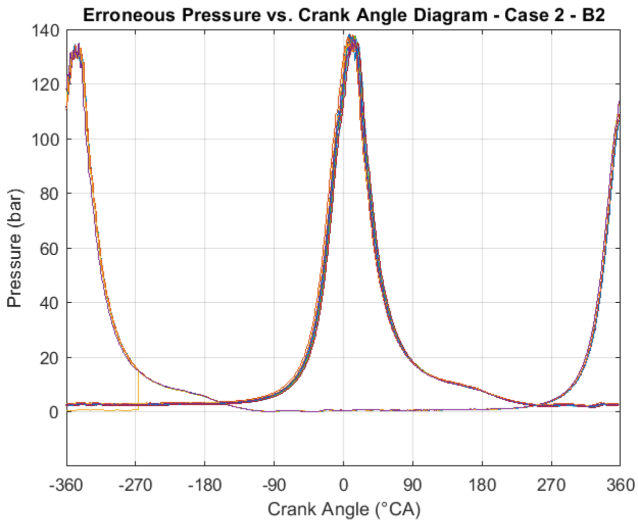

Figure D.1: Corrupted pressure data for cylinder B2 (25 cycles). Several traces are visibly offset in crank angle, with erroneous zero-bar minimum pressures.

Several cycles are completely out of phase—misaligned by approximately 360°CA. Additionally, the traces exhibit an unrealistic minimum pressure of 0 bar, indicating that the automatic pressure referencing procedure was evidently not executed correctly. All B-bank cylinders demonstrated similar behavior. Even cycles that appear correct at first glance—those with pressure peaks shortly after top dead center (TDC)—are in fact misaligned, as shown more clearly in Figure D.2a. During the compression stroke, pressure traces should be well aligned; however, the misalignment is clearly evident.

To address these faults, a reference cycle was selected from an unaffected A-bank cylinder. Cylinder A1 was chosen, and the corrupted B-bank traces were manually aligned to match this reference. For each B-bank cylinder (B1–B6), a TDC shift angle was visually determined to best align the compression stroke with that of the reference. Due to the labor-intensive nature of the correction, only the first nine cycles of each measurement were manually corrected per cylinder, resulting in a 6×9 correction matrix of TDC shift angles. The resulting pressure traces, after implementing the TDC shift angles, are shown in Figure D.2b. The pressure traces now are well aligned.

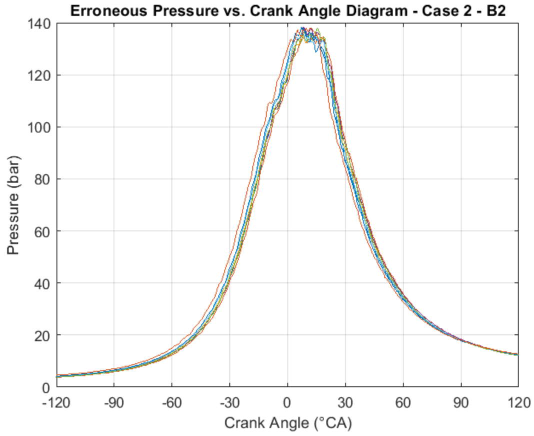

(a) Before correction: misaligned pressure traces of 9 cycles.

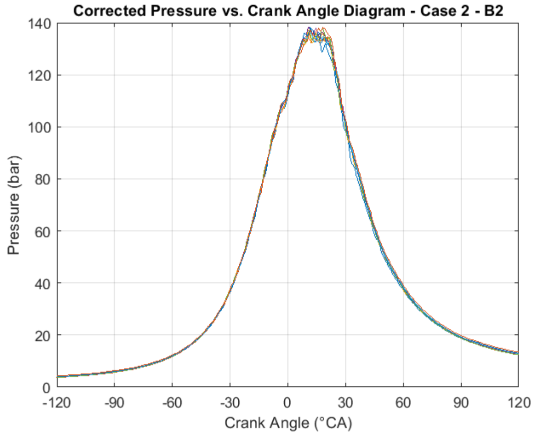

(b) After manual correction: pressure traces are visually aligned.

Figure D.2: Cycle-to-cycle variation in cylinder pressure before and after manual alignment.

This process highlights the necessity for an automated correction method. The automated synchronisation procedure used elsewhere in this thesis—introduced in Section 4.1—relies on pressure data from a stopping engine. However, that method is not applicable in this case, as the correction must be applied within a single measurement taken from an engine operating under load.

The root cause of this anomaly remains unclear. Since A-bank data were unaffected, it is unlikely that the issue stemmed from the trigger sensor, crank angle encoder, pressure sensor, or charge amplifier. Instead, the fault likely originated from the analog-to-digital (A/D) converter. Notably, the system uses separate A/D converters for the A-bank and B-bank cylinders. Strangely, data collected in Case 3, just three days after Case 2, do not exhibit any such issues. Figure D.3 shows pressure traces for cylinder B2 in Case 3, all of which are well aligned and free from anomalies. The same applies to all other cylinders in that measurement. An explanation for this temporary malfunction could not be identified by the author.

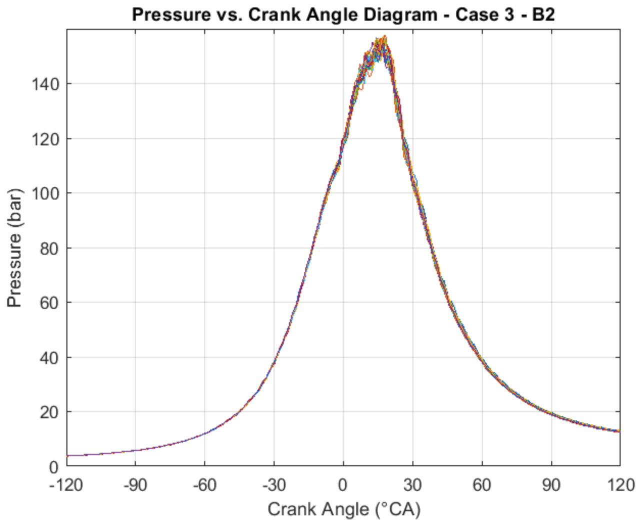

Figure D.3: Correct pressure traces from cylinder B2 in Case 3 (25 cycles).
No misalignment or referencing issues are present.

Bibliography

[1] Antonis Antonopoulos and Dimitrios Hountalas. "Identification and correction of the error induced by the sampling method used to monitor cylinder pressure of reciprocating internal combustion engines". In: *SAE Technical Papers*. SAE International, 2012. DOI: 10.4271/2012-01-1155.

[2] Francesco Baldi, Gerasimos Theotokatos, and Karin Andersson. "Development of a combined mean value–zero dimensional model and application for a large marine four-stroke Diesel engine simulation". In: *Applied Energy* 154 (Sept. 2015), pp. 402–415. ISSN: 03062619. DOI: 10.1016/j.apenergy.2015.05.024.

[3] Urban Žvar Baškovič et al. "A new method for simultaneous determination of the TDC offset and the pressure offset in fired cylinders of an internal combustion engine". In: *Energies* 10.1 (2017). ISSN: 19961073. DOI: 10.3390/en10010143.

[4] H. Bergh and H. Tijdeman. *Theoretical and experimental results for the dynamic response of pressure measuring systems*. Tech. rep. Amsterdam: National Aero- and Astronautical Research Institute, 1965.

[5] T. Borkowski et al. "Combustion pressure appraisal in marine engine". In: *Journal of KONES Powertrain and Transport* 18.4 (2011).

[6] W L Brown. "Methods for Evaluating Requirements and Errors in Cylinder Pressure Measurement". In: *SAE International* 670008 (1967).

[7] Michael F J Brunt and Christopher R Pond. *Evaluation of Techniques for Absolute Cylinder Pressure Correction*. Tech. rep. SAE Technical Paper Series, 1997. DOI: 10.4271/970036.

[8] Michael F J Brunt, Harjit Rai, and Andrew L Emtage. "The Calculation of Heat Release Energy from Engine Cylinder Pressure Data". In: *SAE Technical Paper Series* 981052 (1998).

[9] Richard Burden and J. Douglas Faires. *Numerical Analysis*. 9th. Brooks/Cole, Cengage Learning, 2011. ISBN: 978-0-538-73564-3.

[10] Michael Casey and Chris Robinson. *A METHOD TO ESTIMATE THE PERFORMANCE MAP OF A CENTRIFUGAL COMPRESSOR STAGE GT2011-45*. Tech. rep. URL: http://www.asme.org/about-asme/terms-of-use.

[11] Riccardo Ceccarelli et al. "Model-based adaptive observers for intake leakage detection in diesel engines". In: *2009 American Control Conference*. IEEE, 2009, pp. 1128–1133. ISBN: 978-1-4244-4523-3. DOI: 10.1109/ACC.2009.5160133.

[12] Andrea Coraddu et al. "Physical and Data-Driven Models Hybridisation for Modelling the Dynamic State of a Four-Stroke Marine Diesel Engine". In: 2022, pp. 145–193. DOI: 10.1007/978-981-16-8618-4{_}6.

[13] Richard S Davis and Gary J Patterson. "Cylinder Pressure Data Quality Checks and Procedures to Maximize Data Accuracy". In: *SAE Technical Paper Series* 01.1346 (2006).

[14] Paul Dempsey. *Troubleshooting and Repairing Diesel Engines*. 4th. McGraw-Hill, 2008. DOI: 10.1036/0071493719.

[15] Y. Ding et al. "A new method to smooth the in-cylinder pressure signal for combustion analysis in diesel engines". In: *Proceedings of the Institution of Mechanical Engineers, Part A: Journal of Power and Energy* 225.3 (May 2011), pp. 309–318. ISSN: 0957-6509. DOI: 10.1177/2041296710394298.

[16] Yu Ding. "Characterising combustion in diesel engines using parameterised finite stage cylinder process models". PhD thesis. Delft University of Technology, 2011. ISBN: 9789065622891.

[17] Michail Drakoulas. *DATA-DRIVEN ENGINE STATE MONITORING APPLYING MULTIVARIATE STATISTICS AND MACHINE LEARNING TO FAULT DETECTION AND ISOLATION*. Tech. rep. Delft University of Technology, 2019. URL: http://repository.tudelft.nl/..

[18] Lars Eriksson and Andreas Thomasson. “Cylinder state estimation from measured cylinder pressure traces - A Survey”. In: *IFAC-PapersOnLine*. Vol. 50. 1. Elsevier B.V., July 2017, pp. 11029–11039. DOI: 10.1016/j.ifacol.2017.08.2483.

[19] R Figliola and D Beasley. *Theory and Design for Mechanical Measurements*. 7th. Wiley, 2021. ISBN: 978-1-119-70640-3.

[20] J. A. Gatowski et al. “Heat Release Analysis of Engine Pressure Data”. In: *SAE Technical Paper Series* 841359 (1984).

[21] Rinze Geertsma. “Autonomous control for adaptive ships with hybrid propulsion and power generation”. PhD thesis. 2019. DOI: 10.4233/uuid:ad81b0ee-76be-4054-a7e8-bd2eeecdb156. URL: https://doi.org/10.4233/uuid:ad81b0ee-76be-4054-a7e8-bd2eeecdb156.

[22] Hla Gharib and György Kovács. “Development of a New Expert System for Diagnosing Marine Diesel Engines Based on Real-Time Diagnostic Parameters”. In: *Strojniški vestnik - Journal of Mechanical Engineering* 68.10 (Oct. 2022), pp. 642–655. ISSN: 2536-3948. DOI: 10.5545/sv-jme.2022.298.

[23] J. I. Ghojel. “Review of the development and applications of the Wiebe function: A tribute to the contribution of Ivan Wiebe to engine research”. In: *International Journal of Engine Research* 11.4 (Aug. 2010), pp. 297–312. ISSN: 14680874. DOI: 10.1243/14680874JER06510.

[24] Christoph Gosweiller, Bryan Willson, and Thomas Walter. “Application of an Improved Model for the Determination of Acoustic Resonances in Indicator Passages for Combustion Pressure Measurements”. In: *ASME 2006 Internal Combustion Engine Division Spring Technical Conference (ICES2006)*. ASMEDC, Jan. 2006, pp. 769–779. ISBN: 0-7918-4206-1. DOI: 10.1115/ICES2006-1373.

[25] Jie Gu et al. “Real-time prediction of fuel consumption and emissions based on deep autoencoding support vector regression for cylinder pressure-based feedback control of marine diesel engines”. In: *Energy* 300 (Aug. 2024), p. 131570. ISSN: 03605442. DOI: 10.1016/j.energy.2024.131570.

[26] Mamoru Hasegawa et al. “Study on Ignition Timing Control for Diesel Engines Using In-Cylinder Pressure Sensor”. In: Apr. 2006. DOI: 10.4271/2006-01-0180.

[27] Maria Henningsson, Per Tunestål, and Rolf Johansson. “A virtual sensor for predicting diesel engine emissions from cylinder pressure data”. In: *IFAC Proceedings Volumes (IFAC-PapersOnline)*. Vol. 45. 30. IFAC Secretariat, 2012, pp. 424–431. ISBN: 9783902823168. DOI: 10.3182/20121023-3-FR-4025.00063.

[28] J.B. Heywood. *Internal Combustion Engine Fundamentals*. McGraw-Hill Book Co., 1988. ISBN: 0-07-100499-8.

[29] Günter F Hohenberg. “Advanced Approaches for Heat Transfer Calculations”. In: *SAE International* 790825 (1979).

[30] D. T. Hountalas et al. “Comparative evaluation of various methodologies to account for the effect of load variation during cylinder pressure measurement of large scale two-stroke diesel engines”. In: *Applied Energy* 113 (Jan. 2014), pp. 1027–1042. ISSN: 0306-2619. DOI: 10.1016/J.APENERGY.2013.08.036. URL: https://www.sciencedirect.com/science/article/abs/pii/S0306261913006806?via%3Dihub.

[31] Dimitrios T. Hountalas et al. “Evaluation of a New Diagnostic Technique to Detect and Account for Load Variation during Cylinder Pressure Measurement of Large-scale Four-stroke Diesel Engines”. In: *SAE International* 01.1342 (Apr. 2012). ISSN: 26883627. DOI: 10.4271/2012-01-1342.

[32] Rolf Isermann. *Combustion Engine Diagnosis. Model-based Condition Monitoring of Gasoline and Diesel Engines and their Components*. Springer Vieweg, 2017. DOI: 10.1007/978-3-662-49467-7. URL: http://www.springer.com/series/12236.

[33] Andrew K.S. Jardine, Daming Lin, and Dragan Banjevic. “A review on machinery diagnostics and prognostics implementing condition-based maintenance”. In: *Mechanical Systems and Signal Processing* 20.7 (Oct. 2006), pp. 1483–1510. ISSN: 0888-3270. DOI: 10.1016/J.YMSSP.2005.09.012.

[34] N. B. Jones and Y. H. Li. “A review of condition monitoring and fault diagnosis for diesel engines”. In: *Tribo Test* 6.3 (2000), pp. 267–291. ISSN: 13544063. DOI: 10.1002/tt.3020060305.

[35] Young Jin Kang et al. “Hierarchical level fault detection and diagnosis of ship engine systems”. In: *Expert Systems with Applications* 213 (Mar. 2023), p. 118814. ISSN: 0957-4174. DOI: 10.1016/J.ESWA.2022.118814.

[36] Çağlar Karatuğ and Yasin Arslanoğlu. “Development of condition-based maintenance strategy for fault diagnosis for ship engine systems”. In: *Ocean Engineering* 256 (July 2022), p. 111515. ISSN: 00298018. DOI: 10.1016/j.oceaneng.2022.111515.

[37] Hans Klein Woud and Douwe Stapersma. *Design of Propulsion and Electric Power Generation Systems*. IMarEST, 2002.

[38] D A Kouremenos and D T Hountalas. *Diagnosis and Condition Monitoring of Medium-Speed Marine Diesel Engines*. Tech. rep. 1. 1997, pp. 1354–4063.

[39] V.T. Lamaris and D.T. Hountalas. “A general purpose diagnostic technique for marine diesel engines – Application on the main propulsion and auxiliary diesel units of a marine vessel”. In: *Energy Conversion and Management* 51.4 (Apr. 2010), pp. 740–753. ISSN: 01968904. DOI: 10.1016/j.enconman.2009.10.031.

[40] Steffen Leonhardt, Norbert Müller, and Rolf Isermann. “Methods for Engine Supervision and Control Based on Cylinder Pressure Information”. In: *IEEE/ASME TRANSACTIONS ON MECHATRONICS* 4.3 (1999), pp. 7434–7441.

[41] Y Linden. *NO-emission prediction in a Diesel Engine Using a two zone in-cylinder simulation model*. Tech. rep. Delft University of Technology, 2017. URL: http://repository.tudelft.nl/..

[42] Jinlong Liu and Cosmin E. Dumitrescu. “Analysis of two-stage natural-gas lean combustion inside a diesel geometry”. In: *Applied Thermal Engineering* 160 (Sept. 2019), p. 114116. ISSN: 1359-4311. DOI: 10.1016/J.APPLTHERMALENG.2019.114116. URL: https://www.sciencedirect.com/science/article/abs/pii/S1359431118373435?via%3Dihub.

[43] Yaqiong Lv et al. “Fault detection and diagnosis of marine diesel engines: A systematic review”. In: *Ocean Engineering* 294 (Feb. 2024), p. 116798. ISSN: 00298018. DOI: 10.1016/j.oceaneng.2024.116798.

[44] Ravindra R. Malagi. “Estimation of blowby in multi-cylinder diesel engine using finite element approach”. In: *SAE International* 01.0559 (Apr. 2012). ISSN: 26883627. DOI: 10.4271/2012-01-0559.

[45] MAN Diesel & Turbo. *MAN V28/33D Technical Documentation Engine Operating Instructions*. 2010.

[46] MAN Diesel SE. *MAN Diesel Engine 28/33D Project Guide for Marine Plants*. 2008.

[47] A.J. Martyr. *Engine Testing - Theory and Practice*. 3rd. Butterworth-Heinemann, 2007.

[48] K Mollenhauer and H Tschoeke. *Handbook of Diesel Engines*. Springer Berlin Heidelberg, 2010. DOI: 10.1007/978-3-540-89083-6.

[49] M. Moran et al. *Principles of Engineering Thermodynamics*. 8th. Wiley, 2012. ISBN: 978-1-118-96088-2.

[50] M. Namazian and John B. Heywood. “Flow in the Piston-Cylinder-Ring Crevices of a Spark-Ignition Engine: Effect on Hydrocarbon Emissions, Efficiency and Power”. In: Feb. 1982. DOI: 10.4271/820088.

[51] A. Namigtle-Jiménez et al. “Online ANN-based fault diagnosis implementation using an FPGA: Application in the EFI system of a vehicle”. In: *ISA Transactions* 100 (May 2020), pp. 358–372. ISSN: 00190578. DOI: 10.1016/j.isatra.2019.11.003.

[52] Ylva Nilsson and Lars Eriksson. “Determining TDC Position Using Symmetry and Other Methods”. In: Mar. 2004. DOI: 10.4271/2004-01-1458.

[53] G J J Oskam. *Optimizing diesel engine condition monitoring Research on diagnostic representation techniques based on in-cylinder pressure measurement*. Tech. rep. Delft University of Technology, 2014.

[54] Jose Antonio Pagán Rubio et al. "Marine diesel engine failure simulator based on thermodynamic model". In: *Applied Thermal Engineering* 144 (Nov. 2018), pp. 982–995. ISSN: 13594311. DOI: 10.1016/j.applthermaleng.2018.08.096.

[55] F Payri et al. "New methodology for in-cylinder pressure analysis in direct injection diesel engines—application to combustion noise". In: *Measurement Science and Technology* 16.2 (Feb. 2005), pp. 540–547. ISSN: 0957-0233. DOI: 10.1088/0957-0233/16/2/029.

[56] F. Payri et al. "Digital signal processing of in-cylinder pressure for combustion diagnosis of internal combustion engines". In: *Mechanical Systems and Signal Processing* 24.6 (2010), pp. 1767–1784. ISSN: 10961216. DOI: 10.1016/j.ymssp.2009.12.011.

[57] E Pipitone et al. "The Experimental Validation of a New Thermodynamic Method for TDC Determination". In: *SAE International* 2007-24-0052 (2007).

[58] Andrew L Randolph. "Cylinder-Pressure-Transducer Mounting Techniques to Maximize Data Accuracy". In: *JOURNAL OF PASSENGER CARS* 99 (1990), pp. 201–219. URL: https://about.jstor.org/terms.

[59] Andrew L Randolph. "Methods of Processing Cylinder-Pressure Transducer Signals to Maximize Data Accuracy". In: *JOURNAL OF PASSENGER CARS* 99 (1990), pp. 191–200. URL: https://www.jstor.org/stable/44553970.

[60] Otto Redlich and J N S Kwong. *ON THE THERMODYNAMICS OF SOLUTIONS. V k EQUATION OF STATE. FUGACITIES OF GASEOUS SOLUTIONS'*. Tech. rep. 1949.

[61] Christian H. Reinsch. "Smoothing by spline functions". In: *Numerische Mathematik* 10.3 (Oct. 1967), pp. 177–183. ISSN: 0029-599X. DOI: 10.1007/BF02162161.

[62] David R Rogers. *Engine Combustion: Pressure Measurement and Analysis*. SAE International, 2010. ISBN: 978-0-7680-1963-6. URL: http://books.sae.org..

[63] Richard Scott. *RNLN patrol ship Hull Vane retrofit matches predicted performance*. Dec. 2023. URL: https://www.navalnews.com/naval-news/2023/12/rnln-patrol-ship-hull-vane-retrofit-matches-predicted-performance/.

[64] D Stapersma. *Lecture notes WB4408A Diesel Engines Volume 1 Performance Analysis*. Delft University of Technology, 2010.

[65] D Stapersma. *Lecture notes WB4408A Diesel Engines Volume 2 Turbocharging*. Delft University of Technology, 2010.

[66] D Stapersma. *Lecture notes WB4408B Diesel Engines Volume 3 Combustion*. Delft University of Technology, 2010.

[67] D Stapersma. *Reader WB4408B Diesel Engines Volume 4 Emissions and Heat transfer*. Delft University of Technology, 2010.

[68] Marek J Stas. "Thermodynamic Determination of T.D.C. in Piston Combustion Engines". In: *SAE Technical Paper series* 960610 (1996).

[69] M Tazerout, O Le Corre, and S Rousseau. "TDC Determination in IC Engines Based on the Thermodynamic Analysis of the Temperature-Entropy Diagram". In: *SEA Technical Paper Series* 01-1489 (1999). ISSN: 0148-7191.

[70] Wieger Tiddens. "Setting sail towards predictive maintenance : developing tools to conquer difficulties in the implementation of maintenance analytics". PhD thesis. Enschede, The Netherlands: University of Twente, Sept. 2018. ISBN: 9789036546034. DOI: 10.3990/1.9789036546034. URL: http://purl.org/utwente/doi/10.3990/1.9789036546034.

[71] Konstantinos Marios Tsitsilonis et al. "Health assessment framework of marine engines enabled by digital twins". In: *International Journal of Engine Research* (2023). ISSN: 20413149. DOI: 10.1177/14680874221146835.

[72] P. Tunestal, J.K. Hedrick, and R. Johansson. "Model-based estimation of cylinder pressure sensor offset using least-squares methods". In: *Proceedings of the 40th IEEE Conference on Decision and Control (Cat. No.01CH37228)*. IEEE, 2001, pp. 3740–3745. ISBN: 0-7803-7061-9. DOI: 10.1109/.2001.980445.

[73] Mr Raimo Turunen et al. "Cylinder pressure measurement via indicating cock". In: *CIMAC Counsil on Combustion* paper no. 79 (2007).

[74] Christian Velasco-Gallego et al. "Recent advancements in data-driven methodologies for the fault diagnosis and prognosis of marine systems: A systematic review". In: *Ocean Engineering* 284 (Sept. 2023), p. 115277. ISSN: 00298018. DOI: 10.1016/j.oceaneng.2023.115277.

[75] Jeremy Worm. "An Evaluation of Several Methods for Calculating Transient Trapped Air Mass with Emphasis on the "Delta P" Approach". In: Apr. 2005. DOI: 10.4271/2005-01-0990.

[76] G Woschni. "A Universally Applicable Equation for the Instantaneous Heat Transfer Coefficient in the Internal Combustion Engine". In: *SAE International* 670931 (1967), pp. 3065–3083.

[77] Nan Xu et al. "Research on thermoeconomic fault diagnosis for marine low speed two stroke diesel engine". In: *Mathematical Biosciences and Engineering* 19.6 (2022), pp. 5393–5408. ISSN: 1551-0018. DOI: 10.3934/mbe.2022253.

[78] Yahui Zhang and Tielong Shen. "In-cylinder Pressure Pegging Algorithm Based on Cyclic Polytropic Coefficient Learning". In: *Intyernational Journal of Automotive Engineering* 20174097 (2017), pp. 79–86.

[79] Yilong Zhang, Sanghoon Kook, and Kenneth S Kim. "Assessments of Pressure-Based Ignition Delay Measurements of Various Cetane Number Fuels in a Small-Bore Compression Ignition Engine". In: *Source: SAE International Journal of Engines* 14.5 (2021), pp. 683–696. DOI: 10.2307/27099236. URL: https://www.jstor.org/stable/10.2307/27099236.

[80] Lurun Zhong, N A Henein, and W Bryzik. *Effect of Smoothing the Pressure Trace on the Interpretation of Experimental Data for Combustion in Diesel Engines*. Tech. rep. 2004, pp. 525–543. URL: https://www.jstor.org/stable/44723528.

Cylinder pressure measurement of diesel engines can be a step toward enabling condition-based maintenance, rather than maintenance based solely on engine running hours. This thesis investigates the application of a *continuous* cylinder pressure measurement system for the condition monitoring of marine diesel engines. It addresses the question of how such a system can be used effectively for the analysis of engine performance, combustion, and the fault detection and diagnosis of a naval vessel's main engines. To answer this question, a comprehensive methodology was developed and tested on an ocean-going patrol vessel of the Royal Netherlands Navy. The main diesel engines of this vessel were retrofitted with a permanent, multi-cylinder pressure measurement system, enabling simultaneous, crank-angle-resolved pressure acquisition.

Following the preprocessing of the raw cylinder pressure data—including synchronisation, referencing, and smoothing—the data were ready for quantitative analysis. Key performance parameters such as peak pressure, indicated mean effective pressure, and compression pressure were directly extracted from the pressure traces. Combustion-related quantities, including the net apparent heat release rate and thermodynamic efficiency, were computed using a single-zone heat-release model. All parameters were evaluated on a per-cylinder basis and subsequently compared across cylinders and against a reference dataset. The measurement campaign covered an 18-month operational period and revealed several noteworthy anomalies. It also included the replacement of a suspected malfunctioning fuel-injection pump.

TU Delft

Materiel and IT Command
Ministry of Defence